CNIC-00858
CNDC-0014
INDC(CPR)-032/L

COMMUNICATION OF NUCLEAR DATA PROGRESS

No. 11(1994)

China Nuclear Information Center
Chinese Nuclear Data Center
Atomic Energy Press

CNIC-00858
CNDC-0014
INDC(CPR)-032 / L

COMMUNICATION OF NUCLEAR DATA PROGRESS

No. 11 (1994)

Chinese Nuclear Data Center

China Nuclear Information Centre

Atomic Energy Press

Beijing, June 1994

EDITORIAL NOTE

This is the eleventh issue of *Communication of Nuclear Data Progress* (CNDP), in which the nuclear data progress in China during the last year is carried, including the measurements of ^{64,67}Zn(n,p), ^{199}Ir(n,2n) and ^{151,153}Eu (n,γ) activation cross sections, the level structure of ^{154}Gd and ^{182}W; photonuclear data calculations of ^{27}Al, ^{54}Fe and ^{209}Bi, introduction to the codes SPEC and DDCS, the evaluations and calculations of reactions ^{54,56,Nat}Fe(n,x)^{51}Cr, ^{52,54}Mn, ^{197}Au(n,3n) and (n,4n), an open problem on photon production calculation, intermediate–high energy nuclear reaction kinetic simulation and QMD, systematics of H(n,n); the evaluation of neutron induced data on ^{56}Fe, nuclear data sheets update for A = 52, 54, 195, level spin assignment of superdeformed bands; Chinese Evaluated Nuclear Parameter Library (CENPL) (III), an auxiliary plotting code of UNF code, management program system of Chinese evaluated nuclear decay database; a method for evaluation of uncertainties for DDX, the spline fitting for multi–set of correlative data; and activities and cooperations on nuclear data in China during 1993.

For limited experience and knowledge, there might be some shortcomings and errors, welcome to make comments on them.

Please write to Drs. Liu Tingjin and Zhuang Youxiang
Mailing Address : Chinese Nuclear Data Center
China Institute of Atomic Energy
P. O. Box 275 (41), Beijing 102413
People's Republic of China
Telephone : 86–1–9357729 or 9357830
Telex : 222373 IAE CN
Facsimile : 86–1–935 7008
E–mail : CIAEDNP@VXIHEP.IHEP.CERN.CH

EDITORIAL BOARD

CONTENTS

I EXPERIMENTAL MEASUREMENT

Cross Section Measurement of $^{64}Zn(n,p)^{64}Cu$ Reaction from 4 to 7 MeV

Tang Guoyou Cheng Jinxiang Zhang Guohui Shi Zhaomin

(Peking University, Beijing)

Lu Hanlin Zhao Wenrong Yu Weixiang Cheng Jiangtao

(China Institute of Atomic Energy, Beijing)

Introduction

In the areas of activation and neutron scattering cross sections, there are still deficiencies in the nuclear database. Activation cross sections were found to be unsatisfactory in 83 of the 183 reactions reviewed[1]. The excitation curve for $^{64}Zn(n,p)^{64}Cu$ reaction has been measured from threshold to 10 MeV by different authors[2~8]. All of these measured cross sections are not in very good agreement with each other. To clarify the discrepancy it is necessary to measure the cross sections for $^{64}Zn(n,p)^{64}Cu$ reaction once again.

1 Experimental Measurement

The cross sections for $^{64}Zn(n,p)^{64}Cu$ reaction were measured with activation technique and the cross sections of $^{58}Ni(n,p)^{58}Co$ reaction[5~8] were used as reference for neutron fluence rate measurement. The values of $^{58}Ni(n,p)^{58}Co$ cross section are given in Table 1. It was taken from our evaluated results according to ENDF / B-6 and experimental data[9, 10].

The 4.0~ 7.0 MeV neutrons from $D(d,n)^3He$ reactions were used in the measurement. The deuteron beam was accelerated by 4.5 MV Van de Graaff

accelerator of Peking University. The energy range of deuterons was in 1.21～4.08 MeV, beam current was about 6 μA. The deuteron beam was incident to a solid D–Ti target with 1.65 mg / cm^2 in thickness.

The samples are naturally metallic Zinc disks with a diameter of about 20 mm and a mass of about 1040 mg. The purity was better than 99.9%. In irradiation, Zinc disk was sandwiched between two disks in diameter of 20 mm and 1000 mg mass. The distance from sample to source is 1～2 cm. The samples were irradiated for about 12 h. The fluctuation of neutron fluence rate was monitored by BF_3 long counter, which was placed at 0 ° with a beam current, at distance of 150 cm from the source. After irradiation, the activities from residual nuclei were measured with HPGe γ–detector (105 cm^3). The detector was calibrated with standard gamma sources in the energy range of 0.1～1.5 MeV and the efficiency curve was fitted with the least– square method. Their half–life, γ–ray intensity and γ–ray energy[11] of the residual nuclei measured in this experiment are listed in Table 2.

From the measured γ–spectrum, counting number under the concerned total energy peaks was obtained. After corrections to the detector efficiency, cascade effect, γ–intensity and fluctuation of neutron fluence rate, the cross sections of the ^{64}Zn(n,p)^{64}Cu reaction are obtained with the following formula :

$$\sigma = \sigma_0 \frac{N_\gamma \lambda \, e^{\lambda t} M_0 \, (1 - e^{\lambda_0 \Delta t_0}) \, K_0 \, (1 - e^{-\lambda_0 T}) \, \varepsilon_0 I_0}{N_{\gamma 0} \lambda_0 \, e^{\lambda_0 t_0} \, M \, (1 - e^{\lambda \Delta t}) \, K \, (1 - e^{-\lambda T}) \, \varepsilon I} \tag{1}$$

where suffix 0 represents corresponding terms concerning the reference ^{58}Ni σ —cross section, N_γ—total counting number under total energy peak of the measured characteristic γ–ray, λ—decay constant of the residual nucleus, t—cooling time, M—nucleus number of the sample, Δt—total time of the γ–ray measurement, K—fluctuation factor of neutron fluence rate, T—irradiated time, ε—detection efficiency for the total energy peak, I—γ–ray intensity.

The fluctuation factor of neutron fluence rate

$$K = \frac{\sum_{i=1}^{n} (1 - e^{-\lambda \Delta t_i}) \, \Phi_i \, e^{-\lambda T_i}}{\Phi \, (1 - e^{-\lambda T})} \tag{2}$$

where N is the number of time intervals for the irradiation time, Δt_i is the i–th time interval, T_i is time from interval Δt_i to the end of irradiation, Φ_i is the

relative neutron fluence in interval Δt_i and Φ is the average neutron fluence during the irradiation T.

Table 1 Cross sections for $^{58}Ni(n,p)^{58}Co$ reaction

Energy (MeV)	4.0	4.9	6.0	7.0
Cross section (mb)	352.5 ± 5.6	474.7 ± 7.5	584.4 ± 14.0	638.2 ± 15.9

Table 2 Half-life, γ-ray energy and intensity of measured residual nuclei

Reaction	Residual nuclei	Half-life	Energy of γ-ray (keV)	γ-intensity
$^{64}Zn(n,p)$	^{64}Cu	12.701 h	511, 1346	36%, 0.48%
$^{58}Ni(n,p)$	^{58}Co	70.8 d	811	99.46%

2 Result and Discussion

The measured results of the cross sections are listed in Table 3. The main errors are given in Table 4.

Table 3 Results of cross section measurements for $^{64}Zn(n,p)^{64}Cu$ reaction

Energy (MeV)	4.00 ± 0.16	4.90 ± 0.10	6.00 ± 0.13	7.00 ± 0.15
Cross Section (mb)	132.9 ± 3.8	181.6 ± 6.3	205.2 ± 7.9	219.5 ± 8.4

Table 4 Main errors of $^{64}Zn(n,p)^{64}Cu$ cross section

Source of error	Relative error (%)
Reference cross section	1.6 ~2.5
γ-counting statistics for ^{64}Cu	0.45~2.9
γ-counting statistics for ^{58}Co	0.6 ~1.9
γ-detection efficiency for ^{64}Cu	1.5
γ-detection efficiency for ^{58}Co	1.5
^{64}Zn target nuclei number	0.01
^{58}Ni target nuclei number	0.02

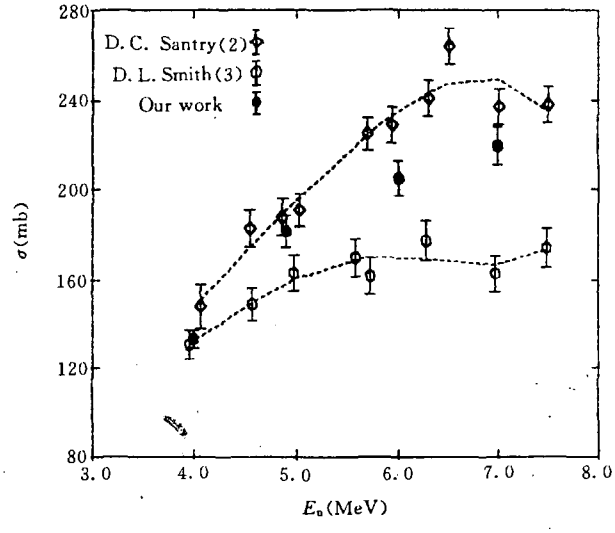

Fig 1 $^{64}Zn(n,p)^{64}Cu$ activation curve

For the residual nucleus ^{64}Cu, γ–rays of energy 511 keV and 1346 keV were measured by HPGe γ–detector. Their intensities are 36% and 0.48% respectively. So the counting statistics of 511 keV γ–ray are better than that of 1346 keV γ–ray. 511 keV γ–ray is produced by the positron annihilation of ^{64}Cu β^+ decay. To ensure that positron annihilation occurred within measured geometry, ^{64}Cu measurements must be made with thick metal covers placed behind each irradiated sample. It shows that the results by measuring γ–ray of 1346 keV and both γ– rays of 511 keV intensities of residual nuclei ^{64}Cu are concerted in our measurement.

The measured cross sections of the present work are plotted in Fig. 1, along with the data of D. L. Smith[3] and D. C. Santry[2] for comparison. These data are not in very good agreement with each other. The cross section values of Santry are considerably larger than that of Smith in the entire measured range. In Santry's work, he completed many corrections but he did not correct the effect of ^{67}Cu β counting number in measuring β counting number of ^{64}Cu, and he took more large half life of ^{64}Cu. In Smith's measurement, maybe, the correction for low energy neutron was not enough, and he took more large γ–intensity. Our cross section values are larger than Smith's values and smaller than Santry's, but closer to Santry's value.

References

[1] D. L. Smith et al., ANL / NDM 123, p. 11(1991)
[2] D. C. Santry et al., Can. J. Phys., 50, 2536(1972)
[3] D. L. Smith et al., Nucl. Sci. Eng., 58, 314(1976)
[4] K. Nakai et al., J. Phys. Soc. Japan. 17, 1215(1962)
[5] H. A. Hussain et al., J. Appl. Radiation Isotopes, 34, 731(1983)
[6] J. Rapaport et al., Phys. Rev., 114, 565(1959)
[7] C. H. King et al., Nucl. Sci. Taiwan, 16, 71(1979)
[8] Y. A. Nemilov et al., P. YFI., 26, 25(1978)
[9] D. L. Smith, Proceedings of Nuclear Data for Sci. & Tech., p. 282(1992)
[10] Li Tingyan et al., High Energy Physics and Nuclear Physics, 16, 151(1992)
[11] C. M. Lederer et al., Table of Isotopes, 7th Edition, p. 169, 197

Progress on 14 MeV Neutron Activation Cross Section Measurement at Lanzhou University

Yuan Junqian Kong Xiangzhong Yang Jingkang Wang Yongchang

(Department of Modern Physics, Lanzhou University)

Radioactivity in fusion reactors is primarily induced by D–T neutrons and depends entirely on the materials chosen for constructing the reactor components. A lot of work on measurement and evaluation of activation cross sections for 14 MeV neutrons has been done recently. The development of a comprehensive activation data library for fusion applications is also being developed. The needs for activation cross sections leading to the production of long–lived (half–life longer than five years) radionuclides have become obvious in the recent years because of the worldwide concerns for the production of high level nuclear waste from fusions reactors.

Since 1992 we have measured some activation cross sections for the $^{137}Ba(n,p)^{137}Cs$, $^{136}Ba(n,p)^{136}Cs$, $^{134}Ba(n,p)^{134}Cs$, $^{132}Ba(n,p)^{132}Cs$, $^{134}Ba(n,2n)^{133}Cs$, $^{132}Ba(n,2n)^{131}Ba$, $^{204}Pb(n,2n)^{203}Pb$, $^{206}Pb(n,\alpha)^{203}Hg$, $^{67}Zn(n,p)^{67}Cu$, $^{66}Zn(n,2n)^{65}Zn$, $^{193}Ir(n,2n)^{192m2}Ir$ reactions at 13.5~ 14.8 MeV neutron energy

region. The cross sections for $^{193}Ir(n,2n)^{192m2}Ir$ and $^{137}Ba(n,p)^{137}Cs$ reactions are high-priority request long-lived activation cross sections for fusion reactor technology [1]. At present, for $^{137}Ba(n,p)^{137}Cs$ reaction only one published datum can be found and for the $^{193}Ir(n,2n)^{192m2}Ir$ reaction no measured cross section can be found.

The results obtained for the above reactions are given in the Table 1.

The papers on the reactions relative to the Pb and Zn have been published (see Refs. [2], [3]). The cross section measurement for the reaction of $^{137,136,134,132}Ba(n,p)$ and $^{134,132}Ba(n,2n)$ will be published (see Ref. [4]). In this paper the measurement of activation cross section for $^{193}Ir(n,2n)^{192m2}Ir$ which has not been published yet is described in detail.

Irradiation of the Ir sample was carried out in June 16, 1990 at Intense Neutron Generator of Lanzhou University. The sample of Ir with 20 mm in diameter and 3 $\times$ 0.4 mm in thickness was made by natural metal foil. The sample in question was sandwiched between two niobium foils to monitor the neutron fluence on the sample. In order to obtain high neutron fluxes the sample was positioned close to the back of the rotating tritium target. The distance of the sample from target is about 8 mm. At the position, the neutron energy was determined by the method of cross section ratio of zirconium to niobium. It was determined at 14.80 MeV. The irradiation lasted up to 12 h with neutron intensity of about $1\sim 3\times 10^{12}$ n / s in the 4π space. The cooling time of the sample was 3.5 a.

After irradiation the activities were measured by γ-ray spectroscopy using a CH8403 coaxial HPGe detector made in China in conjunction with a EG & G ORTEC 7450 Multichannel Analyzer. The efficiency of the detector was calibrated by using the standard γ source, SRM4275, made in U. S. A. The relative photopeak detection efficiency of the detector was known within an error of $\pm$ 2%. The counting time for the $^{192m2}Ir$ was 103.6 h. The total number of counts recorded by the γ-ray detector under the full energy peak area was 3134.

The decay data for ^{92m}Nb used in the present work were taken from the literature[5]: half-life 10.15 d, γ-ray energy of 934.5 keV, and γ-ray intensity 99.0%. The abundance of ^{93}Nb is 100% for the $^{93}Nb(n,2n)^{92m}Nb$ reaction. For the $^{193}Ir(n,2n)^{192m2}Ir$ reaction, the ^{199}Ir abundance is 62.7%. The half-life, γ-ray energy, and intensity used for $^{192m2}Ir$ are 241 $\pm$ 9 a, 155.16 keV, and 0.097 $\pm$ 0.004%, respectively. In the measurement of γ activities, some corrections were made for the effects of neutron intensity fluctuation during irradiation and γ-ray self-absorption in the sample. The low energy neutrons from contamination of neutron source (D-D reaction) and scattered neutron produced in the vicinity of neutron source and sample package were not considered in this

work.

The main experimental errors in present work are as follows : peak area analysis (29.9%), efficiency of γ–ray detector (2%), γ–ray self–absorption (5%), decay constant (4%), γ–ray branching (4%) and standard cross section (2%).

The measured cross section for the $^{193}Ir(n,2n)^{192m2}Ir$ at 14.8 MeV is 246 ± 76 mb. The result is only regarded as a preliminary one. In order to determine the final cross section for $^{193}Ir(n,2n)^{192m2}Ir$ reaction, we will measure it repeatedly.

References

[1] E. T. Cheng, "Review of the Nuclear Data Status and Requirements for Fusion Reactors", Proc. Int. Conf. Nucl. Data for Sci. & Tech., Mito, Japan, 30, June 3, 1988

[2] Yuan Junqian et al., Nuclear Techniques 16, 9 (1993) (in Chinese)

[3] Kong Xiangzhong et al., J. of Lanzhou University, 28, 2 (1992) (in Chinese)

[4] Yuan Junqian et al., Trends in Nuclear Physics, to be published (in Chinese)

[5] E. Browne et al., Table of Radioactive Isotopes, 1986

Table 1 Values of measured activation cross sections

Reaction	Neutron energy (MeV)	Cross section (mb)
$^{204}Pb(n,2n)^{203}Pb$	13.50	1951 ± 85
	13.84	1907 ± 90
	14.18	2027 ± 81
	14.38	2070 ± 79
	14.67	1931 ± 77
	14.81	1928 ± 75
$^{206}Pb(n,\alpha)^{203}Pb$	14.38	1.2 ± 0.2
$^{67}Zn(n,p)^{67}Cu$	13.50	56.5 ± 2.3
	13.66	57.1 ± 2.3
	14.29	61.6 ± 2.5
	14.37	62.7 ± 2.5
	14.70	68.1 ± 2.7
	14.80	69.3 ± 2.8
$^{66}Zn(n,2n)^{65}Zn$	13.50	479 ± 24
	13.66	523 ± 25
	14.29	617 ± 30
	14.37	632 ± 31
	14.70	698 ± 35
	14.80	711 ± 36
$^{137}Ba(n,p)^{137}Cs$	14.20	9.1 ± 0.8
$^{136}Ba(n,p)^{136}Cs$	14.20	3.7 ± 0.3
$^{134}Ba(n,p)^{134}Cs$	14.20	16.4 ± 1.4
$^{132}Ba(n,p)^{132}Cs$	14.20	35.0 ± 1.5
$^{134}Ba(n,2n)^{133}Ba$	14.20	1790 ± 152
$^{132}Ba(n,2n)^{131}Ba$	14.20	1596 ± 136
$^{193}Ir(n,2n)^{192m2}Ir$	14.80	246 ± 76

Activation Cross Section Measurement for the Eu(n,γ) Reactions

Xia Yijun Long Xianguan Luo Xiaobing Yang Zhihua Liu Mantian
Wang Chunhao Yang Jingfu He Fuqing Peng Xiufeng

(Institute of Nuclear Science and Technology, Sichuan University)

Lu Hanlin

(China Institute Atomic Energy, Beijing)

Abstract

The cross sections for $^{151}Eu(n,\gamma)^{152m}Eu$, $^{151}Eu(n,\gamma)^{152g}Eu$ and $^{153}Eu(n,\gamma)^{154}Eu$ reactions have been measured relatively to that of ^{197}Au for neutron energy from 22 to 1100 keV, using the activation technique. Neutrons were generated via the $^{7}Li(p,n)^{7}Be$ and $T(p,n)^{3}He$ reaction with a 4.5 MV Van de Graaff accelerator at Peking University. The activities after irradiation were measured with two calibrated high resolution HPGe detectors. The accuracy of the measurement is 6～7%. The experiment results were compared with existing data.

Introduction

Along with the development of fusion reactor research, more activation cross section data for the generation of long-lived radionuclides are needed for estimation of radioactive waste and selection of materials leading to low-level activities. These important activation cross sections, which still need to be measured, were listed by E. T. Cheng[1] and adopted by working group 1 of 16th INDC meeting as high priority data requested for fusion technology. The cross section of $^{151}Eu(n,\gamma)^{152g}Eu$ reaction is an important for fusion reactor design. In this work, we measured the cross sections for the $^{151}Eu(n,\gamma)^{152g}Eu$, $^{151}Eu(n,\gamma)^{152m}Eu$ and $^{153}Eu(n,\gamma)^{154}Eu$ reactions by activation method in the energy range from 22 to 1100 keV.

1 Measurement

The samples were made of natural oxide europium, which were pressed into a disk with 20 mm in diameter and 2.5 mm in thickness and packed in Al film. The gold disks 20 mm in diameter and 0.1 mm in thickness were used as the neutron fluence monitors. Each sample was sandwiched between two gold disks. Considering the effect of 5 eV neutron from background on gold resonant absorption, we put two other gold disks of the same diameter but only 0.05 mm in thickness outside the gold monitors. The sample groups were wrapped in cadmium foils of 0.5 mm in thickness. A group of samples mounted on the surface of Al ring (70 mm in daimeter) centered at the neutron source were irradiated simultaneously at 0, 45, 90, and 135 degrees with respect to the incident proton beam. Therefore neutrons between 22 to 230 keV were produced by the $^{7}Li(p,n)^{7}Be$ reaction, and 173 to 1100 keV by the $T(p,n)^{3}He$ reaction. Two irradiation runs for each proton energy were performed. The proton beam currents were generally 8 to 15 μA and the duration of irradiation was about 80 to 90 hours in each run. The neutron flux was monitored with a long counter at 0 degree at a distance of 2.2 m from the source. In order to record the neutron flux as a function of time during the irradiation, the integral count rate of the long counter per 6 minutes was recorded continuously by microcomputer multiscaler and stored on magnetic disk for calculating the correction of nonuniform irradiation history. To determine the effect of background neutron, another europium sample was placed at 1.8 m from the target and irradiated simultaneously.

The activities of the samples and the gold disks were measured with two calibrated high resolution HPGe detectors. Because the activities of samples were rather weak, they were placed on the surface of the detector for measurement. The counts of the γ–ray full energy peaks were about 10000. Table 1 lists some parameters for calculation of the results.

Table 1 Some parameters

Sample	Molecular weight	Isotope	Abundance	Product nucleus	Half–Life	E_γ (keV)	I_γ (%)
Au	196.9665	^{197}Au	1.0	^{198}Au	2.6935 d	412	95.5
Eu_2O_3	351.9182	^{151}Eu	0.478	^{152m}Eu	9.32 h	842	14.6
				^{152g}Eu	13.33 a	344	26.6
		^{153}Eu	0.522	^{154}Eu	8.8 a	1274	35.5

2 Results

The cross sections for the $^{151}Eu(n,\gamma)^{152m}Eu$, $^{151}Eu(n,\gamma)^{152g}Eu$ and $^{153}Eu(n,\gamma)^{154}Eu$ reactions obtained with the standard cross section of $^{197}Au(n,\gamma)$ reaction recommended by ENDF / B–6 are listed in Table 2 and plotted in Figs. 1～3 together with experiment errors. For comparisons, the data of other authors are also plotted in Figs. 1～3.

Table 2 Present results of the cross sections in mb

E_n, keV	$^{151}Eu(n,\gamma)^{152m}Eu$	$^{151}Eu(n,\gamma)^{152g}Eu$	$^{153}Eu(n,\gamma)^{154}Eu$
1100±80	130±9	284±19	245±15
817±167	163±11	348±23	313±20
376±116	321±20	641±40	541±34
230±20	475±30	860±54	841±55
173±40	547±36	994±63	966±61
160±40	516±34	1040±65	1041±68
57±25	683±48	1734±110	1741±113
22±16	1524±99	2822±170	2521±164

It can be seen from Figs. 1～3 that our results for the $^{151}Eu(n,\gamma)^{152g}Eu$ and $^{153}Eu(n,\gamma)^{154}Eu$ reactions are in good agreement with the data of Yu Weixiang[2] and Macklin[3] .within the experiment error. Our results for $^{151}Eu(n,\gamma)^{152m}Eu$ reaction are also agreement with the data of Yu Weixiang within the experiment error.

The authors thank the International Atomic Energy Agency and Chinese Nuclear Data Center for their encouragement and financial support. In addition, the Van de Graaff crew in Peking University is gratefully acknowledged.

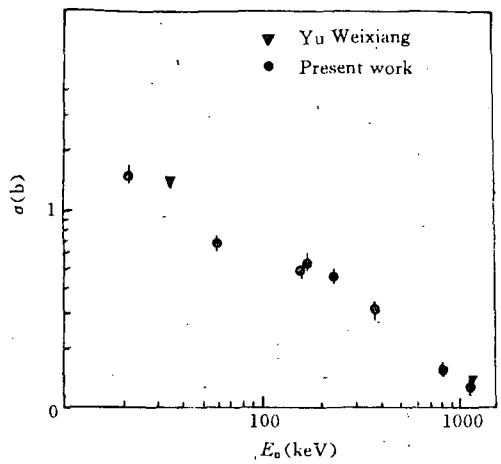

Fig. 1 $^{151}Eu(n,\gamma)^{152m}Eu$ cross sections

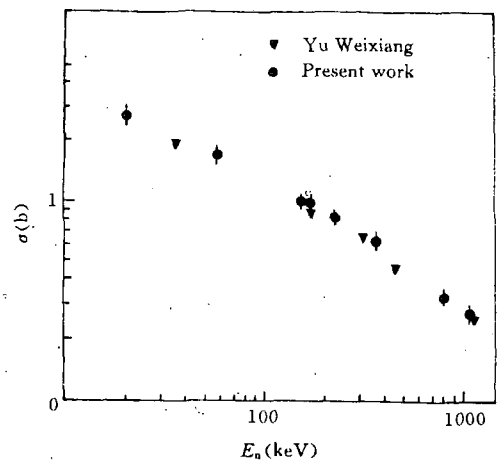

Fig. 2 $^{151}Eu(n,\gamma)^{152g}Eu$ cross sections

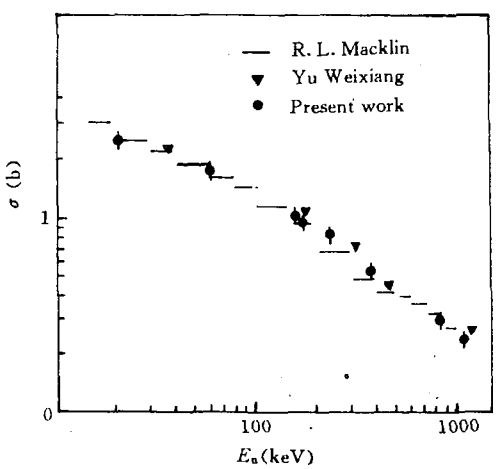

Fig. 3 $^{153}Eu(n,\gamma)^{154}Eu$ cross sections

References

[1] E. T. Cheng, Minutes of the 16th INDC Meeting–INDC / P (89)–7, p. 29 (October 1987, Beijing, China)

[2] Yu Weixiang, Chinese Journal of Nuclear Physics, 15, 71(1993)

[3] R. L. Macklin, Nucl. Sci. Eng., 95, 189(1987)

Progress on Nuclear Data Measurement at Nuclear Physics Laboratory of Jilin University

Huo Junde Liu Yunzuo

(Department of Physics, Jilin University)

1 On Some New Levels in ^{182}W

In recent study[1], five new γ–rays and two new levels were claimed to have been observed in the decay of ^{182}Ta. The energies and relative intensities of these γ–rays are: 49.43 keV (4.49), 136.65 keV (0.12), 146.72 keV (0.04), 169.34 keV (0.20) and 1294.57 keV (0.03), where the intensities are given in parentheses and normalized to the 1121.33 keV γ–ray (I_γ (rel) = 100). The level at 1624.07 keV is depopulated by two γ–rays : 1294.57 and 136.65 keV. The level at 1656.64 keV is depopulated by two γ–rays : 146.72 and 169.34 keV. Fig. 2 of Ref. [1] was given to show the coincidence relation 1294.57~100.10 keV. Fig. 3 of Ref. [1] was intended to show the coincidence relations 136.65~1001.67 keV and 169.34~1001.67 keV. The 146.72 keV γ–ray was also claimed to be seen in weak coincidence with the 100.10 and 229.33 keV γ–rays, but they were not indicated in the coincidence spectra of Ref. [1].

Our study shows that the intensities of the γ–rays (if they exist) depopulating the new levels are too weak to be observed in the coincidence spectra of Ref. [1] and that the claimed observation of the coincidence relations in Ref. [1] is in contradiction with the γ–ray intensities and level scheme of Ref. [1]. The evidence and arguments were presented in Ref. [2].

2 Study on the Level Structure of ^{154}Gd Through the Decay of ^{154}Eu

The nucleus ^{154}Eu lies at the edge of the region of strongly deformed nuclei and its decay has been studied for several times. Refs. [3] and [4] are the latest studies of the decay of ^{154}Eu and large amount of discrepancies exist between these two studies[3]. Reported 172 γ–rays in 1968 and only 82 of them were confirmed by A. K. Sharma et al.[4] in 1980. In the evaluation of nuclear structure and nuclear decay data of 1987[5], 140 γ–rays of Ref. [3] were adopted by the

evaluator. Trying to clarify the discrepancies, the singles and coincidence spectra of γ–rays emitted in the decay of ^{154}Eu were reinvestigated in our laboratory. Data analysis are in progress.

References

[1] J. K. Jabber et al., J. Phys. G: Nucl. Phys., 16, 271(1990)

[2] Liu Yunzuo et al., J. Phys. G: Nucl. Part. Phys., 19, 213(1993)

[3] R. A. Meyer, Phys. Rev., Vol. 170, 1089(1968)

[4] A. K. Sharma et al., J. Phys. Soc., Japan, Vol. 48, 1407(1980)

[5] R. G. Helmer, Nuclear Data Sheets, Vol. 52, No. 1(1987)

II THEORETICAL CALCULATION

Progress on Nuclear Theory and Its Application at the Theory Group of CNDC

Han Yinlu

(Chinese Nuclear Data Center, IAE)

In 1993, the theory group of CNDC made progress in theory research, model programs making, data calculations of nuclear reaction, parameter library construction and so on. The main works are described briefly as follows:

I The Nuclear Reaction Theory Research

1. The multistep compound formalism of FKK theory is developed in pre–equilibrium reaction as follows:

(1) Determining the angular momentum compound coupling factors in both the transition matrix element and geometrical coefficient of double differential cross sections formula, the nucleon treated as a fermion, the target spin can be any value, and the coupling is treated rigorously.

(2) The neutrons and protons are distinguished rigorously in wave function, so the two–component FKK theory is rigorous.

(3) The transmission coefficients (T) of optical model (OM) taking the place of $2\pi < \Gamma_1^{in} > / < D_1 >$ of FKK theory are advanced, the calculated result not only is consistent with OM, but also gives out a basis for calculating the portions of P and Q space in first step.

(4) Because compound system becomes in equilibrium in r space, and the detailed balance principle is applicable, the escaping width can be calculated by T of OM. In lower energy and equilibrium states, it degenerates HF theory completely, the compound process and pre–equilibrium process can be described by the same theory, and it overcomes the confines of exciton model being

classical also.

2. The channel theory of fission with diffusive dynamics is proposed based on Bohr channel theory of fission and Fokker–Planck equation. It is assumed that the single particle motion degrees of freedom are in equilibrium but the collective deforming variable is not in equilibrium inside the saddle point of the excited nucleus. Therefore the Fokker–Planck equation can be used to describe the collective deforming motion at other degrees of freedom (single particle motion) acting as a heat bath with temperature T. The diffusion is caused by the coupling between the deforming variable and the other degrees of freedom of the system as a heat bath with temperature T to attain random or stochastic.

The result shows the channel theory of fission with diffusive dynamics are sensibly influenced by all quantities of friction coefficient β, kT and the fission barrier parameters. Since the model is physically insight, and consistent with Bohr–Wheele formula when $T\to 0$ or $\beta\to 0$, and also rather easy to work with, it is useful in the analysis of fission cross section and many other applications in high energy range.

3. The semi–classical multi–step compound and direct double differential cross section formulations of light composite particle projectile considering (1,m) and (2,m) pick–up type reactions simultaneously are presented. The calculated results of cross sections, spectra, and double differential cross sections indicate that the contributions of the (2,m) pick–up type reactions are about 15 $\sim$ 25% when incident energies are less than 50 MeV and become dominant when incident energies are larger than 50 MeV in some region of the outgoing energies and angles. Whereas the forward tendency of the calculated angular distributions by (2,m) configuration are weaker than that by (1,m) configuration. It also concludes that for the reactions of outgoing composite particle with higher incident energy the semi–classical multi–step direct process must be considered.

4. Since the anisotropic behavior of nucleon–nucleon scattering becomes strong with increasing incident energy and the isotropic picture still used in previous theories of exciton model, the formula of anisotropic free N–N elastic scattering angular distribution in the energy region 2$\sim$ 150 MeV of C. M. system is obtained based on the experimental data of the neutron–hydrogen elastic scattering angular distributions. With considering the influence of the Fermi motion and the Pauli principle and the intranuclear anisotropic N–N

scattering, the more realistic and reasonable elastic scattering angular distribution formulation of N–N scattering in nuclear matter is obtained. Based on the obtained expressions and the semi–classical model of multi–step direct and compound reactions the emitted secondary nucleon double differential cross sections are calculated for some nuclei. The calculated results indicate that the anisotropic effect can slightly improve the fitting to the experimental data especially at the small angle region. Meanwhile, the calculated results indicate again that for the reactions at high incident energies the semi–classical multi–step direct reaction must be considered.

5. The systematics of neutron–hydrogen elastic scattering cross sections and angular distributions in energy region 2～150 MeV is obtained based on the experimental data of the neutron–hydrogen elastic scattering angular distributions in the C. M. system for 773 angles of 45 energy points well–distributed between 14.1～150 MeV and the evaluated values of neutron–hydrogen elastic scattering cross sections. The calculated results show that the empirical formula for neutron–hydrogen elastic scattering could reproduce the experimental data successfully.

6. In the intermediate and high energy nuclear reaction, the Kinetic Simulation model is proposed. This model is used to study the thermalization in reaction of 800 MeV proton bombarding iron nucleus. The calculation shows that the thermal equilibrium is reached in a tube–like volume along incident direction. This model is being applied in the nuclear data calculations for intermediate and high energy nuclear reaction.

7. The nuclear photon scattering by structural materials is studied on the bases of the optical theorem and the dispersion relation associated with the absorption process. The particle–hole calculations are adopted, when the incident photon is absorbed by a nucleus, a pair of particle and hole is excited by successive (2p–2h) (3p–3h) ···, as the same as the picture of the exciton model.

With the above model the GUNF code was developed, with which the photon–nuclear data of ^{27}Al, ^{54}Fe, ^{209}Bi ($A = 27 \sim 209$, $Z = 13 \sim 83$) have been calculated. The calculated results are consistent with the existing experimental data.

II The Nuclear Reaction Model Program Making

8. SPEC is a program for calculating the neutron or charged particles (p, d,

t, ^{3}He, α) induced reactions of medium–heavy nuclei in the incident energy range up to 60 MeV including 6 emission processes. For those reaction channels contributed only by 1～5 emission processes the incident energy can go up to 100 MeV. This program is written in FORTRAN–77 on microscopic computer 486.

SPEC is constructed within the framework of optical model, master equation of the exciton model and the evaporation model. In the first and second particle emission processes, pre–equilibrium emission and evaporation are considered; in 3～6 particle emission processes, evaporation is considered only. The pre–equilibrium and direct reaction mechanisms of γ emission are also included in this program. The effect of recoil nucleus is considered for calculating spectra.

The following nuclear data can be calculated with the program SPEC: total emission cross sections and spectra of all emitted particles; the partial emission cross sections and spectra of all emitted particles for first to sixth particle emission processes and different pick–up configurations (l,m); the various yield cross sections; total and elastic scattering cross sections (only for neutron as projectile); total reaction cross sections; nonelastic scattering cross sections; radiative capture cross sections; (x,np), (x,nα), (x,2n), (x,3n), (x,4n), (x,5n), (x,6n) cross sections and so on.

9. DDCS is a program for calculating the neutron or proton induced reactions of medium–heavy nuclei in the incident energy range up to 50 MeV including 5 emission processes. For those reaction channels contributed only by 1～4 emission processes the incident energy can go up to 100 MeV. This program is written in FORTRAN–77 on microscopic computer 486. DDCS is constructed within the framework of optical model, generalized master equation of the exciton model.

The following nuclear data can be calculated with the program DDCS:
the double differential emission cross sections of emitted nucleon (n and p) and composite particle (α, d, t, ^{3}He) in laboratory or C. M. system, as well as total emission cross sections and spectra of all emitted particles; the partial emission cross sections and spectra of all emitted particles for first to sixth particle emission processes and pick–up configurations (1,m) and (2,m); the various yield cross sections; total and elastic scattering cross sections (only for neutron as projectile); total reaction cross sections; nonelastic scattering cross sections; radiative capture cross sections; (x,np), (x,nα), (x,2n), (x,3n), (x,4n), (x,5n) cross sections and so on.

DDCS has been already used to calculate nuclear data.

III The Evaluated Nuclear Parameter Library

10. Optical model parameter sub–library of Chinese Evaluated Nuclear Parameter Library (CENPL–OMP) consists of two parts. One is the global, regional optical model parameter which are for neutron, proton, deuteron, triton, ^{3}He and alpha particle respectively, the other is optical model parameter of nucleus–specific. So far about 70 sets of optimum optical model parameters which were used in calculations of complete neutron data in CENDL–1,2 have been collected in nucleus–specific optical model parameter part. The data file has been set up by means of dBASE. The most of collection and compilation of the optical model parameters have finished according to references list, which was retrieved by IAEA. The collection and compilation of optical model parameters used in ENDF / B–6 and the retrieve–management code for this sub–library is proceeding and have made some progresses.

11. The discrete level schemes and gamma–decay branching ratio data sub–library (DLS) is set up in order to store and retrieve these data conveniently. The format and content of DLS data file are defined. It includes the spins, parities, and half–lives of discrete levels, as well as the final energy levels, branching ratios and multipolarities for transition gamma–rays, and so on. The DLS data are mainly from the Evaluated Nuclear Structure Data File (ENSDF), which is evaluated and compiled by the International Nuclear Structure and Decay Data Network under the coordination of International Atomic Energy Agency. The transformation code have been written, which includes data format and data expression–mode transformation from ENSDF to DLS. The DLS format is suitable for computer reading and listing data table. All data are given by using the same format, and can straight be used as input data for model calculation code. Besides, the drawing code has been also written for the convenience of user's reading and retrieving data, the function of which can arbitrarily select energy scale and make any part of the whole level scheme enlarged.

12. The sub–library of atomic masses and characteristic constants for nuclear ground states (MCC), which constitutes one of Chinese Evaluated Nuclear Parameter Library (CENPL), contains two parts: (1) the data file; (2) the management–retrieval code system. The MCC data file is augmented, improved and perfected further. Data of 4800 nuclides have been contained in the new MCC file, and the half–life of the new nuclides ^{202}Pt, ^{208}Hg and ^{185}Hf as well as the

mass excesses of ^{199}Ir, which were produced and distinguished by Chinese scientists, have been compiled. The format of MCC data file has been adjusted reasonably, and a unity expression for the standard uncertainties of all physical quantities is adopted.

MCC management–retrieval code system has been finished basically. This system provides two retrieval ways. One of them is single nucleus retrieval, for which not only the data listed in MCC data file, such as mass excess, atomic mass, total binding energy, half–life or abundance as well as spin and parity of nuclear ground state, but also other data, for example, the separating energies of neutron n, proton p, deuteron, triton, ^{3}He, ^{4}He, 2n, 2p, and decay energies of beta+ and beta– decay. For natural isotopic composition, this code system can also retrieve the data mentioned above for all stable isotopes simultaneously.

The other is retrieval for a neutron reaction. The code system can calculate the reaction energies Q and threshold energies for all possible reaction channels including up to fourth reaction processes for a studied neutron reaction at first. User could choose the model computation code from four popular used fast neutron reaction model codes (i. e. MUP, FUP, UNF and code with the situation including gamma, n, p and ^{4}He emissions only) according to calculated threshold energies, and the mass excesses or atomic masses, spins and parities of nuclear ground states for all related residual nuclei with the chosen model code and abundance of the target nucleus.

IV The Nuclear Data Calculation

13. Based on the available experimental data, a set of neutron optical potential parameters for ^{56}Fe in energies of 4~100 MeV was obtained. The various calculated cross sections are in pretty agreement with the existed experimental data and the yield cross sections of the activation isotopes ^{51}Cr, ^{52}Mn, ^{54}Mn, and ^{56}Mn are predicted for n+^{56}Fe reaction in energy range up to 60 MeV. Considering $^{57, 58}$Fe are the neighboring nuclei of ^{56}Fe, the yield cross sections of the activation isotopes mentioned above for n+$^{57, 58}$Fe reactions were predicted with the same model parameters for n+^{56}Fe reaction in energy region up to 60 MeV. For n+^{54}Fe reaction, ^{54}Mn can be produced through (n,p) reaction, ^{52}Mn through (n.t), (n,nd), and (n,2np) reactions, and ^{51}Cr through (n,α), (n,2d), (n,pt), (n,n^{3}He), (n,npd), and (n,2n2p) reactions, respectively. Some experimental data can be found in lower energy region for producing ^{54}Mn, ^{52}Mn, and ^{51}Cr in n+^{54}Fe reaction. But there are no enough experimental data to obtain the optical potential parameters in the energy re-

gion up to 60 MeV. Therefore, the optical potential parameters obtained in $n+^{56}Fe$ reaction are also used for $n+^{54}Fe$ reaction. The yield cross sections of the activation isotopes ^{51}Cr, ^{52}Mn, and ^{54}Mn for $n+^{54}Fe$ reaction are calculated after adjusting the charged particle optical potential, the level density and exciton model parameters in the same energy region. The calculated cross sections for reactions $^{56}Fe(n,p)^{56}Mn$, $^{54}Fe(n,p)^{54}Mn$, and $^{54}Fe(n,\alpha)^{52}Mn$ in low energy region should be replaced by the evaluated data based on experimental data. Then the yield cross sections of the 4 activation isotopes for $n+^{Nat}Fe$ reaction can be obtained in the energy region up to 60 MeV through summation according to abundance.

14. A set of neutron optical potential parameters for ^{197}Au in energies of 0.5 ~ 80 MeV was obtained with available experimental data. In higher energy region the calculated total cross sections have good fitting with the experimental data and the calculated nonelastic scattering cross sections are closing to the measured values of ^{208}Pb; in lower energy region the calculated (n,2n), (n,3n), and (n,4n) cross sections also have good fitting with the experimental data. Therefore, the predicted neutron monitor reaction (n,2n), (n,3n), and (n,4n) cross sections in higher energy region are reasonable and reliable.

The Calculations of Photonuclear Data

Zhang Jingshang Zhuang Youxiang Yan Shiwei

(Chinese Nuclear Data Center, IAE)

Abstract

The photonuclear reaction data with the approximate energies up to 30 MeV have been calculated. The formulations are described. The photonuclear reactions include the scattering, absorption and particle production of photons induced on nuclei. For example, the photonuclear data of ^{27}Al, ^{54}Fe and ^{209}Bi were calculated and compared with experimental data.

Introduction

The photonuclear reaction data have been widely used in basic scientific researches on neutron binding energy, nuclear level and deformation, as well as nuclear reaction mechanism; also used in engineering and technology such as medicine, electronics, activation analysis, radiation damage and shielding etc.

There are no nuclear force and charge interaction between photon and nucleus, thus the photonuclear reaction is induced by electromagnetic interaction. It is quite evident that there is always a threshold energy in the photonuclear reaction.

In general, the gamma-ray sources are mainly from the following three categories:

(1) nuclear reaction such as $^{7}Li(p,\gamma)^{8}Be$, $^{19}F(p,\alpha\gamma)^{16}O$; (2) electron beam bremsstrahlung; (3) positron annihilation in flight. The monochromatic photons can be obtained from (1) and (3), and the photons with continuous energies come from the bremsstrahlung.

The giant resonance phenomenon appears in the excitation function of photonuclear reaction. The maximum values σ_{res} of reaction cross section are increased with mass number A of target nuclei, for example σ_{res} = 15.5 mb for $^{27}Al(\gamma,n)^{26}Al$ and 650 mb for $^{209}Bi(\gamma,n)^{208}Bi$; and the resonance energies E_{res} at the peaks are decreased with mass number A, for instance E_{res} = 21.3 MeV for ^{27}Al and 13.5 MeV for ^{209}Bi. They have been explained by the absorption model of collective dipole vibration; of course, the direct process also exists in the photonuclear reaction, especially in (γ,p) reaction.

The theoretical code GUNF has been established, the photonuclear data of ^{27}Al, ^{54}Fe and ^{209}Bi were calculated in ENDF / B-6 format, including files 1, 3, 4, and 6. The comparisons of theoretical results with experimental data are given in this paper.

1 Theoretical Formulations

The nuclear photon scattering by structural materials was studied. On the basis of the optical theorem and the dispersion relation, associated with the absorption process, the nuclear photon scattering process shows a higher order coherent phenomena[1], the total absorption and coherent scattering cross section with the incident photon energy E are expressed by same complex forward scattering amplitude $R(E,\theta=0)$. The total absorption cross section $\sigma_a(E)$ is given by:

$$\sigma_a(E) = 4\pi\lambda Im R(E,0) \qquad \lambda = \frac{hC}{E} \tag{1}$$

The coherent scattering cross section reads

$$\frac{d\sigma}{d\Omega}(E,\theta) = |R(E,\theta)|^2 \tag{2}$$

The dispersion relation gives the connection between the real and imaginary parts of the forward scattering amplitude

$$ReR(E,\theta) = \frac{E}{2\pi^2 hC} P\int \frac{dE' \sigma_a(E')}{E'^2 - E^2} + D \tag{3}$$

where $D = -\dfrac{Z^2 e^2}{AMC^2}$ is the energy independent Thomson scattering amplitude and P means the principal integration. If the photon energies are above 20 MeV, the electrical multipole mechanism should occur, then the retardation correction need to be taken into account. In terms of the long wave approximation[2, 3], the modified Thomson scattering amplitude is obtained by

$$D' = \frac{e^2}{MC^2}\left[\frac{NZ}{A} - Z\left[1 - \frac{1}{3}\left(\frac{E}{hC}\right)^2 \langle r^2 \rangle (1 - \cos\theta)\right]\right] \vec{\varepsilon}\,\vec{\varepsilon}' \tag{4}$$

where $\vec{\varepsilon}$ and $\vec{\varepsilon}'$ are the directions of incident and outgoing photons, respectively, $\langle r^2 \rangle$ is the a. s. r. of nucleus.

The photonuclear giant resonance may often be adequately represented by a Lorentz–shaped resonance line

$$R(E,\theta) = \frac{\Gamma\sigma_0}{4\pi hC} \frac{E^4(E_0^2 - E^2 - \Gamma^2) + i\Gamma E^3 E_0^2}{[(E_0^2 - E^2)^2 + \Gamma^2 E^2] E_0^2} \tag{5}$$

where σ_0, E_0 and Γ stand for the absorption cross section, resonance energy and its width, respectively. In this way, from Eqs. (1) and (3), the nuclear photon scattering cross section can be given by

$$\frac{d\sigma}{d\Omega}(E,\theta)=|\,R^{E_1}(E)+D+\frac{Z^2e^2}{MC^2}\kappa^2\frac{\langle r^2\rangle}{3}\,|^2\frac{(\,1+\cos^2\theta\,)}{2}$$

$$+\frac{1}{2}|\,R^{E_2}(E)\,|^2(\,1-3\cos^2\theta+4\cos^4\theta\,)$$

$$+[\,(\,ReR^{E_1}(E)+D+\frac{Z^2e^2}{MC^2}\kappa^2\frac{\langle r^2\rangle}{3}\,)ReR^{E_2}(E)$$

$$+ImR^{E_1}(E)ImR^{E_2}(E)\,]\,2\cos^3\theta$$

$$+[-\frac{Z^2e^2}{MC^2}\,\kappa^2\,\frac{\langle r^2\rangle}{6}\,]^2\,\frac{(\,1+\cos^2\theta\,)}{2}$$

$$+[\,(\,ReR^{E_1}(E)+D+\frac{Z^2e^2}{MC^2}\kappa^2\frac{\langle r^2\rangle}{3}\,)$$

$$(-\frac{Z^2e^2}{MC^2}\,)\,\kappa^2\frac{\langle r^2\rangle}{6}\,]\,2\cos\theta$$

$$+[-ReR^{E_2}(E)\frac{Z^2e^2}{MC^2}\kappa^2\frac{\langle r^2\rangle}{6}\,]\,(\,3\cos^2\theta-1\,) \qquad (6)$$

where $\kappa=\frac{E}{hC}=\frac{1}{\lambda}$ and the subscript E_1 and E_2 mean the electric $E1$ and $E2$ modes. For the deformed nuclei, the double Lorentz–shaped resonance for $E1$ and $E2$ modes was used in our calculations.

$$\sigma_a=\sum_{i=1}^{2}\sigma_i^{E_1}\frac{(\,\Gamma_i^{E_1}E\,)^2}{[\,(\,E^2-(\,E_i^{E_1}\,)^2\,)^2+(\,\Gamma_i^{E_1}E\,)^2\,]}$$

$$+\sigma^{E_2}\frac{(\,\Gamma^{E_2}E\,)^2}{[\,(\,E^2-(\,E^{E_2}\,)^2\,)^2+(\,\Gamma^{E_2}E\,)^2\,]} \qquad (7)$$

where $\sigma_i^{E_1}$, $\Gamma_i^{E_1}$, $E_i^{E_1}$ and σ^{E_1}, Γ^{E_1}, E^{E_1} stand for the Lorentz–shaped resonance parameters of dipole and quadrupole multipolarity, respectively.

For structural materials, the particle–hole calculations are adopted. When the incident photon is absorbed by a nucleus, a pair of particle and hole is excited by successive (2p–2h) (3p–3h) ···. The states can be excited as the same as the picture of the exciton model. The dominant mode for the absorption is through the quasideuteron mechanism if the photon energies are above the giant resonance. In this case the photon has the interaction with two–particle

cluster rather than with single particle but the preview study shows that this mechanism is important for photon energies in the range 30～140 MeV. So we do not consider this picture in our calculation.

For the particle–hole exciton, the angular momentum and parity conservations are taken into account. The discrete level effect is also included in the model calculation[4].

2 Theoretical Results and Comparisons with Experimental Data

2.1 Experimental Measurements

The excitation function of $^{27}Al(\gamma,n)^{26}Al$ reaction was measured by A. Veyssiere et al.[5], the incident gamma rays of 13.34～30.28 MeV came from positron annihilation in flight, the cross sections were obtained with the aid of direct registration of photoneutrons.

The measurements of $^{54}Fe(\gamma,n)^{53}Fe$ reaction excitation function were carried out by B. S. Ratner et al.[6] and S. S. Verbitskiy et al.[7], using bremsstrahlung sources of energy range 16～26.4 MeV and 16.6～26.4 MeV, respectively, and photoneutron detectors; and by W. E. Del Bianco et al.[8], using $^{3}H(p,\gamma)^{4}He$ reaction as gamma ray source at 20.48 MeV and activation method. S. S. Verbitskiy et al.[7] gave the relative measured values, which were normalized to the peak value of B. S. Ratner et al.[6]

The experiments of $^{209}Bi(\gamma,n)^{208}Bi$ reaction were accomplished by S. N. Belyaev et al.[9, 10] and L. M. Young et al.[11], using bremsstrahlung source of incident energies 7.595～12.348 MeV and 10.01～14.84 MeV, respectively, and photoneutron detectors; and $^{209}Bi(\gamma,abs)$ reaction by G. M. Gurevich et al.[12], using bremsstrahlung source at 8.45～30.25 MeV and the absorption method.

All the experimental data as mentioned above are available, and the corresponding measurements are in good agreement.

2.2 Comparisons between Calculated Values and Experimental Data

The comparisons of ^{27}Al, ^{54}Fe, $^{209}Bi(\gamma,n)$ and $^{209}Bi(\gamma,abs)$ reactions are shown in Figs. 1～4, respectively.

In general, the coincidences of theoretical results with experimental data are very good. However, due to the existence of intermediate structures in the cross section of $^{27}Al(\gamma,n)$ reaction, the theoretical calculation without this reaction mechanism can not describe these small structures.

3 Summary

By means of the theoretical code GUNF for photonuclear reaction, we have evaluated and calculated the photonuclear data of ^{27}Al, ^{54}Fe and ^{209}Bi ($A = 27 \sim 209$, $Z = 13 \sim 83$). the theoretical values are consistent with the existing experimental data. Therefore, these results are satisfactory for the users.

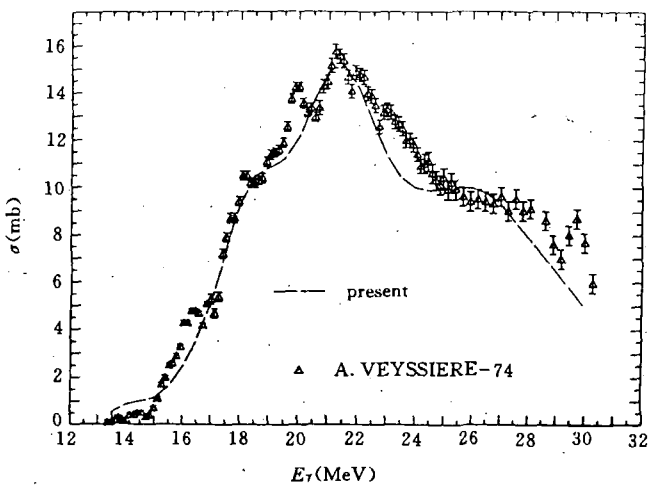

Fig. 1 $^{27}Al(\gamma,n)$ cross section

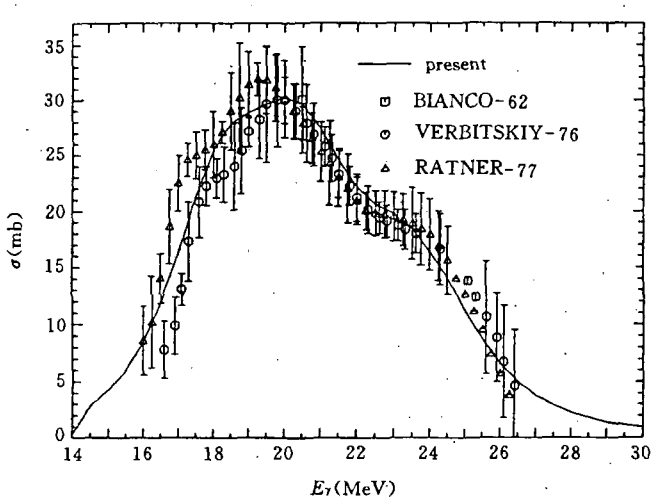

Fig. 2 $^{54}Fe(\gamma,n)$ cross section

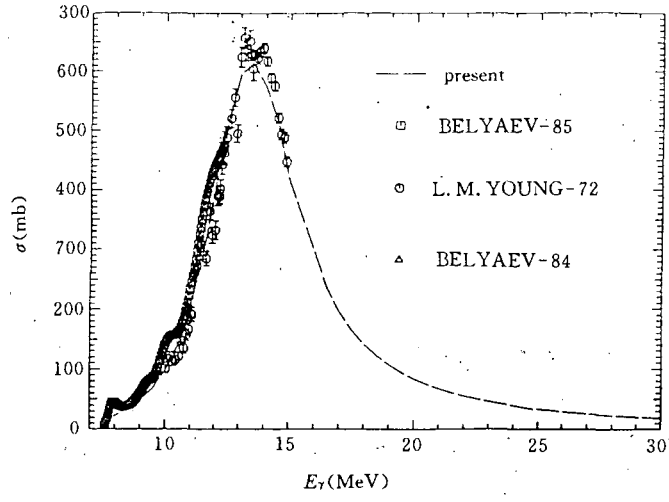

Fig. 3 ^{209}Bi(γ,n) cross section

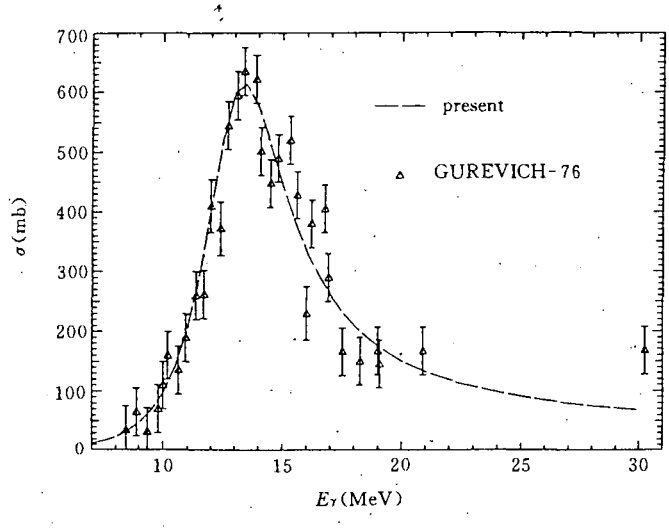

Fig. 4 ^{209}Bi(γ,abs) cross section

References

[1] Hayward. E.,"Photonuclear Reactions" NBS MONOGRAPH 118, Aug., 1970

[2] R. Silbar et al., Nucl. Phys., A109, 146(1968)

[3] T. E. Ericson et al., Nucl. Phys., B57, 604(1973)

[4] Zhang Jingshang, Nucl. Sci. Eng., 114, 55(1993)

[5] A. Veyssiere et al., Nucl. Phys., A227, 513(1974)

[6] B. S. Ratner et al., Nucl. Phys., A285, 71(1977)
[7] S. S. Verbitskiy et al., ZEP 23, 538(1976)
[8] W. E. Del Bianco et al., Phys. Rev., 126, 709(1962)
[9] S. N. Belyaev et al., IZV 48, 1940(1984)
[10] S. N. Belyaev et al., YF 42, 1050(1985)
[11] L. M. Young et al., T. Young 72, EXFOR L0059
[12] G. M. Gurevich et al., ZEP 23., 411(1976)

Program SPEC for Neutron or Charged Particles Induced Reactions up to Tens of MeV

Shen Qingbiao Zhang Jingshang

(Chinese Nuclear Data Center, IAE)

SPEC is a program for calculating the neutron or charged particles (p, d, t, ^{3}He, α) induced reactions on medium–heavy nuclei in the incident energy range up to 60 MeV including 6 emission processes. For those reaction channels contributed only by 1~ 5 emission processes the incident energy can go up to 100 MeV. This program is written in FORTRAN–77 on microscopic computer 486.

SPEC is constructed within the framework of optical model, master equation of the exciton model[1], and the evaporation model. For the first and second particle emission processes, the preequilibrium emission and evaporation are considered, but for 3~ 6 particle emission processes, only the evaporation is considered. The preequilibrium and direct reaction mechanisms of γ emission[2] are also included in this program. The effect of recoil nucleus is considered for calculating spectra. Program SPEC includes the first to the sixth particle emission processes[3].

The life time master equation in exciton model reads[1]

$$-\delta_{n,n_0} = \lambda_-(n+2,E)\ \tau\ (n+2,E) + \lambda_+(n-2,E)\ \tau\ (n-2,E) - [\lambda_+(n,E) + \lambda_-(n,E) + W_t(n,E)\ ]\ \tau\ (n,E) \quad (1)$$

where E is the excitation energy. λ_+ and λ_- are the intranuclear transition rates. For composite particle emission, the pick–up mechanism of cluster formation[4~7] is used in the first and second particle emission processes. The cluster b is constituted according to the arrangement of particles above and below the Fermi surface [l,m]. By means of the detailed balance principle the emission rate of l particles above Fermi surface can be expressed as

$$W_b^l(p,h,E,\varepsilon_b) = \frac{2I_b+1}{\pi^2\hbar^3}\mu_b\varepsilon_b\sigma_b(\varepsilon_b)F_{l,m}(\varepsilon_b)$$
$$Q_{l,m}^b(p,h)\frac{\omega(p-l,h,E-\varepsilon_b-B_b)}{\omega(p,h,E)} \tag{2}$$

where I_b is the spin of the emitted particle b, ω is the exciton state density, $\sigma_b(\varepsilon_b)$ is the inverse cross section of the emitted particle b with outgoing energy ε_b. B_b is the binding energy of particle b in the system. $Q_{l,m}^b(p,h)$ is combination factor[8]. $F_{l,m}(\varepsilon_b)$ is the pick–up factor of the emitted particle[4~7].

The emission rate for a photon with energy ε_γ from a nucleus in the exciton state n is taken as[2]:

$$W_\gamma(n,\varepsilon_b) = \frac{\varepsilon_\gamma^2\sigma_a^\gamma(\varepsilon_\gamma)}{\pi^2\hbar^3C^2\omega_n(E)}\left\{\frac{g^2\varepsilon_\gamma\omega_{n-2}(E-\varepsilon_\gamma)}{g(n-2)+g^2\varepsilon_\gamma}+\frac{gn\omega_n(E-\varepsilon_\gamma)}{gn+g^2\varepsilon_\gamma}\right\} \tag{3}$$

where g is single particle level density. $\sigma_a^\gamma(\varepsilon_\gamma)$ is giant resonance cross section:

$$\sigma_a^\gamma(\varepsilon_\gamma) = \sum_{i=1}^{2}\frac{(\varepsilon_\gamma\Gamma_i)^2\sigma_i^\gamma}{(\varepsilon_\gamma\Gamma_i)^2+(\varepsilon_\gamma^2-E_i^2)^2} \tag{4}$$

where Γ_i, E_i, σ_i^γ are two peak giant resonance parameters.

For the first emission particle b, the spectrum is given by

$$\frac{d\sigma_b}{d\varepsilon_b} = \sigma_a\sum_{n,\lambda}\tau(p,h,E)\sum_l W_b^l(p,h,E,\varepsilon_b) \tag{5}$$

where σ_a is the absorption cross section of the incident particle.

The direct γ emission cross section reads

$$\sigma_{\gamma}^{d} = \sigma_{a} \frac{Y}{Y + \lambda_{+}(1)} \tag{6}$$

where

$$\lambda_{+}(1) = \frac{\pi K}{2} \left(\frac{g}{A} \right)^{3} E \tag{7}$$

$$Y = \frac{1}{\pi^{2} h^{3} C^{2}} \int_{0}^{E} \varepsilon_{\gamma}^{2} \sigma_{a}^{\gamma}(\varepsilon_{\gamma}) \frac{1}{1 + g\varepsilon_{\gamma}} d\varepsilon_{\gamma} \tag{8}$$

where K is exciton model constant. A is mass number of the composite system.

The Gilbert–Cameron level density formula[9] was applied in the program SPEC. The inverse cross sections of the emitted particles used in statistical theory are calculated from the optical model. The partial widths for γ–ray emission are calculated based on the giant dipole resonance model with two resonance peaks in both the evaporation model and exciton model.

In the optical model calculation, we adopt the Becchetti and Greenlees'[10] phenomenological optical potential, whose parameters are obtained by a program for automatically searching. We use Neumanove methods to solve the radial equation in optical model. Coulomb wave functions used in optical model are calculated by the continued fraction method[11].

SPEC does not calculate the direct inelastic scattering and compound nucleus elastic scattering cross sections, but the calculated direct inelastic scattering cross sections by the collective excitation distorted–wave Born approximation [12] and compound nucleus elastic scattering results by Hauser–Feshbach model can be added by the input data of the program SPEC.

The following nuclear data can be calculated by using the program SPEC: total emission cross sections and spectra of all emitted particles; the partial emission cross sections and spectra of all emitted particles from the first to sixth particle emission processes and different pick–up configurations (l,m); the various yield cross sections; total and elastic scattering cross sections (only for neutron as projectile); total reaction cross section; nonelastic scattering cross sections; radiative capture cross section; (x,np), (x,nα), (x,2n), (x,3n), (x,4n), (x,5n), (x,6n) cross sections and so on.

SPEC has been used to calculate reactions of n+^{197}Au in energy region 0.5 ~ 80 MeV and n+^{56}Fe in energy region 2~ 60 MeV. Pretty good results in agreement with the experimental data were obtained. The application practices show that SPEC is a useful and convenient program for users.

References

[1] M. Blann, Ann. Rev. Nucl. Sci., 25, 123(1975)

[2] J. M. Akkermans et al., Phys. Let., 157B, 95(1985)

[3] Shen Qingbiao et al., Commun. of Nucl. Data Prog., 10, 53(1993)

[4] A. Iwamoto et al., Phys. Rev., C26, 1821(1982)

[5] K. Sato et al., Phys. Rev., C28,1527(1983)

[6] Zhang Jingshang et al., Commun. in Theor. Phys., (Beijing, China), 10, 33(1988)

[7] Zhang Jingshang et al., Z. Phys., A344, 251(1992)

[8] Zhang Jingshang et al., INDC(CPR)-014 / L

[9] A. Gilbert et al., Can. J. Phys., 43, 1446(1965)

[10] F. D. Becchetti et al., Phys. Rev., 182, 1190(1969). C. M. Perey et al., Atomic Data and Nuclear Data Tables, 17, 3(1976)

[11] A. R. Barnett et al., Computer Phys. Commun., 8, 377(1974)

[12] P. D. Kunz, "Distorted Wave Code DWUCK4", University of Colorado, USA

The Calculations of $^{56}Fe(n,x)^{51}Cr,^{52,54,56}Mn$ Reactions Cross Sections up to 60 MeV

Shen Qingbiao Yu Baosheng Cai Dunjiu

(Chinese Nuclear Data Center, IAE)

Abstract

A set of neutron optical potential parameters for ^{56}Fe in energies of 4~100 MeV was obtained by fitting available experimental data. The yield cross sections of the activation isotopes ^{51}Cr, ^{52}Mn, ^{54}Mn, and ^{56}Mn in n+^{56}Fe reaction are calculated and predicted in energy range up to 60 MeV.

Introduction

The activation isotopes ^{51}Cr (half life is 27.7 d),^{52}Mn (half life is 5.59 d), ^{54}Mn (half life is 312 d) , and ^{56}Mn (half life is 2.58 h) can be produced in

n+^{56}Fe reaction in which ^{56}Mn is produced through (n,p) reaction, ^{54}Mn is through (n,t), (n,nd), and (n,2np) reactions, ^{52}Mn and ^{51}Cr are through more reaction channels especially in higher energy region. For n+^{56}Fe reaction many experimental data are available to obtain the model parameters. If the calculated results are in pretty agreement with the existing experimental data, the yield cross sections of the above activation isotopes can be predicted.

In Sec.1, the theories and parameters used in the calculation are described. The calculated results and analyses are given in Sec. 2. Finally, a summary is given in Sec. 3.

1 Theories and Parameters

The calculation was made with the program SPEC[1] including the first to the sixth particle emission processes. In this program, the optical model, evaporation model, and the master equation of exciton model[2] are included. The preequilibrium and direct reaction mechanisms of γ emission[3] are also included. The direct inelastic scattering cross sections were obtained by the collective excitation distorted-wave Born approximation[4]. The compound-nucleus elastic scattering contributions were calculated by Hauser-Feshbach model.

For composite particle emissions, the pick-up mechanism of cluster formation[5~7] was included in the first and second particle emission processes.

Firstly, based on various experimental data of ^{56}Fe from EXFOR data a set of optimum neutron optical potential parameters in energy region 4~ 100 MeV was obtained as follows:

$$V = 54.5279 - 0.45651E + 0.0019002E^2 - 24.0(N-Z)/A \quad (1)$$

$$W_s = \max\ \{\ 0,\ 11.36608 - 0.23766E - 12.0(N-Z)/A\ \} \quad (2)$$

$$W_v = \max\ \{\ 0,\ -0.96252 + 0.15836E - 0.000195E^2\ \} \quad (3)$$

$$U_{so} = 6.2 \quad (4)$$

$$r_r = 1.1956,\quad r_s = 1.33457,\quad r_v = 1.41732,\quad r_{so} = 1.1956, \quad (5)$$

$$a_r = 0.6312,\quad a_s = 0.52102,\quad a_v = 0.36,\quad a_{so} = 0.6312, \quad (6)$$

This set of optical potential parameters is used in the calculation of n+^{56}Fe reaction.

The Gilbert-Cameron level density formula[8] is applied in the calculation, but some parameters are changed and read as

$$U_x = 2.1 + 395 / A \tag{7}$$

$$a = (0.0032 \times S + 0.142) A \tag{8}$$

where S is shell correction factor.

In exciton model, the K value is taken as 1800 MeV[3]. Some charged particle optical potential parameters are also adjusted.

2 Calculated Results and Analyses

Fig. 1 shows the comparison of neutron total cross sections between the calculated values and the experimental data in the energy region 4~ 100 MeV. The theoretical values are in good agreement with the experimental data. The calculated elastic scattering cross sections and angular distributions agree with the experimental data pretty well. The calculated neutron nonelastic cross sections are generally in agreement with the experimental data. Based on above fitting process, a set of neutron optical potential parameters in the energy region 4 ~ 100 MeV for n+^{56}Fe reaction are determined.

The calculated inelastic scattering cross sections including the direct reaction contributions calculated by DWBA method agree with the experimental data pretty well. The calculated (n,2n) cross sections of ^{56}Fe are basically in agreement with the experiments. Fig. 2 shows that the calculated (n,p) cross sections of ^{56}Fe are lower than experimental data below 10 MeV. In order to obtain a better yield cross sections of ^{56}Mn in n+^{56}Fe reaction, the evaluated (n,p) cross sections data should be adopted in lower energy region instead of the calculated ones. The calculated (n,α) cross sections are also lower than experimental data below 10 MeV. The main reason for above disagreement is that the discrete levels are not taken into account in the calculation. The calculated (n,d) cross section curve just passes through the only one existent experimental error bar. Fig. 3 shows that the calculated (n,t) cross section curve approaches the two existent experimental error bars. The activation isotope ^{54}Mn can be produced through this reaction in low energy region. The calculated (n,p–em) and (n,α–em) cross sections basically agree with the experimental data.

Fig. 4 shows the calculated ^{51}Cr, ^{52}Mn, ^{54}Mn, and ^{56}Mn yield cross sections for n+^{56}Fe reaction in energy range up to 60 MeV. Because the calculated results for many channels of n+^{56}Fe reaction are quite in agreement with the existing experimental data, the predicted yield cross sections of the activation isotopes are reasonable, except the ^{56}Mn yield cross sections in lower energy region should use the evaluated data.

3 Summary

Based on the available experimental data, a set of neutron optical potential parameters for ^{56}Fe in energies of 4~ 100 MeV was obtained. Various calculated cross sections are in pretty agreement with the existing experimental data and the yield cross sections of the activation isotopes ^{51}Cr, ^{52}Mn, ^{54}Mn, and ^{56}Mn are predicted in energy range up to 60 MeV. The calculated cross sections for reactions $^{56}Fe(n,p)^{56}Mn$ in low energy region should use the evaluated data. The final yield cross sections of the 4 activation isotopes for $n+^{56}Fe$ reaction can be obtained in the energy region up to 60 MeV.

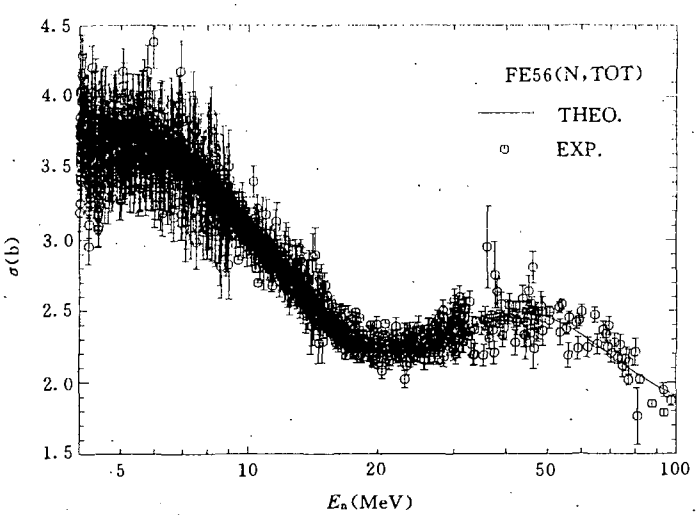

Fig. 1 Comparison of neutron total cross sections of ^{56}Fe between the calculated values and the experimental data

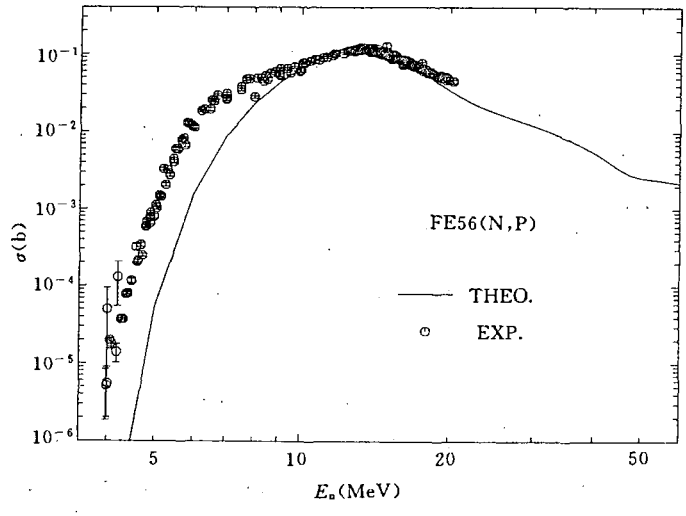

Fig. 2 Comparison of (n,p) cross sections of ^{56}Fe between the calculated values and the experimental data

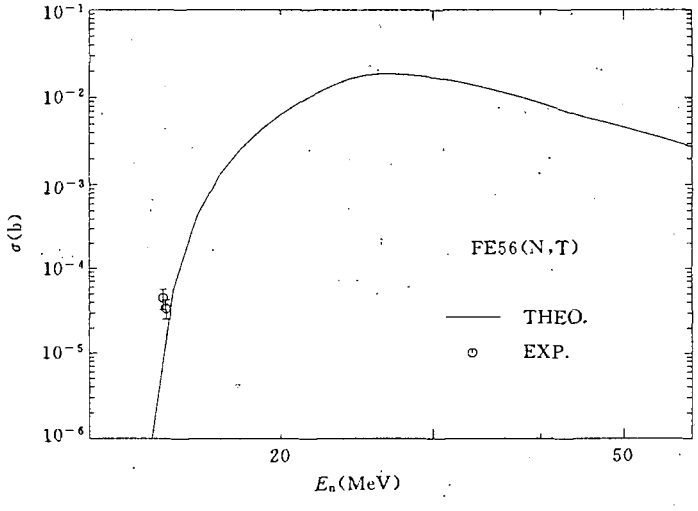

Fig. 3 The same as Fig.2 but for (n,t) cross sections

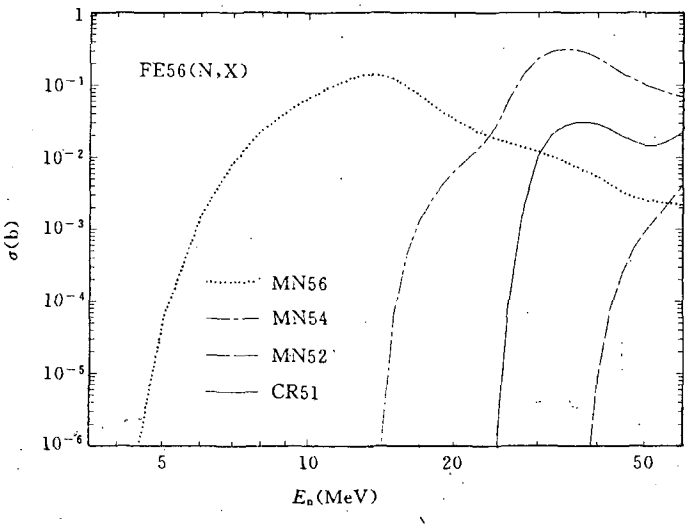

Fig. 4 The calculated yield cross sections for n+^{56}Fe reaction

References

[1] Shen Qingbiao et al., Commun. of Nucl. Data Progress, 11, 29(1994)

[2] M. Blann, Ann. Rev. Nucl. Sci., 25, 123(1975)

[3] J. M. Akkermans et al., Phys. Let., 157B, 95(1985)

[4] P. D. Kunz, "Distorted Wave Code DWUCK4", University of Colorado

[5] A. Iwamoto et al., Phys. Rev., C26, 1821(1982)

[6] K. Sato et al., Phys. Rev., C28, 1527(1983)

[7] Zhang Jingshang et al., Commun. in Theor. Phys., (Beijing, China), 10, 33(1988)

[8] A. Gilbert et al., Can. J. Phys., 43, 1446(1965)

An Open Problem on Photon Production Calculation

Zhang Jingshang

(Chinese Nuclear Data Center, IAE)

The Hauser–Feshbach model and the unified Hauser–Feshbach and exciton model[1] conserve angular momentum and parity, then the angular momentum and the parity distribution at each excitation energies of the residual nuclei for every reaction channels can be obtained by the model calculation. The photon production calculation will be performed by the gamma cascade decay processes. So far the level structure of a residual nucleus is usually described by two parts, the discrete levels at low excitation states labeled by their spins and parities obtained from the experiment data, the continuum region at high excitation states described by level density formula. The level density formula has the common form which reads

$$\rho(E,J,\pi) = \rho(E)R(J)P(\pi) \tag{1}$$

where E is the excitation energy, $\rho(E)$ stands for the J π–independent level density, the parity factor $P(\pi) = 0.5$ is often used. Based on the Fermi gas model the spin distribution factor $R(J)$ has the form

$$R(J) = \frac{2J+1}{2\sigma^2} \exp\left[-\frac{\left(J+\frac{1}{2} \right)^2}{2\sigma^2} \right] \tag{2}$$

where σ is the spin cut–off factor.

The transition probabilities of the gamma decay are the branching ratios between discrete levels. For continuum part, it has to be divided into small bins, like the discrete levels but have the angular momentum and the parity distribution. The transition probabilities must be calculated between the bins or from a bin to the discrete levels mainly with the E_1, M_1 and E_2 modes by means of the giant resonance model. For the gamma cascade decay process the routine tool can be used if all of the transition rates and the initial angular momentum and the parity distribution are available.

Performing the photon production calculation in this way, a problem was

discovered. The energy conservation could not be held. The reason is that when the cascade processes performed to the lowest bin located at the boundary between the continuum and the discrete parts, the angular momentum distribution in this bin can be extended in a wide region, for instance $J \approx 20$. In this case the high spin parts in the lowest bin could not decay into the discrete levels with the E_1, M_1 and E_2 modes which are restricted by the angular momentum conservation $\Delta J = 1, 2$. Therefore the lowest bin becomes into a spurious isomerical level. As an example, the percentages of the forbidden decaying from the lowest bin to the discrete levels in neutron induced ^{56}Fe reactions at $E_n = 14$ and 18 MeV are shown in Table 1. The results indicate that the percentages increase with incident energy increasing, and strongly dependent on the level structure of the residual nuclei.

Table 1 Percentage of the lowest bin forbidden decaying in reactions n+^{56}Fe for $E_n = 14, 18$ MeV

channel	(n,g)	(n,n′)	(n,p)	(n,a)	(n,d)	(n,t)	(n,2n)	(n,np)
14 MeV	57.8	15.2	64.3	24.0	22.1			
18 MeV	69.5	22.7	87.4	56.4	70.6	12.9	48.7	74.4

It is impossible to expect that the discrete level sheets can be given even for high excitation energy region. On the other hand, we do not have the formula which is available to calculate the transition rates for large angular momentum transfer. Now we have this problem opened to the present photon production calculations.

References

[1] Zhang Jingshang, Nuc. Sci. Eng., 114, 55(1993)

Program DDCS for Nucleon and Composite Particle DDX of Nucleon Induced Reactions up to Tens of MeV

Shen Qingbiao

(Chinese Nuclear Data Center, IAE)

DDCS is a program for calculating the neutron or proton induced reactions of medium–heavy nuclei in the incident energy range up to 50 MeV including 5 emission processes. For those reaction channels contributed only by 1 ~4 emission processes the incident energy can go up to 100 MeV. This program is written in FORTRAN–77 on microscopic computer 486.

DDCS is constructed within the framework of optical model, generalized master equation of the exciton model[1~6], and the evaporation model. In the first and second particle emission processes, we consider preequilibrium emission and evaporation; in 3~ 5 particle emission processes, we only consider evaporation. The preequilibrium and direct reaction mechanisms of γ emission[7] are also included in this program. The effect of recoil nucleus is considered in this program.

Based on the anisotropic free N–N scattering, we get the energy–angle distributions of N–N collision in nuclear matter as follows:

$$A=\frac{\mathrm{d}^2\sigma_0}{\mathrm{d}E_{L'_1}\mathrm{d}\Omega_{L'_1}}=\frac{3\sigma_{el}}{8\pi E_f}\sqrt{\frac{QE_{L'_1}}{E_fE_{L_1}}}\left\{g_0\frac{E_{L_1}-E_{L'_1}}{Q}-g_1\ln\frac{F_2(Q)}{F_1(Q)}\right.$$
$$+g_2\frac{Q^3(E_{L_1}-E_{L'_1})}{F_1(Q)F_2(Q)}-g_3\frac{Q^5\,[F_1(Q)+F_2(Q)]\,(E_{L_1}-E_{L'_1})}{(F_1(Q)F_2(Q))^2}$$
$$\left.+g_4\frac{Q^7\,[F_1^2(Q)+F_1(Q)F_2(Q)+F_2^2(Q)]\,(E_{L_1}-E_{L'_1})}{(F_1(Q)F_2(Q))^3}\right\}; \qquad (1)$$

$$B=\frac{\mathrm{d}^2\sigma_0}{\mathrm{d}E_{L'_1}\mathrm{d}\Omega_{L'_1}}=\frac{3\sigma_{el}}{8\pi E_f}\sqrt{\frac{QE_{L'_1}}{E_fE_{L_1}}}\left\{g_0\frac{D(Q)}{Q^2}-g_1\ln\frac{F_2(Q)}{F_3(Q)}\right.$$

$$+g_2\frac{Q^2D(Q)}{F_3(Q)F_2(Q)} - g_3\frac{Q^4[F_3(Q)+F_2(Q)]D(Q)}{(F_3(Q)F_2(Q))^2}$$

$$+g_4\frac{Q^6[F_3^2(Q)+F_3(Q)F_2(Q)+F_2^2(Q)]D(Q)}{(F_3(Q)F_2(Q))^3}\Big\}, \tag{2}$$

where

$$\begin{aligned} g_0 &= 1+3f_1+5f_2+7f_3+9f_4, \\ g_1 &= 6(f_1+5f_2+14f_3+30f_4), \\ g_2 &= 120(f_2+7f_3+27f_4), \\ g_3 &= 560(f_3+9f_4), \\ g_4 &= 3360f_4. \end{aligned} \tag{3}$$

$$\begin{aligned} F_1(Q) &= Q^2+2(E_f+E_{L'_1})Q-(E_{L_1}-E_{L'_1})^2, \\ F_2(Q) &= Q^2+2(E_f+E_{L_1})Q-(E_{L_1}-E_{L'_1})^2, \\ F_3(Q) &= \frac{3}{2}Q^2+(E_{L_1}+E_{L'_1})Q-\frac{1}{2}(E_{L_1}-E_{L'_1})^2. \end{aligned} \tag{4}$$

$$D(Q) = E_{L_1}E_{L'_1}\sin^2\Theta_{L'_1}-(E_{L'_1}-E_f)Q \tag{5}$$

$$Q = E_{L_1}+E_{L'_1}-2\sqrt{E_{L_1}E_{L'_1}}\cos\Theta_{L'_1}. \tag{6}$$

where the Legendre coefficients f_l can be found in Ref. [8]. The A– and B–areas are the allowed collision parts in the angle–energy plane in nuclear matter. The boundary values are given by:

$$\left.\begin{matrix}\alpha_1\\ \beta_1\end{matrix}\right\} = \frac{1}{\sqrt{E_{L_1}E_{L'_1}}}\left[E_{L_1}-E_f\overline{+}\sqrt{E_f(E_f-E_{L_1}+E_{L'_1})}\right]$$

$$\left.\begin{matrix}\alpha_2\\ \beta_2\end{matrix}\right\} = \frac{1}{\sqrt{E_{L_1}E_{L'_1}}}\left[E_{L'_1}-E_f\overline{+}\sqrt{E_f(E_f+E_{L_1}-E_{L'_1})}\right] \tag{7}$$

If f_1, f_2, f_3, and f_4 are taken to be equal to zero, that is just the free N–N scattering in the C. M. system, which is assumed to be isotropic, and the expressions (1) and (2) reduce to the Kikuchi–Kawai formula[2, 3].

For composite particle emission in the leading particle model [2], the pick–up mechanism needs to be taken into account[9~12]. If the emitted leading

particle picks up some nucleons in the composite system to form a cluster, then the composite particle emission processes happen. We denote the momentum distribution of the composite system at the exciton state n as $D_n(p)$. According to the momentum conservation, the outgoing momentum of the composite particle is the vector summation over the momentum of the nucleons in the cluster. In this model the leading particle must be one of the nucleons of the emitted composite particle. To be consistent with the previous model, when integrating over the angle, one gets the spectra of the outgoing particle. For the composite particle b with the emitted energy ε_b and outgoing direction Ω_b, the normalized angular factor of exciton state n for semi–classical multi–step compound processes is introduced by[13~15]

$$A_\lambda(n,\Omega_b,\varepsilon_b)=\frac{1}{N_\lambda}\int d\mathbf{p}_1\cdots d\mathbf{p}_{A_b}\,\delta(\mathbf{p}_b-\sum_{i=1}^{A_b}\mathbf{p}_i)\prod_{j=\lambda+1}^{A_b}D_n(\mathbf{p}_j)\;\tau\;(n\Omega_1), \tag{8}$$

where

$$|\mathbf{p}_i|>p_f,\quad \text{if } i\leqslant\lambda;\qquad |\mathbf{p}_i|<p_f,\quad \text{if } i>\lambda, \tag{9}$$

where $\lambda=1$, 2 represent (1,m) and (2,m) pick–up configuration, respectively. $\tau(n\Omega_1)$ is the lifetime of the leading particle in direction Ω_1. The δ function implies the momentum conservation. p_f is the Fermi momentum, p_b is the momentum of the outgoing composite particle b with the mass number A_b. N_λ is the normalization factor which can be obtained with the following normalization condition

$$\int A_\lambda(n,\Omega_b,\varepsilon_b)\;d\Omega_b=1. \tag{10}$$

For multi–step compound processes, the lifetime of the leading particle is independent of the energy. The Fermi gas model is employed to give the momentum distribution of the nucleons below the Fermi surface

$$D_n(\mathbf{p})=\begin{cases}\dfrac{3}{4\pi p_f^3} & \text{for}\quad p\leqslant p_f\\ 0 & \text{for}\quad p>p_f\end{cases}. \tag{11}$$

Thus the integration of (8) can be carried out analytically. The explicit expression of the angular factor of the emitted composite particle can be obtained

in the partial wave expansion form as

$$A_\lambda(n,\Omega_b,\varepsilon_b)=\frac{1}{4\pi}\sum_l\frac{\zeta_{l,\lambda}(n)}{\zeta_{0,\lambda}(n)}R^b_{l,\lambda}(\varepsilon_b)P_l(\cos\theta_b), \tag{12}$$

where

$$R^b_{l,\lambda}(\varepsilon_b)=\frac{G^b_{l,\lambda}(\varepsilon_b)}{G^b_{0,\lambda}(\varepsilon_b)}, \tag{13}$$

For (1,m) pick–up configuration one has[13~15]

$$G^b_{l,1}(\varepsilon_b)=\frac{1}{x_b}\int_{\max\{1,x_b-(A_b-1)\}}^{\sqrt{1+E/\varepsilon_f}}x_1\,dx_1 \int_{x_b-x_1}^{A_b-1}S_b(Y)P_l\left(\frac{x_b^2+x_1^2-Y^2}{2x_bx_1}\right)dY, \tag{14}$$

with

$$\begin{aligned}&S_d(Y)=Y,\\ &S_{t(\text{or }^3\text{He})}(Y)=Y(1-0.5Y)^2(4+Y),\\ &S_\alpha(Y)=(3-Y)^4[210-126(3-Y)+21(3-Y)^2-(3-Y)^3].\end{aligned} \tag{15}$$

E is excitation energy. For (2,m) pick–up configuration the following formulas are obtained

$$G^b_{l,2}(\varepsilon_b)=\frac{1}{x_b}\int_1^{\sqrt{1+E/\varepsilon_f}}\Theta(1-\gamma)x_1\,dx_1 \int_{\max(1,x_b-x_1)}^{\min(A_b-2+Z,X_b+x_1)}Q_b(Y)P_l\left(\frac{x_b^2+x_1^2-Y^2}{2x_bx_1}\right)dY, \tag{16}$$

with

$$\gamma=\frac{x_b^2+x_1^2-(A_b-2+Z)^2}{2x_bx_1}, \tag{17}$$

$$Z=\sqrt{2+E/\varepsilon_f-x_1^2}\,. \tag{18}$$

and

$$Q_d(Y)=Y, \tag{19}$$

$$\begin{aligned}Q_{t(\text{ or }^3\text{He})}(Y)&=\Theta(Y-2)\{\Theta(Z_1-Y)I_1+\Theta(Y-Z_1)(I_2+I_7)\}+\\&\Theta(2-Y)\{\Theta(Z_1-Y)(I_5+I_3)+\Theta(Y-Z_1)[\Theta(Z-\sqrt{2})(I_5+I_4+I_7)\\&+\Theta(\sqrt{2}-Z)((\Theta(Y-Z_2)+\Theta(Z_3-Y))(I_5+I_4+I_7)\\&+(1-\Theta(Y-Z_2)-\Theta(Z_3-Y))(I_6+I_9+I_8))]\},\end{aligned} \tag{20}$$

$$\begin{aligned}Q_\alpha(Y)&=\Theta(Z+1-2Y)\{\Theta(Y-Z+2)(J_1+J_4+J_{10})\\&+\Theta(Z-2-Y)[\Theta(3-Y)(J_1+J_5)+\Theta(Y-3)J_3]\}\\&+\Theta(2Y-Z-1)\Theta(Z-Y)\{\Theta(3-Y)(J_2+J_6+J_{11})\\&+\Theta(Y-3)[\Theta(Y-Z+2)(J_2+J_8)+\Theta(Z-2-Y)J_3]\}\\&+\Theta(Y-Z)\{\Theta(3-Y)(J_7+J_{11})+\Theta(Y-3)J_9\},\end{aligned} \tag{21}$$

where

$$Z_1=Z-1,\ Z_2=Z+\sqrt{2-Z^2},\ Z_3=Z-\sqrt{2-Z^2}\,. \tag{22}$$

$$x_b^2=A_b^2+\frac{A_b}{\varepsilon_f}(\varepsilon_b+B_b)-\frac{3}{4}A_b(A_b-1)\frac{\hbar\omega_b}{\varepsilon_f}, \tag{23}$$

B_b is binding energy. I_j in (20) and J_j in (21) can be found in Ref. [16]. The cluster harmonic oscillator parameter $\hbar\omega_b$ are taken as 8.1, 14.4, 11.7, 18.2 for d, t, ^{3}He, α, respectively. And the step function is defined as

$$\Theta(x)=\begin{cases}1 & \text{if}\quad x\geqslant 1\\ 0 & \text{if}\quad x<0\end{cases} \tag{24}$$

In the extended generalized master equation[5, 6] of semi-classical multi-step direct processes, for the composite particle b with the emitted energy ε_b and outgoing direction Ω_b, the normalized angular factor of exciton state n is introduced by

$$A_\lambda(n,\Omega_b,\varepsilon_b)=\frac{1}{N_\lambda}\int d\mathbf{p}_1\cdots d\mathbf{p}_{A_b}\,\delta(\mathbf{p}_b-\sum_{i=1}^{A_b}\mathbf{p}_i)$$

$$\prod_{j=\lambda+1}^{A_b} D_n(\mathbf{p}_j)\ \tau\ (n\Omega_1\varepsilon_1), \tag{25}$$

The explicit expression of the angular factor of the emitted particle b can be obtained as follows

$$A_\lambda(n,\Omega_b,\varepsilon_b)=\frac{1}{4\pi}\sum_l \frac{\xi_{l,\lambda}(n\varepsilon_b)}{\xi_{0,\lambda}(n\varepsilon_b)} P_l(\cos\theta_b), \tag{26}$$

For (1,m) pick–up configuration one has

$$\xi^b_{l,1}(n\varepsilon_b)=\frac{1}{x_b}\int_{\max\{1,x_b-(A_b-1)\}}^{\sqrt{1+E/\varepsilon_f}} x_1\zeta(n,\varepsilon_f x_1^2)\,dx_1$$
$$\int_{x_b-x_1}^{A_b-1} S_b(Y)P_l\left(\frac{x_b^2+x_1^2-Y^2}{2x_bx_1}\right)dY. \tag{27}$$

For (2,m) pick–up configuration one has

$$\xi^b_{l,2}(n\varepsilon_b)=\frac{1}{x_b}\int_1^{\sqrt{1+E/\varepsilon_f}} \Theta(1-\gamma)x_1\zeta(n,\varepsilon_f x_1^2)\,dx_1$$
$$\int_{\max(1,x_b-x_1)}^{\min(A_b-2+Z,x_b+x_1)} Q_b(Y)P_l\left(\frac{x_b^2+x_1^2-Y^2}{2x_bx_1}\right)dY, \tag{28}$$

In order to avoid the appearance of negative calculated values of double differential cross sections at some backward angle, for the first step ($n=n_0$) direct process, the following expressions of the angular factor of the emitted particle b are used

$$A_\lambda(n_0,\Omega_b,\varepsilon_b)=\frac{D^b_\lambda(\Omega_b,\varepsilon_b)}{\int D^b_\lambda(\Omega'_b,\varepsilon_b)\,d\Omega'} \tag{29}$$

For (1,m) pick–up configuration one has

$$D_1^b(\Omega_b,\varepsilon_b)=\frac{1}{x_b}\int_{\max\{1,x_b-(A_b-1)\}}^{\sqrt{1+E/\varepsilon_f}} x_1\,dx_1\int_{x_b-x_1}^{A_b-1} S_b(Y)G(E,\varepsilon_b,\cos\theta)\,dY. \quad (30)$$

For (2,m) pick–up configuration one has

$$D_2^b(\Omega_b,\varepsilon_b)=\frac{1}{x_b}\int_1^{\sqrt{1+E/\varepsilon_f}}\Theta(1-\gamma)x_1\,dx_1$$
$$\int_{\max(1,x_b-x_1)}^{\min(A_b-2+Z,X_b+x_1)} Q_b(Y)G(E,\varepsilon_b,\cos\theta)\,dY, \quad (31)$$

where

$$\cos\theta\cong\cos\theta'\cos\theta_b, \quad (32)$$

$$\cos\theta'=\frac{x_b^2+x_1^2-Y^2}{2x_bx_1}. \quad (33)$$

$G(E,\varepsilon_b,\cos\theta)$ is given by (1) and (2).

DDCS does not calculate the direct inelastic scattering and compound nucleus elastic scattering data,but the calculated direct inelastic scattering cross sections and angular distributions by the collective excitation distorted–wave Born approximation[17] and compound nucleus elastic scattering cross sections and elastic scattering angular distributions by Hauser–Feshbach model and optical model can be added by the input data of the program DDCS.

The following nuclear data can be calculated with the program DDCS: the double differential cross sections of emitted nucleons (n and p) and composite particle (α, d, t, ^{3}He) in laboratory or C. M. system, as well as total emission cross sections and spectra of all emitted particles; the partial emission cross sections and spectra of all emitted particles for first to sixth particle emission processes and pick–up configurations (1,m) and (2,m); the various yield cross sections; total and elastic scattering cross sections (only for neutron as projectile); total reaction cross section; nonelastic scattering cross sections; radiative capture cross section; (x,np), (x,nα), (x,2n), (x,3n), (x,4n), (x,5n) cross sections and so on.

DDCS has been used to calculate reactions of n+^{56}Fe, n+^{93}Nb, p+^{120}Sn, p+^{197}Au, and p+^{209}Bi. Pretty good results in agreement with the experimental

data were obtained. The application practices show that DDCS is a useful and convenient program for users.

References

[1] G. Mantzouranis et al., Phys. Lett., 57B, 220(1975). G. Mantzouranis et al., Z. Phys., A276, 145(1976)

[2] Sun Ziyang et al., Z. Phys., A305, 61(1982)

[3] K. Kikuchi et al., " Nuclear Matter and Nuclear Reaction," North–Holland, Amsterdam, p. 33, 1968

[4] C. Costa et al., Phys. Rev., C28, 587(1983)

[5] A. Iwamoto et al., Nucl. Phys., A419, 472(1984)

[6] Wen Yuanqi et al., Z. Phys., A324, 325(1986)

[7] J. M. Akkermans et al., Phys. Let., 157B, 95(1985)

[8] Shen Qingbiao, Commun. of Nucl. Data Progress, 11, 52(1994)

[9] A. Iwamoto et al., Phys. Rev., C26, 1821(1982)

[10] K. Sato et al., Phys. Rev., C28, 1527(1983)

[11] Zhang Jingshang et al., Commun. in Theor. Phys., 10, 33(1988)

[12] Zhang Jingshang et al., Z. Phys., A344, 251(1992)

[13] Zhang Jingshang, Commun. Theor. Phys., 14, 41(1990)

[14] Zhang Jingshang et al., Chinese J. Nucl. Phys., 13, 129(1991)

[15] Zhang Jingshang, Nucl. Sci. Eng., to be published

[16] Shen Qingbiao, "The Angular Distribution of Light Composite Particle Projectile in Preequilibrium Reactions", Chin. J. Nucl. Phys., to be published

[17] P. D. Kunz, "Distorted Wave Code DWUCK4", University of Colorado, USA

Intermediate–High Energy Nuclear Reaction Kinetic Simulation and QMD

Lu Zhongdao

(Chinese Nuclear Data Center, IAE)

Introduction

The intermediate and high energy nuclear reaction has caused much interest for physicists in the last two decades. Great progress has been made both in theory and experiment. When the projectile with high incident energy bombarding the target, the nuclei are highly compressed and violent collisions between projectile nucleons and target nucleons will occur when they pass through from each other. In the reaction zone, the condensed nuclear matter will be formed with high energy density and high temperature in which besides the leading particles or their excited state like delta particles, other particles such as pions, kaons will be produced. If one uses the hadron language, this state of nuclear matter is the hadronic gas (HG). If the incident energy is very high, the nuclear matter is extremely compressed, the hadrons will be melted into quark and anti–quark, and a so–called quark gluon plasma (QGP) will be formed. Then this highly compressed nuclear matter will be undergone the adiabatic expansion and reaches to a stage of 'freeze–out'. Produced particles and their clusters (nuclear fragments) fly away from each other are measured by detectors.

In the theoretical aspect of kinetic studies, two kinds of models are available to describe the collision process of two nuclei with intermediate and high energy. One is macroscopic such as the hydrodynamic model[1~3]. It concerns with the state equation and thermal quantities such as entropy, free energy, pressure. It also discusses the time–space evolution of thermal quantities in the reaction zone and searches for the possibly reached largest densities of nuclear medium and energy or temperature. Another kind of models are microscopic, such as MCM[4, 5], SSIENC[6], QMD[7, 8] (or RQMD[9]) and BUU[10, 11] (or RBUU[12]). They treat the movement of each particle (nucleon and meson) and their collisions in time and space and concern with the new particle production. It is more interested in the variation of densities of nuclear medium and

energy and searches for the possible phase transition.

IHENRKS is the abbreviation of Intermediate–High Energy Nuclear Reaction Kinetic Simulation. It belongs to the second kind of models. It combines the idea and method of MCM (the abbreviation of multiple collision model[4,5]), SSIENC [6] and QMD (the abbreviation of quantum molecular dynamics[7, 8]). We proposed the model for the following purposes : first, to study the change of reaction mechanism from one–body interaction domain to two–body interaction domain and to search for the characters involved in the two–body interaction such as the mass and charge distribution of emitted particles and their energy spectrum. Second, to study the characteristic behaviors of nuclear matter at extreme condition e. g. phase transition, state equation, entropy ··· . Third, to apply it to calculate the intermediate and high energy nuclear data. So far, no model is available for the intermediate and high energy nuclear data calculations. So this will be a good try. Forth, other limited purposes such as to study the thermalization in p–nucleus and nucleus–nucleus reactions and to check the validity of the assumption of thermal equilibrium in these reactions.

Next section is the main features of the model, then its application in the study of thermalization for reaction of 830 MeV p + ^{56}Fe.

I Main Feature of IHENRKS

Compared to the low and extremely relativistic energy reactions, intermediate and high energy nuclear reaction has its own characters. It is mainly shown in quantum effect and mean field effect. The following are the main features of the model and the treatments of these effects.

1. Both the particle effect and wave effect are important in this energy range. It can be treated as each nucleon wearing a wave packet around its centroid in the phase space. The Gaussian type of wave packet is taken as follows :

$$f_i(\vec{r},\vec{p},t) = N\ e^{-\alpha^2(\vec{r}-\vec{r}_{i0})^2}\ e^{-\frac{(\vec{p}-\vec{p}_{i0})^2}{\hbar^2\alpha^2}} \tag{1}$$

where N is the normalization constant. α is the reverse width of wave packet and taken to be 0.5 fm^{-1}. The density of nuclear medium is the summation for all nucleons in the nucleus and integral in momentum space.

2. In low energy reaction, the interaction between nucleons can be reduced to

one–body interaction. While in intermediate and high energy reaction, two–body interaction must be taken into account. Each nucleon moves in the mean field built up by all possible pairs of nucleons and is acted by the field. In IHENRKS, the following effective interaction potential is adopted which contains Skyrme, Yukawa and Coulomb potential :

$$V_{ij} = V_{ij}^{S} + V_{ij}^{Y} + V_{ij}^{C} \tag{2}$$

$$V_{ij}^{S} = t_1 \delta (\vec{r}_i - \vec{r}_j) + t_2 \delta (\vec{r}_i - \vec{r}_j) \delta (\vec{r}_i - \vec{r}_k)$$

$$V_{ij}^{Y} = t_3 \frac{e^{-\mu|\vec{r}_i - \vec{r}_j|}}{\mu|\vec{r}_i - \vec{r}_j|}$$

$$V_{ij}^{C} = \frac{Z_1 Z_2 e^2}{|\vec{r}_i - \vec{r}_j|}$$

The parameters are taken from Ref. [8].

3. The movement of each nucleon in the phase space obeys the following Newton equations :

$$\frac{d\vec{r}_i}{dt} = \frac{\partial H}{\partial \vec{p}_i}$$

$$\frac{d\vec{p}_i}{dt} = -\frac{\partial H}{\partial \vec{r}_i} \tag{3}$$

Where H is the Hamiltonian. If two particles close enough i. e. $|\vec{r}_i - \vec{r}_j| \leqslant \sqrt{\frac{\sigma_t(\sqrt{s})}{\pi}}$ ($\sigma_t(\sqrt{s})$ is the total cross section for nucleon–nucleon c. m. energy $\sqrt{s}$), the collision will occur.

4. Pauli blocking is one of quantum effects which is considered in IHENRKS by introducing the Pauli blocking factor G. After the collision of particles i and j, their momenta are changed : $\vec{p}_i \to \vec{p}'_i$, $\vec{p}_j \to \vec{p}'_j$. The Pauli blocking factor for i particle is

$$G_i = \int_{\Omega_i} \sum_{k(k \neq i)} f_k(\vec{r},\vec{p},t) \, d\vec{r} \, d\vec{p} \tag{4}$$

where Ω_i is a volume in phase space around $(\vec{r}_{i0}, \vec{p}'_i)$ [6, 8].

5. In the energy range for the model suitable, a few pions will be produced. The pion production and absorption is approximated by the production of delta particle and its decay. The following 5 channels are considered in collisions :

$$\begin{aligned} N + N &\rightarrow N + N \\ N + N &\rightarrow N + \Delta \\ N + \Delta &\rightarrow N + N \\ N + \Delta &\rightarrow N + \Delta \\ \Delta + \Delta &\rightarrow \Delta + \Delta \end{aligned} \tag{5}$$

Both the elastic and inelastic scattering cross sections are parameterized and taken from Ref. [10].

6. The reaction process is kinetically simulated by Monte Carlo technique. Monte Carlo sampling is involved in the determination of the original space positions and momenta of nucleons, and the determination of reaction type ··· .

II Thermalization in p + ^{56}Fe Reaction

Thermalization is one of the basic issue in nuclear reaction. In intermediate and high energy reaction, it is generally assumed that the thermal equilibrium (sufficient thermalization) is reached before the fragmentation. In order to clarify the validity of this assumption, we studied the thermalization in reaction 830 MeV p + ^{56}Fe.

At first we studied the squared components of the momentum as the function of time. The incident direction is taken as z direction. The time evolution of these quantities is shown in Fig. 1. At the beginning, because of the large incident momentum, p_z^2 is much larger than p_x^2 and p_y^2 (they are only contributed by Fermion momentum). Later on, the collision between incident proton and target nucleons occurs, the incident proton looses its energy and converts it into the collided nucleons. So, the p_z^2 drops drastically and p_x^2, p_y^2 increase. But obviously, these curves do not reach to a same line. That means that the incident proton still keeps more energy than other nucleons when it leaves from the target. This shows that the energy conversion in collisions is not sufficient. The thermal equilibrium is not reached in the whole nucleus, more likely,

is reached in a tube along incident direction. As to the gap between p_x^2 and p_y^2, it comes from the statistical fluctuations in the original momenta.

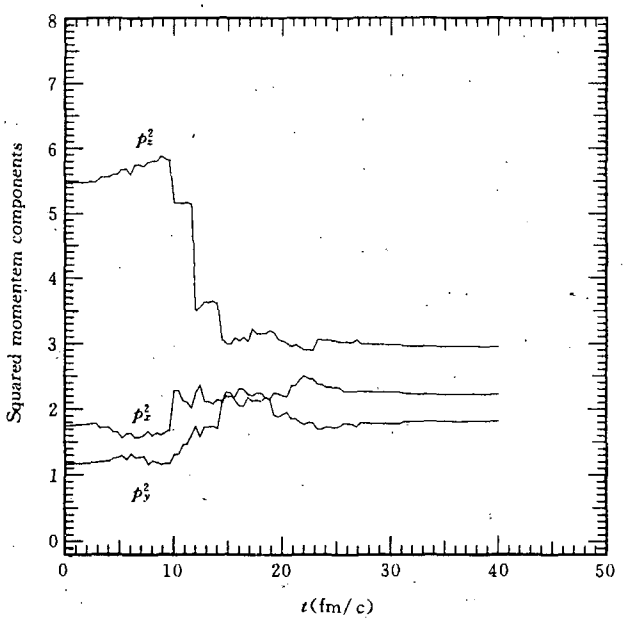

Fig. 1 Time evolution of squared momentum components for 830 MeV p+^{56}Fe reaction

Secondly, we calculated the distribution of kinetic energy density in $z-\rho$ ($\rho=\sqrt{x^2+y^2}$) plane as a function of time. It can be found that at the original position of the incident proton, the kinetic energy density has a sharp peak. Then the peak moves forward along z direction and lowered and fattened. Although the peak is still lowered and fattened when it moves forward, the peak is not dispersed enough to the whole nucleus along ρ direction. So the same conclusion is reached as in the calculation of the squared components of momentum that the thermal equilibrium is only reached in a tube–like volume.

From above calculations for 830 MeV proton bombarding reactions, it can be concluded that the nucleus is not wholely thermalized, but locally thermalized. Whether this conclusion can be used for other incident proton energy,further work is needed. For higher incident energy, this conclusion may be more reasonable, but for lower incident energy, the incident proton will stay in target longer time and suffered more collisions, and the nucleus may be thermalized in a wider area. The further work is undertaking.

References

[1] J. D. Bjorken, Phys. Rev., D27, 140(1982)
[2] K. Kajantie et al., Nucl. Phys., B222, 152(1983)
[3] Zhuang Pengfei et al., Z. Phys., C32, 93(1986)
[4] C. Y. Wong et al., Phys. Rev., D39, 2606(1989)
[5] Lu Zhongdao et al., Chinese Phys. Lett., 7, 145(1990)
[6] Zheng Yuming et al., Chinese Phys. Lett., 6, 117(1989)
[7] J. Aichelin et al., Phys. Rev., C37, 2451(1988)
[8] J. Aichelin, Phys. Rep., 202, 233(1991)
[9] H. Sorce et al., Ann. Phys., 192, 266(1989)
[10] G. F. Bertsch et al., Phys. Rep., 160, 189(1988)
[11] A. Lang et al., Nucl. Phys., A541, 507(1992)
[12] C. M. Ko, Nucl. Phys., A495, 321C(1989)

Systematics of H(n,n) Cross Sections and Angular Distributions

Shen Qingbiao

(Chinese Nuclear Data Center, IAE)

Nucleon–nucleon interaction is the most basic one in nuclear physics. The data of nucleon–nucleon elastic scattering cross sections and angular distributions are very useful in the study of nuclear many–body problems and nuclear reactions as well as the nuclear engineering design. The neutron–hydrogen nuclear data below 30 MeV have been studied[1]. In order to meet the needs in higher energy region, a systematics of neutron–hydrogen elastic scattering cross sections and angular distributions in energy region 2~150 MeV is given in this paper.

The neutron–hydrogen elastic scattering angular distribution in the C. M. system is written in the form of Legendre polynomial :

$$\frac{d\sigma}{d\Omega_c} = \frac{\sigma_{el}}{4\pi} \sum_{l=0}^{4} (2l+1)\ f_l P_l(\cos\theta_c) \tag{1}$$

where σ_{el} is the elastic scattering cross section, f_l is the elastic scattering Legendre coefficient. The sum of l is only up to 4 which is determined by the shape of the experimental data of the neutron–hydrogen elastic scattering angular distributions in the C. M. system. In order to find the relations of the σ_{el} and f_l with incident neutron energy E_n in laboratory system, the experimental data of the neutron–hydrogen elastic scattering angular distributions in the C. M. system for 773 angles of 45 energy points well–distributed between 14.1 ~ 150 MeV were retrieved from EXFOR library. The evaluated values of neutron–hydrogen elastic scattering cross sections were taken from ENDF / B–6 for our fitting calculations. The relations of σ_{el} and f_l with energy E_n are obtained through search of the minimum deviation between the calculated results and experimental data:

$$\begin{aligned}\sigma_{el}(\text{mb}) = {} & 35.341 - 3.3673E_n^{1/2} - 0.82562E_n + 0.057394E_n^{3/2} \\ & + 896.67E_n^{-1/2} + 48.752E_n^{-1} + 5629.0\ \exp\ (-0.68362E_n^{1/2})\end{aligned} \tag{2}$$

$$\begin{aligned}f_0 &= 1.0, \\ f_1 &= -0.0044225E_n^{1/2} + 0.0011536E_n - 0.00011839E_n^{3/2}, \\ f_2 &= -0.0056356E_n^{1/2} + 0.0021873E_n - 0.00002694E_n^{3/2}, \\ f_3 &= -0.00043554E_n^{1/2} + 0.00000007E_n + 0.00000837E_n^{3/2}, \\ f_4 &= 0.00059991E_n^{1/2} + 0.00003287E_n + 0.00001177E_n^{3/2}.\end{aligned} \tag{3}$$

Fig. 1 shows the comparison of neutron–hydrogen elastic scattering cross sections between the calculated values by expression (2) and the evaluated values taken from ENDF / B–6 in energy range 2~ 150 MeV. The very good agreements are obtained. Figs. 2~9 give the comparisons of neutron–hydrogen elastic scattering angular distributions in C. M. system between the calculated results by expressions (1) to (3) and the experimental data taken from EXFOR library at energies E_n=25.8, 50, 63.1, 80, 90, 108.5, 130, and 150 MeV, respectively. The empirical formula of neutron–hydrogen elastic scattering angular distributions in C. M. system could reproduce the experimental data quite well. Therefore, the empirical formulas (1), (2), and (3) could reproduce the ex-

perimental data successfully.

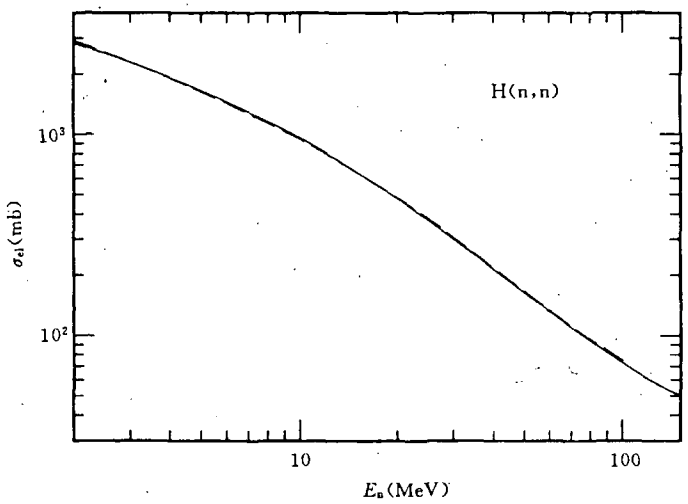

Fig. 1 Comparison of neutron–hydrogen elastic scattering cross sections between the calculated and the evaluated values taken from ENDF / B–6

——— calculated values, – – – – evaluated values.

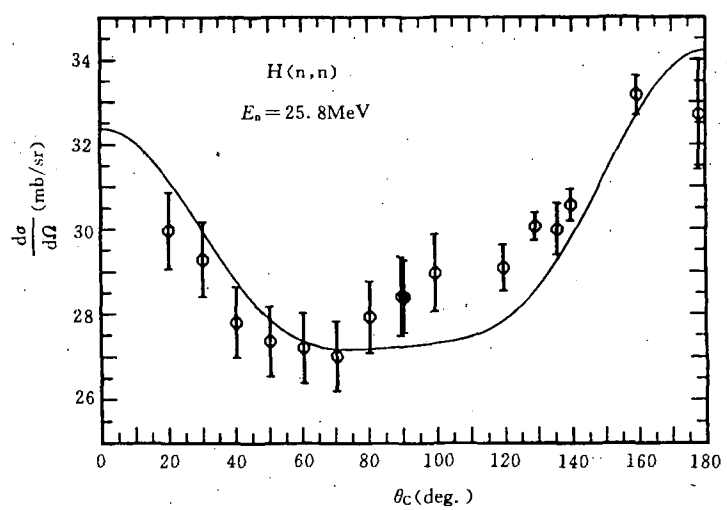

Fig. 2 Comparison of neutron–hydrogen elastic scattering angular distribution in the C. M. system between the calculated values and the experimental data taken from EXFOR library at energy E_n = 25.8 MeV

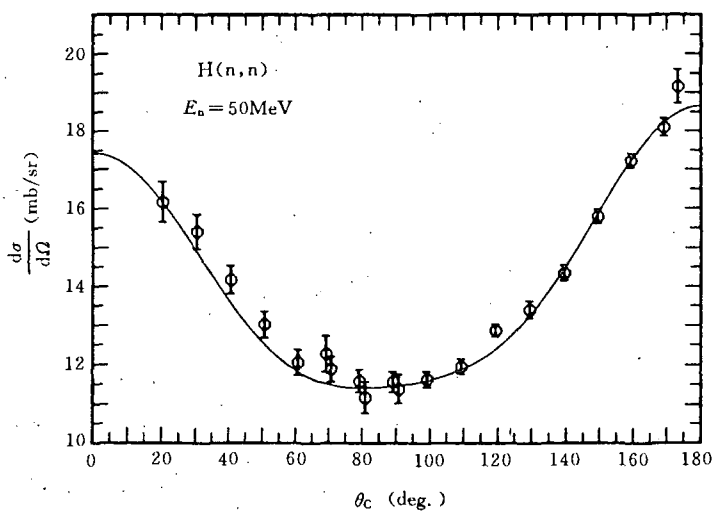

Fig. 3 The same as Fig. 2 but for $E_n = 50$ MeV

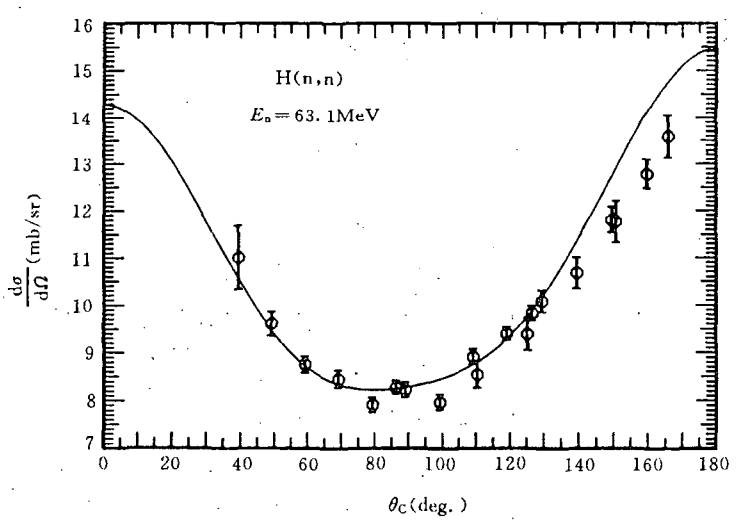

Fig. 4 The same as Fig. 2 but for $E_n = 63.1$ MeV

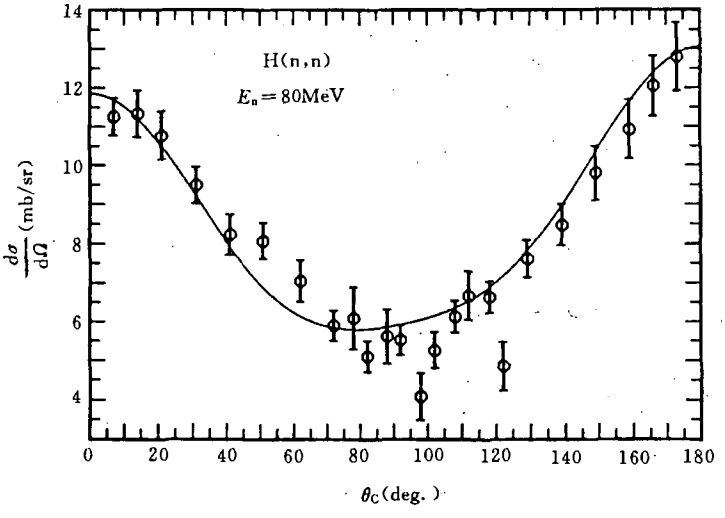

Fig. 5 The same as Fig. 2 but for $E_n = 80$ MeV

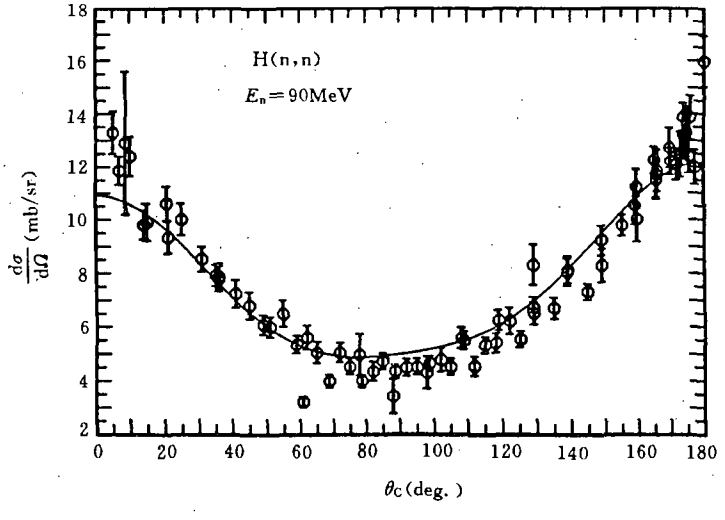

Fig. 6 The same as Fig. 2 but for $E_n = 90$ MeV

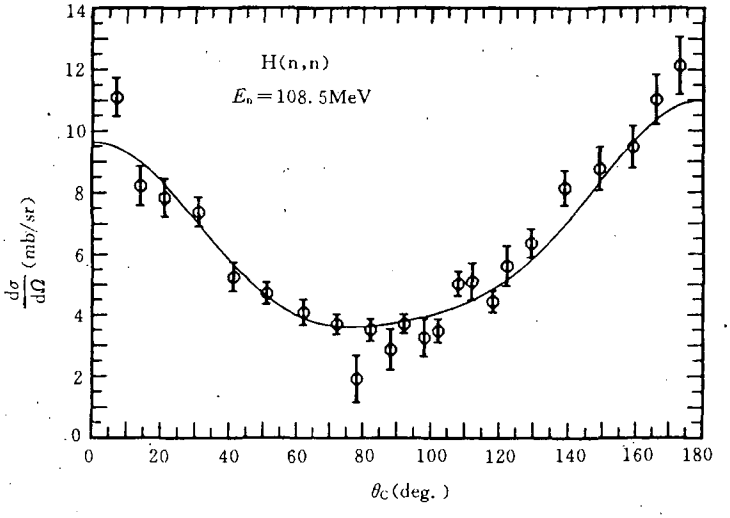

Fig. 7 The same as Fig. 2 but for E_n = 108.5 MeV

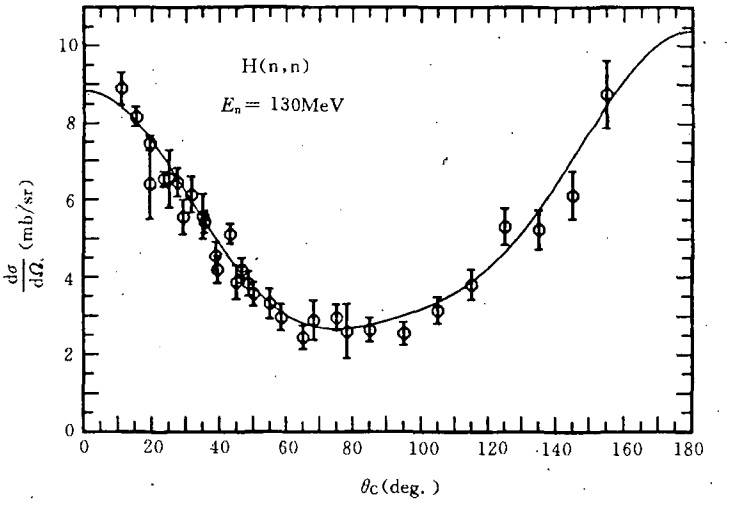

Fig. 8 The same as Fig. 2 but for E_n = 130 MeV

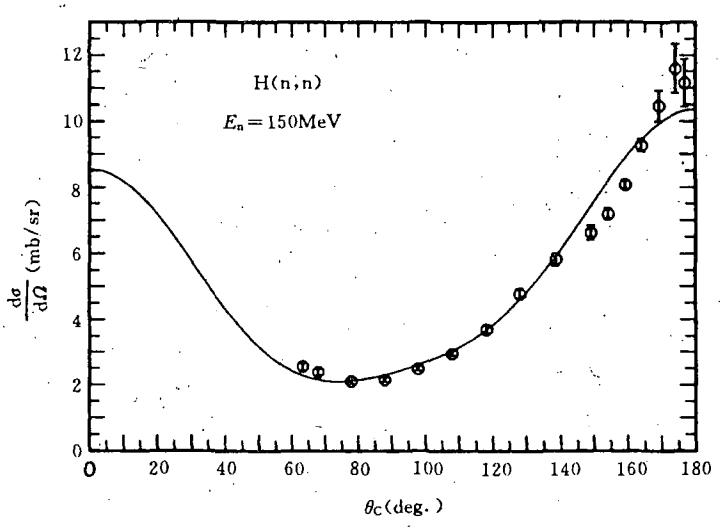

Fig. 9 The same as Fig. 2 but for $E_n = 150$ MeV

References

[1] Li Gengyuan et al., "Calculations of total cross sections, differential cross sections, and polarization data for neutron–hydrogen reaction", Collection of Theoretical Method on Nuclear Reactions and Their Applications, p. 1, (1980) (in Chinese)

Analytical Expression of Mean Force in Quantum Molecular Dynamics

Lu Zhongdao

(Chinese Nuclear Data Center, IAE)

Introduction

In the intermediate and high energy nuclear reaction, the nuclear mean field is very important. The field is constructed by the interaction of nucleons in the nucleus and acts on each nucleon. In the microscopic dynamic models, such as QMD[1, 2] or RQMD[3], SSIENC[4], BUU[5, 6] or RBUU[7, 8], and MCM[9, 10], the effective interaction potential such as the Skyrme–type potential is generally adopted as the mean field, which contains two–body and three–body interactions. The movement of nucleons obeys the Newton equation. To solve the Newton differential equations the forces, which are the minus gradient of the potential, should be calculated firstly. If one adopts the difference method to calculate the forces, six potentials need to be calculated for each nucleon at each time step, (three coordinate directions with each direction having two potentials). To calculate a potential at a point in the phase space spends much CPU time for it counts in each pair of nucleons in the nucleus. In studying the evolution of nuclear system, such calculation will cost big amount of CPU time, especially for large nuclear system. Furthermore, the dull calculations will lead to the results poor accuracy and sometimes make it unacceptable. So it is important to improve the method of solving equations and reduce the calculation of potentials. This can be realized by introducing the analytical forces instead of the potential difference.

In next section, we give out the analytical force expressions derived from the Skyrme–type potentials which include the two–body Skyrme interaction, two–body Yukawa and two–body Coulomb interactions, and a three–body Skyrme interaction[1]. In the third section, the comparison is made for the two methods. From the comparison, one can see that the application of the analytical force expressions not only save much CPU time but also raise the calculation accuracy.

1 Analytical Force Expressions

In the microscopic dynamic theory, the following Skyrme–type potential [1, 2] is generally adopted, which includes the two–body Skyrme potential(U^{S}), two–body Yukawa potential (U^{Y}) and two–body Coulomb potential (U^{C}), and a three–body Skyrme potential (U^{3}):

$$U_i^{S} = t_1\left(\frac{\alpha}{\sqrt{2\pi}}\right)^3 \sum_{\substack{j \\ (j\neq i)}} e^{-\frac{\alpha^2}{2}r_{ij}^2} \tag{1}$$

$$U_i^{Y} = \frac{t_3}{2\mu} \sum_{\substack{j \\ (j\neq i)}} \frac{e^{-\frac{\alpha^2}{2}r_{ij}^2}}{r_{ij}} \left(\operatorname{err}\left(\frac{\mu}{\sqrt{2}\alpha} - \frac{\alpha}{\sqrt{2}} r_{ij}\right) - \operatorname{err}\left(\frac{\mu}{\sqrt{2}\alpha} + \frac{\alpha}{\sqrt{2}} r_{ij}\right) \right) \tag{2}$$

$$U_i^{C} = Z_1 Z_2 e^2 \sum_{\substack{j \\ (j\neq i)}} \frac{1}{r_{ij}} \operatorname{erf}\left(\frac{\alpha}{\sqrt{2}} r_{ij}\right) \tag{3}$$

$$U_i^{(3)} = t_2\left(\frac{\alpha}{\sqrt{\pi}}\right)^6 \frac{1}{3\sqrt{3}} \sum_{\substack{j \\ (j\neq i)}} e^{-\frac{\alpha^2}{3}r_{ij}^2} \sum_{\substack{k>j \\ (k\neq i)}} e^{-\frac{\alpha^2}{3}(r_{ik}^2 + r_{jk}^2)} \tag{4}$$

where r_{ij} is the distance between particles i and j. t_1, t_2, t_3 and μ are parameters of potential, α is the parameter of wave packet. The erf and err are the error function and modified error function respectively defined as

$$\operatorname{erf}(x) = \frac{2}{\sqrt{\pi}} \int_0^x e^{-t^2} dt, \qquad \operatorname{err}(x) = 1 - \operatorname{erf}(x)\ e^{-x^2}$$

According to above potential formulas, the analytical forces, which is defined as the minus gradient of potential, i. e. $\vec{F} = -\nabla_r U$, can be derived. From formulas (1)~ (3), the two–body Skyrme, Yukawa and Coulomb forces in x direction are derived as follows:

$$F_{x_i}^{S} = t_1\left(\frac{\alpha}{\sqrt{2\pi}}\right)^3 \alpha^2 \sum_{\substack{j \\ (j\neq i)}} (x_i - x_j)\ e^{-\frac{\alpha^2}{2}r_{ij}^2} \tag{5}$$

$$F_{x_i}^{Y} = \frac{t_3}{2\mu} \sum_{\substack{j \\ (j\neq i)}} \frac{x_i - x_j}{r_{ij}^2} e^{-\frac{\alpha^2}{2}r_{ij}^2} \left(\left(\frac{1}{r_{ij}} + \mu \right) \operatorname{err}\left(\frac{\mu}{\sqrt{2}\alpha} - \frac{\alpha}{\sqrt{2}} r_{ij} \right) - \right.$$

$$\left(\frac{1}{r_{ij}}-\mu\right)\operatorname{err}\left(\frac{\mu}{\sqrt{2}\alpha}+\frac{\alpha}{\sqrt{2}}r_{ij}\right)-2\sqrt{\frac{2}{\pi}}\alpha\Bigg) \tag{6}$$

$$F_{x_i}^{C}=Z_1Z_2e^2\sum_{\substack{j\\(j\neq i)}}\frac{x_i-x_j}{r_{ij}^2}\left(\frac{1}{r_{ij}}\operatorname{erf}\left(\frac{\alpha}{\sqrt{2}}r_{ij}\right)-\sqrt{\frac{2}{\pi}}\alpha\, e^{-\frac{\alpha^2}{2}r_{ij}^2}\right) \tag{7}$$

The three–body Skyrme force is derived from formula (4), which reads

$$F_{x_i}^{(3)}=t_2\left(\frac{\alpha}{\sqrt{\pi}}\right)^6\frac{4}{9\sqrt{3}}\alpha^2\sum_{\substack{j\\(j\neq i)}}e^{-\frac{\alpha^2}{3}r_{ij}^2}\sum_{\substack{k>j\\(k\neq i)}}(2x_i-x_j-x_k)\,e^{-\frac{\alpha^2}{3}(r_{jk}^2+r_{jk}^2)} \tag{8}$$

In y and z directions, the force expressions are the same except x replaced by y and z.

2 Numerical Results and Comparisons

The calculations of forces for nucleus ^{56}Fe are shown in Tables 1～3. The No is the ordering number of the nucleons, the ID specifies the sort of nucleons : 1 is for proton and 2 for neutron. The x, y and z are the spatial positions of the nucleons. The forces are shown in other columns. Among them, columns 4 to 6 and 11 to 13 are the forces calculated by the following difference formulas :

$$F_{x_i}=-\frac{U(x_i+l)-U(x_i-l)}{2l}$$

$$F_{y_i}=-\frac{U(y_i+l)-U(y_i-l)}{2l}$$

$$F_{z_i}=-\frac{U(z_i+l)-U(z_i-l)}{2l}$$

For comparison, we have calculated them with three l values, i. e. $l=$ 1.0, 0.5 and 0.1 fm. They are shown in columns 4 to 6 and 11 to 13 respectively. The forces calculated by the analytical expressions are shown in the seventh and the last column. From comparison between the results of difference formulas and that of analytical expressions, it is easy to see that the smaller l can have higher accuracy. For $l=$ 0.1 fm the accuracy can reach 2～3 effective digits. For $l=$ 0.5 fm the accuracy reaches 1～2 effective digits. But for $l=$ 1.0 fm, the accuracy is poor. For some particles the error is severe. For instance, in x direction,

the magnitude of force for the 3rd particle is only 1 / 6 of that calculated by the analytical expression. For 19th and 33rd particles, the forces calculated by the two methods even have different signs. The reason for that is due to the potential being the nonmonotonic function of spatial coordinates. For some particles, the potential has large fluctuations around their locations. The differences in y and z directions can also been seen in Tables 2 and 3. So the application of analytical forces can raise the accuracy for the calculation of forces and for solving the Newton equations.

Saving CPU time is the second advantage. In the calculation of difference method, for each nucleon at each time step, six potentials need to be calculated in three coordinate directions with each direction having two potentials. While in the calculation by analytical expressions, only three components of force need to be calculated. Furthermore, if one examines the three components carefully, he will easily find that only one component of CPU time is needed to calculate the three components, for they have the same calculations except the factors $x_i - x_j$, $y_i - y_j$ and $z_i - z_j$ which need almost no time. The CPU time is only a little increased to calculate an analytical force than to calculate a potential. So the application of analytical mean force can save about 5 / 6 CPU time.

The analytical force expressions have been put into the code IHENRKS (the abbreviation of Intermediate and High Energy Nuclear Reaction Kinetic Simulation). The improvement is great in both running speed and accuracy.

Table 1 x–component of force (in MeV • fm^{-1}). $\Delta x = 2l$, l = 1.0, 0.5 and 0.1 fm.

No	ID	x	$-\Delta U/\Delta x$			Fx	No	ID	x	$-\Delta U/\Delta x$			Fx
			1.0	0.5	0.1					1.0	0.5	0.1	
1	1	1.35	−5.581	−5.386	−5.310	−5.315	29	2	−2.38	8.747	8.873	8.921	8.932
2	1	−1.91	11.509	12.539	12.896	12.920	30	2	−1.10	5.840	5.693	5.637	5.638
3	1	−0.92	−0.260	−1.172	−1.497	−1.511	31	2	2.10	−9.681	−9.832	−9.895	−9.904
4	1	−0.18	−2.867	−3.153	−3.251	−3.256	32	2	0.14	2.278	2.688	2.826	2.835
5	1	0.88	1.276	2.045	2.323	2.332	33	2	−0.41	0.337	0.032	−0.082	−0.086
6	1	4.18	−19.986	−20.543	−20.716	−20.734	34	2	−0.16	0.742	0.722	0.717	0.716
7	1	−0.46	5.213	5.449	5.518	5.524	35	2	0.28	0.476	0.923	1.085	1.090
8	1	−2.99	15.743	16.296	16.472	16.489	36	2	4.12	−20.920	−21.706	−21.954	−21.977
9	1	−2.52	12.081	12.242	12.288	12.298	37	2	1.78	−9.584	−9.593	−9.596	−9.605
10	1	−2.85	11.466	11.537	11.554	11.561	38	2	−2.60	13.019	13.576	13.754	13.769
11	1	−2.80	14.334	14.445	14.465	14.476	39	2	2.06	−11.156	−11.371	−11.445	−11.457
12	1	1.53	−5.138	−4.982	−4.930	−4.933	40	2	2.37	−9.642	−10.022	−10.159	−10.174
13	1	−1.51	2.182	1.338	1.041	1.031	41	2	−0.26	1.539	1.364	1.290	1.288
14	1	−3.88	17.437	17.922	18.082	18.102	42	2	2.31	−18.656	−19.850	−20.260	−20.287
15	1	−1.08	9.471	9.730	9.818	9.831	43	2	−1.78	9.659	10.188	10.371	10.386
16	1	−1.56	5.901	5.329	5.136	5.134	44	2	1.20	−5.743	−5.530	−5.443	−5.442
17	1	0.23	2.378	2.856	3.007	3.015	45	2	−1.60	6.003	5.452	5.266	5.264
18	1	2.40	−8.914	−9.438	−9.624	−9.639	46	2	−3.49	17.537	18.533	18.867	18.892
19	1	−0.59	0.650	−0.175	−0.478	−0.492	47	2	0.54	3.450	4.021	4.219	4.226
20	1	−1.29	10.499	10.960	11.124	11.137	48	2	1.65	−10.077	−10.185	−10.212	−10.218
21	1	1.01	−0.475	0.560	0.934	0.948	49	2	−2.13	11.393	11.631	11.707	11.718
22	1	3.09	−12.646	−13.137	−13.306	−13.320	50	2	−1.28	8.514	8.853	8.969	8.978
23	1	2.36	−14.657	−14.986	−15.089	−15.102	51	2	1.81	−11.425	−11.466	−11.462	−11.468
24	1	3.61	−13.977	−14.478	−14.637	−14.653	52	2	1.49	−11.161	−11.048	−10.986	−10.991
25	1	0.76	−3.718	−3.549	−3.489	−3.489	53	2	−0.37	−3.056	−3.733	−3.970	−3.982
26	1	−3.48	19.601	20.675	21.034	21.061	54	2	−3.94	17.262	17.645	17.772	17.789
27	2	2.11	−12.910	−13.225	−13.336	−13.350	55	2	1.83	−7.601	−7.801	−7.861	−7.867
28	2	−1.15	1.754	1.388	1.265	1.261	56	2	3.46	−18.525	−19.164	−19.371	−19.390

Table 2 y–component of force (in MeV • fm^{-1}). $\Delta y = 2l$, l = 1.0, 0.5 and 0.1 fm.

No	ID	y	$-\Delta U/\Delta y$			Fy	No	ID	y	$-\Delta U/\Delta y$			Fy
			1.0	0.5	0.1					1.0	0.5	0.1	
1	1	0.32	−3.729	−4.622	−4.952	−4.970	29	2	0.99	−2.324	−2.849	−3.040	−3.051
2	1	−3.87	15.025	15.562	15.743	15.763	30	2	−3.00	12.020	11.675	11.542	11.545
3	1	2.07	−7.214	−6.933	−6.816	−6.816	31	2	0.20	−3.473	−4.576	−4.975	−4.997
4	1	1.63	−13.408	−13.937	−14.110	−14.125	32	2	0.29	−0.248	−0.894	−1.139	−1.152
5	1	−1.01	8.374	8.914	9.117	9.134	33	2	3.40	−17.687	−18.536	−18.824	−18.848
6	1	−0.69	3.484	3.546	3.570	3.573	34	2	1.94	−13.470	−12.965	−12.761	−12.762
7	1	0.19	−3.712	−4.185	−4.371	−4.379	35	2	3.40	−20.756	−21.683	−22.005	−22.033
8	1	−2.14	9.235	9.099	9.043	9.044	36	2	−0.22	−1.534	−2.027	−2.204	−2.213
9	1	2.91	−16.380	−17.195	−17.468	−17.488	37	2	2.22	−11.671	−10.830	−10.507	−10.498
10	1	−1.18	4.013	4.090	4.121	4.124	38	2	2.21	−11.391	−11.644	−11.722	−11.730
11	1	1.29	−5.038	−4.623	−4.467	−4.463	39	2	1.90	−10.307	−10.224	−10.176	−10.180
12	1	2.73	−16.992	−17.279	−17.363	−17.379	40	2	−1.19	11.606	12.465	12.771	12.792
13	1	−0.24	9.027	9.651	9.863	9.878	41	2	−2.95	13.829	14.096	14.174	14.185
14	1	0.14	1.865	2.060	2.123	2.125	42	2	−0.93	2.204	2.053	1.995	1.995
15	1	−0.75	2.968	3.184	3.268	3.276	43	2	−3.23	13.718	13.973	14.047	14.059
16	1	−0.41	10.456	11.118	11.345	11.359	44	2	−3.05	19.216	19.605	19.720	19.734
17	1	−0.83	3.829	3.987	4.049	4.055	45	2	1.34	−4.097	−3.795	−3.691	−3.693
18	1	−0.57	4.673	4.713	4.720	4.725	46	2	−0.03	8.250	9.049	9.322	9.337
19	1	−2.56	12.227	12.156	12.113	12.123	47	2	−1.96	13.809	14.462	14.677	14.695
20	1	−1.22	4.153	4.200	4.231	4.237	48	2	3.34	−17.506	−18.146	−18.366	−18.388
21	1	0.63	−2.595	−2.880	−2.979	−2.985	49	2	3.03	−18.740	−19.581	−19.854	−19.875
22	1	−2.99	16.345	16.860	17.016	17.032	50	2	0.52	−1.852	−1.476	−1.348	−1.342
23	1	0.92	−10.280	−10.706	−10.842	−10.853	51	2	−2.62	19.457	20.609	20.992	21.018
24	1	3.04	−12.128	−12.613	−12.778	−12.792	52	2	−0.77	4.575	4.486	4.455	4.457
25	1	0.25	−7.338	−7.620	−7.711	−7.718	53	2	−4.66	18.702	19.531	19.817	19.840
26	1	1.50	−6.245	−6.653	−6.794	−6.802	54	2	−0.57	4.188	4.378	4.438	4.443
27	2	−1.39	11.324	11.845	12.035	12.050	55	2	−1.61	5.993	6.293	6.391	6.398
28	2	2.78	−19.424	−20.359	−20.679	−20.704	56	2	1.43	−5.168	−4.872	−4.760	−4.759

Table 3 z–component of force (in MeV • fm^{-1}). $\Delta z = 2l$, $l = 1.0, 0.5$ and 0.1 fm.

No	ID	z	$-\Delta U/\Delta z$			Fz	No	ID	z	$-\Delta U/\Delta z$			Fz
			1.0	0.5	0.1					1.0	0.5	0.1	
1	1	0.01	0.803	1.271	1.441	1.449	29	2	3.22	−18.984	−20.110	−20.492	−20.520
2	1	−0.62	0.325	0.956	1.190	1.201	30	2	0.74	−14.156	−15.295	−15.690	−15.715
3	1	2.64	−15.283	−15.901	−16.108	−16.126	31	2	1.57	−8.233	−8.394	−8.457	−8.464
4	1	−3.35	16.506	16.926	17.057	17.075	32	2	1.18	−8.838	−9.093	−9.188	−9.201
5	1	0.84	−7.288	−7.480	−7.555	−7.564	33	2	2.40	−12.203	−12.795	−12.992	−13.008
6	1	0.06	5.401	6.022	6.233	6.243	34	2	−0.77	5.073	5.038	5.023	5.026
7	1	−1.20	3.552	3.355	3.293	3.297	35	2	0.62	2.914	3.491	3.688	3.697
8	1	0.59	−6.394	−6.639	−6.722	−6.729	36	2	1.68	−7.484	−7.895	−8.031	−8.042
9	1	0.00	3.515	3.887	4.013	4.017	37	2	0.72	−2.443	−2.587	−2.638	−2.643
10	1	−3.29	13.340	13.957	14.163	14.180	38	2	−2.66	12.509	12.903	13.038	13.052
11	1	−1.44	5.435	4.809	4.588	4.583	39	2	2.91	−15.652	−16.045	−16.167	−16.181
12	1	−1.08	12.134	12.702	12.892	12.907	40	2	2.09	−12.738	−13.175	−13.321	−13.336
13	1	3.57	−17.662	−18.421	−18.676	−18.698	41	2	−3.45	15.279	15.774	15.941	15.957
14	1	−0.05	0.340	0.075	−0.020	−0.025	42	2	−2.97	12.055	11.817	11.726	11.732
15	1	−0.14	−3.053	−3.204	−3.249	−3.253	43	2	−2.56	11.856	11.927	11.927	11.933
16	1	1.71	−7.758	−7.546	−7.476	−7.479	44	2	0.61	−5.465	−5.676	−5.757	−5.763
17	1	−2.39	11.261	10.907	10.772	10.775	45	2	0.91	0.234	1.101	1.399	1.410
18	1	3.45	−18.522	−19.185	−19.399	−19.416	46	2	2.57	−9.942	−9.992	−9.999	−10.006
19	1	−0.87	1.532	2.111	2.326	2.338	47	2	3.29	−15.042	−14.963	−14.915	−14.922
20	1	−1.59	6.183	6.096	6.064	6.068	48	2	1.78	−9.032	−9.322	−9.411	−9.420
21	1	3.97	−18.899	−19.583	−19.813	−19.835	49	2	1.93	−7.114	−6.937	−6.867	−6.868
22	1	0.54	−0.873	−0.696	−0.638	−0.639	50	2	−3.56	19.947	20.826	21.118	21.144
23	1	−2.24	12.951	13.067	13.096	13.106	51	2	−2.65	6.018	5.166	4.858	4.848
24	1	−0.26	1.686	1.530	1.468	1.465	52	2	−1.54	5.148	4.599	4.402	4.398
25	1	−3.58	20.076	20.943	21.235	21.261	53	2	0.16	−3.487	−3.544	−3.560	−3.562
26	1	1.58	−2.721	−2.128	−1.917	−1.911	54	2	−1.71	5.543	5.507	5.491	5.494
27	2	−0.20	2.969	3.912	4.253	4.269	55	2	−4.20	19.568	20.899	21.361	21.393
28	2	−1.91	8.719	8.409	8.299	8.301	56	2	−0.78	6.339	6.609	6.702	6.707

References

[1] J. Aichelin et al., Phys. Rev., C37, 2451, 1988

[2] J. Aichelin, Phys. Rep., 202, 233, 1991

[3] H. Sorce et al., Ann. Phys., 192, 266, 1989

[4] Zheng Yuming et al., Chinese Phys. Lett., 6, 117, 1989

[5] G. F. Bertsch et al., Phys. Rep., 160, 189, 1988

[6] A. Lang et al., Nucl. Phys., A541, 507, 1992

[7] C. M. Ko, Nucl. Phys., A495, 321C., 1989

[8] Zheng Yuming et al., Chinese Science Bulletin, 39, 1994, (in press)

[9] C. Y. Wong et al., Phys. Rev., D39, 2606, 1989

[10] Lu Zhongdao et al., Chinese Phys. Lett., 7, 145, 1990

III DATA EVALUATION

Progress on Nuclear Data Evaluation at Nuclear Physics Laboratory of Jilin University

Huo Junde

(Department of Physics, Jilin University)

1 A = 54 Mass Chain

The nuclei involved in the evaluation of nuclear structure and decay data for A = 54 mass chain are ^{54}K, ^{54}Ca, ^{54}Sc, ^{54}Ti, ^{54}V, ^{54}Cr, ^{54}Mn, ^{54}Fe, ^{54}Co, ^{54}Ni, ^{54}Cu. The evaluation for A = 54 (published in Nuclear Data Sheets, Vol. 50, 255 (1987)) has been revised by using the experimental data measured for nuclear reaction and decay studies. In comparison with the last evaluation there are some new data in the following data types (sets) :

^{54}K adopted levels	^{54}Ca adopted levels
^{54}Sc adopted levels	^{54}Ti adopted levels
^{54}Mn ε decay	^{52}Cr(α,^{2}He)
^{52}Cr(n,γ), (pol n,γ)	^{54}Cr(d,d), (α,α)
^{54}Cr coulomb excitation	^{46}Ti(12C,αpγ)
^{52}Cr(^{14}O, ^{14}C)	^{54}Fe(π,π')
^{54}Fe(n,n'γ)	^{54}Fe(p,p')
^{54}Fe(^{3}He,2pnγ)	^{54}Fe(p,n)
^{54}Fe(^{3}He,t) E = 600~2000 MeV	^{54}Fe(π+,π−)
^{54}Cu adopted levels	

In the text, the detailed level schemes, decay schemes, and related experimental data are presented. Adopted values for levels and γ−radiations, as well

as other nuclear properties are given.

The updated data for $A = 54$ have been published in Nuclear Data Sheets, Vol. 68, 887 (1993).

2 $A = 52$ Mass Chain

The nuclear data sheets for $A = 52$ published in 1989, (Vol. 58, 677) has been updated using experimental nuclear structure and decay data. Many of the data sets presented in the evaluation are re-evaluated. In comparison with the last evaluation there are some new data in the following data types (sets) :

^{52}K adopted levels	^{52}Ca adopted levels
^{52}Sc adopted levels	^{52}Ti adopted levels
^{51}V(n,γ) E = thermal	^{52}Mn ε decay(5.591 d)
^{50}Ti(^{16}O, ^{14}C)	^{50}Cr(α,^{2}He)
^{51}V(α,t)	^{52}Cr(π+,π+), (π+,π+$'$)
^{52}Cr(n,n$'\gamma$)	^{52}Cr(p,p$'$)
^{52}Cr(α,α')	^{52}Fe ε Decay(8.275 h)
^{52}Fe adopted levels	^{52}Co adopted levels
^{52}Ni adopted levels	

In the text, the information obtained in various reaction and decay experimental data are summarized and presented,together with adopted level schemes and properties.

The evaluated result has been sent to National Nuclear Data Center, U.S.A., and will be published in Nuclear Data Sheets.

Evaluation of Cross Sections for ^{197}Au(n,3n) and ^{197}Au(n,4n) Reactions from Threshold to 50 MeV

Yu Baosheng Shen Qingbiao Cai Dunjiu

(Chinese Nuclear Data Center, IAE)

Abstract

The measured data of cross sections for ^{197}Au(n,3n) and ^{197}Au(n,4n) reactions were collected and analysed. The theoretical calculations of above mentioned reactions were carried out to predict the data in higher energy region. The sets of cross sections for ^{197}Au(n,3n) and ^{197}Au(n,4n) reactions from threshold to 50 MeV were recommended on the basis of the experimental and calculated data.

Introduction

The cross sections of ^{197}Au(n,3n) and ^{197}Au(n,4n) reactions are very important for monitoring of high energy neutron fields in the context of radiation induced material damage research, space radiation effects and neutron dosimetry etc..

Most of cross sections of ^{197}Au(n,3n) and ^{197}Au(n,4n) reactions have been measured by activation method. Part of them have been measured by using a large liquid scintillator to detect the emitted neutrons. The measured data were only existed below 30 MeV. The data above 30 MeV were supplemented by using theoretical calculations. The present work attempts to give a consistent description of cross section data for ^{197}Au(n,3n) and ^{197}Au(n,4n) reactions based on available experimental and calculated data. In Sec. 1, the experimental data are analysed and evaluated. The model calculations are described in Sec. 2. In Sec. 3, the recommended data are introduced. Finally, a summary is given.

1 Analysis and Evaluation for Experimental Data

There are several difficulties in cross section measurements for ^{197}Au(n,3n) and ^{197}Au(n,4n) reactions above 20 MeV. One of them is that the neutron

fluxes of gas–target source are rather low and the types of reactions induced in the samples are numerous. Another difficulties are that the D(d,n) and T(d,n) reactions are not monoenergetic neutron sources and the breakup neutrons arise from a three–body system when deuterium breakup is energetically possible. The unwanted neutrons will affect measurements if the incident neutron energies are higher than the threshold of the reactions being studied. Five relevant references for ^{197}Au(n,3n) reaction and only one reference for ^{197}Au(n,4n) reaction were collected.

The cross sections of ^{197}Au(n,3n) reaction were measured by using activation method, except one gadolinium–loaded liquid scintillator method. These data are shown in Fig. 1. Most of experimental data were retrieved from EXFOR master files, the newly experimental results of CIAE are included.

Among those experimental data sets for ^{197}Au(n,3n) reaction, 5 laboratories provided 34 energy points[1~5] from 14 MeV to 28 MeV. The collected values were corrected and normalized by using the nice nuclear decay data and standard cross sections. We found some information on the shape of cross sections among those measured data. The data of Bayhurst[3], Lu Hanlin[9] and Veeser[2] are consistent within errors from 16 to 20 MeV. Meanwhile, the data of Bayhurst[3] span a wide energy region (from 16 to 28 MeV). There are only the data of Bramlitt[4] and Hankla[1], at about 14 MeV both of them deviate from the shape of cross section among the measured data.

The abundance of isotope ^{197}Au in natural gold is 100%. The half–life of ^{195}Au is very well known with the value of 183 d, the characteristic gamma rays of 99.8 keV of the product has a branching ratio of 9.34 %. Meanwhile the half–life of ^{194}Au is 1.625 d and its characters of gamma rays have not changed to any significant extent for many years.

Finally strong gamma–transitions with well–known decay characteristics were used. the errors due to uncertainties in decay data were small and were within the limits of quoted errors.

For ^{197}Au(n,3n) reaction, only part of the measured data can be corrected because some authors didn't describe the necessary information in their papers. In order to evaluate measured data, the weighting factors of reciprocal of squared errors were used. Some errors given by authors were enlarged for getting reasonable weighting factors. The evaluated uncertainty in the vicinity of threshold is about 25% and about 15% near 30 MeV region.

As for the measured cross sections for ^{197}Au(n,4n) reaction, there were only 3 data at 3 energy points from 24 to 28 MeV. They are not enough to get a fitting curve from threshold to 50 MeV. But the experimental data can be used to adjust the model parameters for the theoretical calculation.

2 Experimental Data Needed for Model Calculation

To supplement the scarce data in high energy range, the program SPEC[7] was used. First, based on total, nonelastic cross sections and elastic angular distribution data of ^{197}Au from EXFOR data, a set of optimum neutron potential parameters in energy region 0.5~ 80 MeV was obtained. Second, adjusting some charged particle optical potential and level density parameters as well as taking larger exciton model constant, various calculated nuclear data are in good agreement with the experimental data.

1) For inelastic scattering cross section, the direct reaction contribution was considered. The calculated curves can pass through the experimental data.

2) For (n,γ) cross section, the calculated curves are basically agreement with the experimental data.

3) For (n,p) and (n,α) cross sections, the calculated data can reproduce experimental data very well.

4) For ^{197}Au(n,2n) reaction cross section, there are a large number of experimental data. The data at 14.7 MeV of Lu Hanlin[5], Ryves[8], Vonach[9] are consistent within errors. Therefore, those experimental data were normalized at 14.7 MeV. The evaluated values of ^{197}Au(n,2n) reaction were obtained by us. The calculated values are in agreement with the evaluated cross sections of (n,2n) reaction below 30 MeV.

According to the model parameters used, the predicated neutron reaction ^{197}Au(n,3n) and ^{197}Au(n,4n) cross sections in higher energy region were obtained.

3 Recommended Data

For ^{197}Au(n,3n) reaction cross section, the experimental data have been evaluated below 30 MeV. There are 4 multiple–value sets (about 32 points) in the energy range 14~ 30 MeV. The calculated data have been given from threshold to 50 MeV and closed to the experimental data.

The evaluated data were performed for above mentioned data by using a program of orthogonal polynomial fit from threshold to 30 MeV. The weighted factors used in the evaluation were based on the given errors by authors and quoted errors by us. The theoretical calculated values were very closed to the experimental data. They were almost overlapped with the experimental data between 28 and 30 MeV. Therefore, the calculated data above 30 MeV were recommended. The recommended data for ^{197}Au(n,3n) reaction from threshold to

50 MeV were obtained based on experimental and calculated data, and are given in Fig. 1.

For ^{197}Au(n,4n) reaction cross section, the calculated results were recommended based on experimental data by Bayhurst[3] and are given in Fig. 2.

Acknowledgements

The authors are indebted to IAEA (International Atomic Energy Agency), CNNC (China National Nuclear Corporation) and CIAE for their supports, and thanks to Drs. N. P. Kocherov, Wang Dahai, T. Benson, O. Schwerer, Lu Hanlin and Zhao Wenrong for their kind help and suggestions.

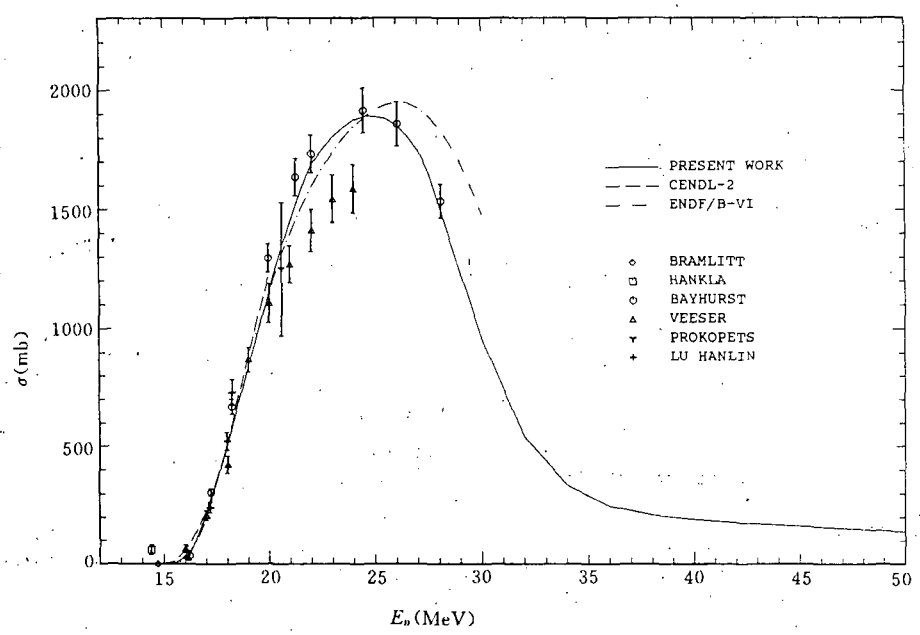

Fig. 1 Comparison among evaluation data with experimental data for Au(n,3n) reaction cross section

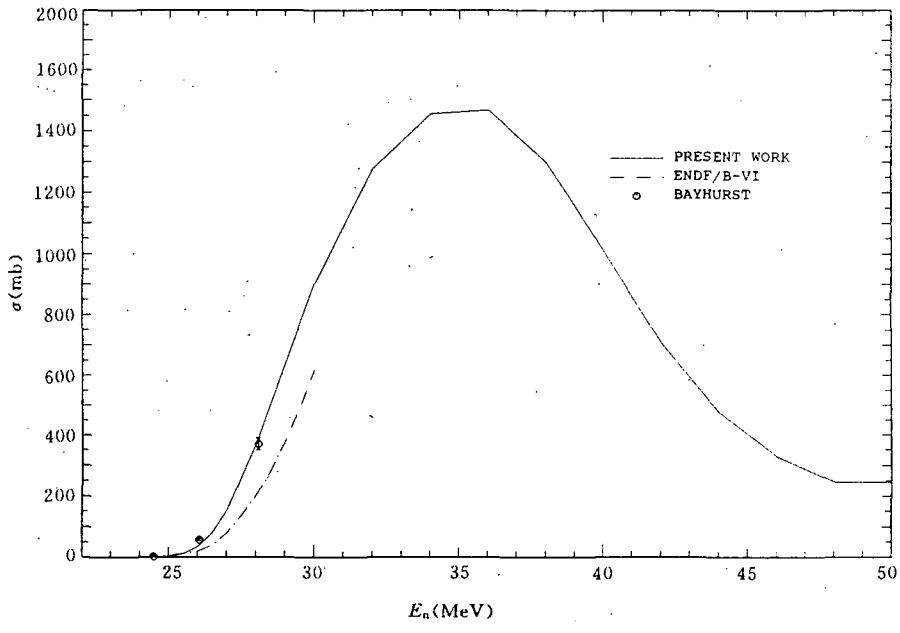

Fig. 2 Comparison among evaluation data with experimental data for Au(n,4n) reaction cross section

References

[1] A. K. Hankla et al., Nucl. Phys., A180, 157(1972)
[2] L. R. Veeser et al., Phys. Rev., C16, 1792(1977)
[3] B. P. Bayhurst et al., Phys. Rev., C12, 451(1975)
[4] E. T. Bramlitt et al., Phys. Rev., 131, 2649(1963)
[5] Zhao Wenrong et al., INDC(CPR)–16(1989)
[6] G. A. Prokopets, EXFOR 88009005
[7] Shen Qingbiao et al., CNDP, 11, (1994)
[8] T. B. Ryves, European Appl. Res. Rept. Nucl. Sci. Tech. Vol., 7, 1241(1989)
[9] H. Vonach et al., private communication (1992)

Evaluation of Neutron Induced Data on ^{56}Fe

Zhao Zhixiang Liu Tong Zhang Jingshang Shen Qingbiao Yan Shiwei

(Chinese Nuclear Data Center, IAE)

Introduction

By means of the semi-classical theory code UNF[1], the optical model code APOM[2] and the distorted-wave Born approximation code DWUCK[3], a consistent theory calculation was carried out for neutron induced data, including cross sections, angular distributions, double differential cross sections (DDX) and γ-ray production data. Based on this calculation and measured data available, an evaluation for neutron induced data on ^{56}Fe up to 20 MeV is completed. This evaluation also includes the uncertainty files for resonance parameters, cross sections, angular distributions, DDX and γ-ray production data.

In Section 1, the model parameters used in the theory calculations will be given. Section 2 will discuss evaluation procedure. And finally, a short summary will be given in Section 3. The methods and results used in generating uncertainty files are presented in Refs. [4] and [5].

1 Model Parameters Used in Theory Calculations

1.1 Optical Model Parameters

The Woods-Saxon optical potential shape is used in the spherical optical model.

The depth of real volume potential is expressed as

$$V_r = V0 + V1 \times E + V2 \times E^2 + V3 \times (A - 2Z) / A + V4 \times Z / A \qquad (1)$$

And the depth of imaginary surface and volume potential are described as

$$W_s = W0 + W1 \times E + W2 \times (A - 2Z) / A \qquad (2)$$

and

$$U_r = U0 + U1 \times E + U2 \times E^2 \tag{3}$$

The diffusivities AR, AS, AV, $AS0$ are constants. But for proton, the diffusivities are modified as :

$$AS' = AS + A2S \times (A - 2Z) / A \tag{4}$$

$$AV' = AV + A2V \times (A - 2Z) / A \tag{5}$$

Table 1 Optical model parameters

Parameter	n	p	α	^{3}He	d	t
AR, fm	0.6071	0.55	0.61	0.72	0.96	0.96
AS, fm	0.4818	0.45	0.56	0.88	0.95	0.95
AV, fm	0.7587	0.45	0.56	0.88	0.95	0.95
AS0, fm	0.6072	0.55	0.61	0.72	0.96	0.96
RR, fm	1.1895	1.25	1.35	1.20	1.37	1.37
RS, fm	1.2564	1.25	1.35	1.40	1.43	1.40
RV, fm	1.2823	1.25	1.35	1.40	1.43	1.40
RS0, fm	1.1895	1.25	1.35	1.20	1.37	1.37
RC, fm	1.2500	1.25	1.40	1.30	1.30	1.30
U0, MeV	−1.0236	−2.70	21.0	46.59	0.00	38.14
U1, MeV	0.172	0.32	0.25	−0.33	0.00	−0.33
U2, MeV	0.0016	0.00	0.00	0.00	0.00	0.00
V0, MeV	56.8317	58.0	133.0	151.9	80.13	165.00
V1, MeV	−0.5072	−0.32	−0.03	−0.17	0.00	−0.17
V2, MeV	0.0024	0.00	0.001	0.0	0.00	0.00
V3, MeV	−24.000	24.0	0.00	50.0	0.00	−6.4
V4, MeV	0.0000	0.40	0.00	0.00	2.20	0.00
VS0, MeV	6.2000	6.20	0.00	2.50	7.00	2.50
W0, MeV	12.0235	16.8	0.00	0.00	14.89	0.00
W1, MeV	−0.2940	−0.05	0.00	0.00	0.00	0.00
W2, MeV	−12.000	12.0	0.00	0.00	0.00	0.00
A2S, fm		0.7				
A2V, fm		0.7				

1.2 Level Density Parameters

The discrete levels data and back-shifted Fermi gas model is used in the calculation.

Table 2 Level density parameters

Nuclei	a, 1 / MeV	Δ, MeV
^{52}Cr	5.416	2.29
^{53}Cr	7.620	0.84
^{54}Cr	5.676	2.35
^{54}Mn	6.337	0.00
^{55}Mn	5.534	2.17
^{56}Mn	8.465	−0.20
^{55}Fe	7.761	0.80
^{56}Fe	6.6620	1.85
^{57}Fe	7.3067	1.10

1.3 Level Information and Branching Ratios for γ-Ray Decay

These data can be found in the file 12 of the evaluated data file.

1.4 Deformation Parameters

The deformation parameters for ^{56}Fe are taken from Ref. [6] and given in Tab.3 for the direct reaction processes.

Table 3 Deformation parameters of ^{56}Fe levels

E, keV	J^{π}	β
846.8	2+	0.252
2085.1	4+	0.2
2657.5	2+	0.062
2959.9	2+	0.04
3122.9	4+	0.11
3369.7	2+	0.095
3601.9	2+	0.063
3832.0	2+	0.047
4120.0	4+	0.1
4401.0	2+	0.059
4510.0	3−	0.2

1.5 Giant–Dipole Resonance Parameters

The γ–ray transmission coefficients were calculated by giant–dipole resonance model in UNF, the parameters used in the calculation are given in table 4. The absorption cross section for giant–dipole resonance was assumed to have a double–humped Lorentzian shape.

Table 4 Giant–dipole resonance parameters

Nuclei	σ_1, b	σ_2, b	E_1, MeV	E_2, MeV	Γ_1, MeV	Γ_2, MeV
^{52}Cr	0.059	0.029	17.86	21.22	4.42	5.10
^{53}Cr	0.069	0.059	17.86	21.22	4.42	5.10
^{54}Cr	0.059	0.029	17.86	21.22	4.42	5.10
^{54}Mn	0.059	0.029	17.86	21.22	4.24	4.16
^{55}Mn	0.047	0.045	16.20	19.91	4.24	4.16
^{56}Mn	0.069	0.059	16.20	19.91	4.42	5.10
^{55}Fe	0.047	0.045	16.20	19.91	4.24	4.16
^{56}Fe	0.029	0.025	16.20	19.91	4.24	4.16
^{57}Fe	0.047	0.045	16.20	19.91	4.24	4.16

2 Evaluation of Neutron Induced Data on ^{56}Fe

2.1 Resonance Parameters (MF = 2)

Reich–Moore parameters of ENDF / B–6 are adopted in present work in the energy region from 10^{-5} eV to 850 keV.

2.2 Smooth Cross Sections (MF = 3)

2.2.1 Total Cross Section (MT = 1)

The total cross section was taken from ENDF / B–6 from 850 keV to 2.2 MeV, and calculated by optical model with the parameters given in Tab.1 from 10 MeV to 20 MeV. From 2.2 to 10 MeV, the cross sections were obtained by averaging the measured data of Larson et al.[7].

2.2.2 Elastic Scattering Cross Section (MT = 2)

This cross section is derived by subtracting the non–elastic cross sections from the total cross sections.

2.2.3 Non–Elastic Scattering Cross Section (MT = 3)

This cross section is obtained by summing all the reaction cross sections.

2.2.4 Total Inelastic Scattering Cross Sections (MT = 4)

This cross section is derived by summing all the inelastic scattering cross sections over the discrete levels and the continuum states.

2.2.5 (n,2n), (n,nα) and (n,np) Cross Sections (MT = 16, 22 and 28)

For these cross sections, the values calculated by UNF are adopted.

2.2.6 Inelastic Scattering Cross Sections for Discrete and Continuum Levels (MT = 51 ~ 75, 91)

For the first discrete level (MT = 51), evaluated cross section of ENDF / B–6 is used in this work. Calculated cross sections by UNF were used for other discrete levels (MT = 52 ~ 75). The direct interaction for 11 discrete levels are taken into account by using the results of DWUCK with deformation parameters given in Tab.3 as input data of UNF. The cross section for continuum levels is also given by UNF calculation.

2.2.7 Radiative Capture Cross Section (MT = 102)

This cross section is taken from ENDF / B–6.

2.2.8 (n,p) Cross Sections (MT = 103, 600 ~ 609, 649)

The total (n,p) cross section (MT = 103) is re–evaluated in this work based on measured data available. First, most of ratio measurements and relative measurements to the reference reactions such as $^{27}Al(n,\alpha)$ are renormalized by using standard cross sections of ENDF / B–6. And then, a

least squares fitting is carried out in the energy region of $E_n = 14 \sim 15$ MeV with the following relationship

$$\sigma_{np} = a + b \times E_n \tag{6}$$

where σ_{np} in mb, E_n in MeV. It follows that

$$\hat{a} = 278.395 \qquad \hat{b} = 11.6564 \tag{7}$$

All of data relatively measured to absolute measured cross section around 14.5 MeV are renormalized to those calculated by Eq. (6~ 7). Finally, the least squares fitting is done in the energy region of threshold energy to 14 MeV and 15 to 20 MeV, separately.

For (n,p) cross sections to discrete levels (MT = 600~ 609), the calculated values by UNF are adopted. The cross sections to continuum states in (n,p) process are obtained by subtracting the cross sections of MT = 600~ 609 from those of MT = 103.

2.2.9 (n,d),(n,t) and (n,^{3}He) Cross Sections (MT = 104~ 106)

For these reactions, the evaluated cross sections are given based on the calculation of UNF.

2.2.10 (n,α) Cross Sections (MT = 107, 800~ 812, 849)

The total (n,α) cross section (MT = 107) and (n,α) cross sections to discrete levels (MT = 800~ 812) are given based on the calculation of UNF. The (n,α) cross sections to continuum states (MT = 849) are obtained by subtracting the cross sections of MT = 800~ 812 from those of MT = 107.

2.3 Angular Distribution (MF = 4)

All angular distributions in file 4 are given in the C. M. system with Legendre coefficients.

2.3.1 Elastic Scattering Neutron (MT = 2)

The contributions from shape elastic scattering are calculated by optical model with the parameters given in Tab.1 and from compound elastic scattering by UNF.

2.3.2 Inelastic Scattering Neutron (MT = 51~ 75)

The Legendre coefficients for inelastic scattering to first excited state (MT = 51) are taken from ENDF / B-6 and for those to other excited states (MT = 52~ 75) given based on the calculation of UNF and DWUCK.

2.3.3 Proton and α Particles (MT = 600~ 609, 800~ 812)

For the angular distribution of proton and alpha particles produced in (n,p) and (n,α) processes to discrete levels, the calculations of UNF are adopted.

2.4 DDX of Secondary Particles, Recoils and γ–Rays (MF = 6)

For (n,2n), (n,np), (n,nα) reactions and continuum states of (n,n′), (n,p) and (n,α) reactions, the DDX for secondary particles, recoils and γ–rays are given by UNF calculations.

2.5 Multiplicity of γ Rays Produced by Neutron Reactions (MF = 12)

For MT = 51 ~ 75, 601 ~ 609 and 801 ~ 812, the branching ratios are given. For radiative capture reaction (MT = 102), the multiplicities of γ–rays are calculated by UNF.

2.6 Angular Distributions of Secondary γ–Rays (MF = 14)

For MT = 51 ~ 75, 102, 601 ~ 609 and 801 ~ 812, the angular distribution are assumed isotropic.

2.7 Energy Distributions of Secondary γ–Rays (MF = 15)

For radiative capture reaction (MT = 102), the energy spectra are taken from ENDF / B–6.

3 Concluding Remark

The comparisons between our results and other evaluations for evaluated data and uncertainty files are carried out. Usually, the agreements are good in the case of plenty measured data available as a basis of the evaluation. ^{56}Fe(n,p) cross section is a typical example. Otherwise, the discrepancies among several evaluations exist more or less, especially for inelastic cross sections of discrete levels.

Acknowledgements

The authors would like to thank Dr. Zhou Delin for helpful discussion.

References

[1] Zhang Jinshang, " A Unified HF and Exciton Model for Calculating Double-Differential Cross Section of Neutron Induced Reactions below 20 MeV", Nucl. Sci. and Eng., 114, 55(1993)

[2] Shen Qingbiao et al, Private Communication

[3] P. D. Kunz, "Distorted Wave Code DWUCK4", University of Colorade, 1972

[4] Zhao Zhixiang et al., "Uncertainty Files for Neutron C-S and Elastic Angular Scattering Distributions on ^{56}Fe", CNDP, 10, 140, 1993

[5] Zhao Zhixiang et al., " A Method for Evaluation of Uncertainties for DDX", CNDP, 11, 1994

[6] S. Mellema et al, Phys. Rev., C33, 481, 1986

[7] D. C. Larson et al., ORNL-5787, 174, 1981

Evaluation of Cross Sections for Neutron Monitor Reactions $^{54,56,Nat}Fe(n,x)^{51}Cr$, $^{52,54}Mn$

Yu Baosheng Shen Qingbiao Cai Dunjiu

(Chinese Nuclear Data Center, IAE)

Introduction

Iron is a very important structure material in nuclear engineering. Meanwhile, knowledge of the neutron monitor reactions for natural iron and its isotopes has been used for the evaluation of radiation induced material damage, radiation safety, neutron dosimetry, etc..

The natural iron consists of four isotopes, ^{54}Fe (5.9 %), ^{56}Fe (91.72%), ^{57}Fe (2.1 %) and ^{58}Fe (0.28 %). At present work, the monitor reactions, for which the cross sections were evaluated, are as follows : $^{54}Fe(n,x)^{51}Cr$, $^{52,54}Mn$, $^{56}Fe(n,x)^{51}Cr$, $^{52,54}Mn$ and $^{Nat}Fe(n,x)^{51}Cr$, $^{52,54}Mn$.

The cross section measurement mentioned above exists several difficulties in higher energy above 20 MeV because there are no so good source of monoenergetic neutron and numerous reactions in samples. Therefore, the ex-

perimental data are scarce in higher energy region. The experimental data available below 20 MeV were evaluated so as to guide the theory calculation for higher energy region. A pertinent calculation[1] has already been performed. In present work, the newer information was given for recommendation of $^{54, 56, Nat}Fe(n,x)^{51}Cr$, $^{52, 54}Mn$ reactions.

1 Adjustment of Model Parameters

Based on the experimental data available, a set of neutron optical potential parameters for ^{56}Fe in energy region 4~ 100 MeV was obtained[1]. Adjusting some charged particle optical potential and level density parameters as well as the exciton model constant, calculated various nuclear data are in good agreement with the experimental data. Thus, the predicted various cross sections and yields are reliable.

Because the nonelastic cross sections for ^{54}Fe were very scarce, it is difficult for us to obtain a set of neutron optical potential parameters. In present work the neutron optical potential parameters for ^{54}Fe are taken as same as those for ^{56}Fe. Then, some charged particle optical potential and level density parameters as well as the consentaneous exciton model constant are adjusted so that the calculated nuclear data are in agreement with the experimental data, and they can be used to predict the cross sections in higher energy region.

In natural iron calculation, the parameters used for $^{57, 58}Fe$ come from those of ^{56}Fe because there are no available experimental data. Then the calculation results of natural iron are sum of the calculated results for each isotope multiplied by its abundance.

2 Evaluation of Cross Sections for $^{54, 56, Nat}Fe(n,x)^{51}Cr$, $^{52, 54}Mn$

2.1 $^{54}Fe(n,x)^{51}Cr$, $^{52, 54}Mn$ reactions

According to the analyses of the calculated results for producing activation products, ^{51}Cr and $^{52, 54}Mn$ from $^{56}Fe(n,x)$ reaction, the contribution of the second particle emission can be neglected when $E_n < 20$ MeV. The activation product ^{51}Cr mainly comes from $^{54}Fe(n,\alpha)$ reaction and $^{52, 54}Mn$ come from $^{54}Fe(n,t)$ and $^{54}Fe(n,p)$ reactions below 20 MeV, respectively.

For the cross section of activation product ^{52}Mn from $^{54}Fe(n,t)$ reaction, large discrepancy exists around 14.0 MeV among a few measured data[2~4] at different laboratories. A new relative (ratio between (n,t) and (n,p)) measurement was carried out by Qaim[4] at 14.6 MeV. Our evaluated value

for $^{54}Fe(n,p)$ reaction was combined to renormalize above–mentioned (n,t) experiments, so the discrepancy around 14.0 MeV was removed.

The recommended results for $^{54}Fe(n,x)^{52}Mn$ reaction were taken from theoretical calculation based on experimental data and referred to another knowledge that the measured activation production rates using a deuteron break–up neutron spectrum by Qaim[5] were converted into excitation functions. The recommended data are shown in Fig. 1.

Most of experimental data exist below 20 MeV for $^{54}Fe(n,p)^{54}Mn$. Those experimental data were measured by 36 laboratories. The 14 important experimental data sets[6~19] of them were selected and covered the region from threshold to nearly 20 MeV, and the new data measured by Saraf[19] around 8.0 MeV are more reliable. The calculated data are more closed to the experimental data from 16 to 18 MeV energy region. The recommended cross sections for $^{54}Fe(n,x)^{52}Mn$ reaction are based on the experimental data and adopted theoretical calculated data above 25 MeV, see Fig. 2 .

The 29 experimental data sets for $^{54}Fe(n,\alpha)^{54}Mn$ reaction were measured by different laboratories below 20 MeV. Now selected 14 experimental sets [8~ 12, 14, 18, 19, 21, 25, 26] of them could describe sufficiently the trend for $^{54}Fe(n,\alpha)^{54}Mn$ reaction, and the new one[19] is important to improve the evaluation. The calculated data are closed to the experimental data between 15 and 20 MeV and were used to supplement the scarce data in the higher energy region. Then, cross sections of activation product ^{51}Cr from $^{54}Fe(n,x)$ reaction are recommended and shown in Fig. 3 .

2.2 For $^{56,Nat}Fe(n,x)^{51}Cr$, $^{52,54}Mn$ reaction

Based on some calculated results by Shen Qingbiao et al.[1], the cross sections for monitor reactions $^{56}Fe(n,x)^{51}Cr$, $^{52,54}Mn$ belong to multi–particles emission and the experimental data were very scarce. Therefore, the recommended data come from theoretical calculations. The evaluated cross sections for $^{56}Fe(n,x)^{51}Cr$, $^{52,54}Mn$ reactions were obtained in combination with other available experimental data, such as (n,tot), (n,el), (n,non), (n,2n), (n,γ), (n,d), (n,p), (n,α), (n,t) etc.. Recommended data for $^{56}Fe(n,x)^{51}Cr$, $^{52,54}Mn$ reactions are shown in Fig. 4.

In the evaluation for natural iron, the theoretical parameters of $^{57,58}Fe$ used are the same as ^{56}Fe. The abundances of ^{57}Fe and ^{58}Fe are small, the abundance of ^{54}Fe is larger than $^{57,58}Fe$ and some of its reaction cross sections are very large. Therefore, the effects of ^{54}Fe were considered in evaluation natural iron. At present, the evaluation for $^{54}Fe(n,x)^{51}Cr$, $^{52,54}Mn$ reaction data

mentioned above have been finished, the calculated data for $^{Nat}Fe(n,x)^{51}Cr$, $^{52,54}Mn$ reactions would be corrected by evaluated data of ^{54}Fe. Therefore, the evaluated results of the natural iron are of the sum of the calculated results of $^{56,57,58}Fe$ and the evaluated results of ^{54}Fe multiplied by their abundances, respectively. The recommended data for $^{Nat}Fe(n,x)^{51}Cr$, $^{52,54}Mn$ reactions are shown in Fig. 5.

3 Summary

The cross section for monitor reactions $^{54,56,Nat}Fe(n,x)^{51}Cr$, $^{52,54}Mn$ have been evaluated. The characteristics of the evaluated data are as follows :

1) The present results for $^{54,56,Nat}Fe(n,x)^{51}Cr$, $^{52,54}Mn$ monitor reactions were compared with those of ENDF / B–6 and JENDL–3 below 20 MeV. It was shown that our results could reproduce experimental data very well.

2) The cross sections for monitor reactions $^{54,56,Nat}Fe(n,x)^{51}Cr$, $^{52,54}Mn$ were evaluated based on the experimental data below 20 MeV and the theoretical calculated values[1] of multi–particle emission in higher energies. The model parameters used were determined on the basis of experimental data. Therefore, the recommended data are reliable.

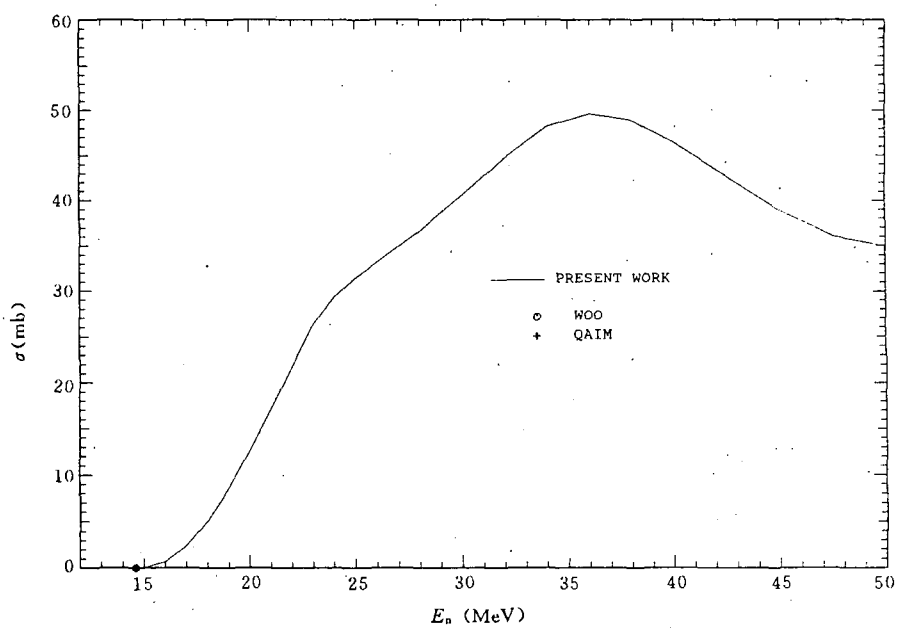

Fig. 1 Comparison among evaluated data with experimental data for $^{54}Fe(n,x)^{52}Mn$ reaction cross section

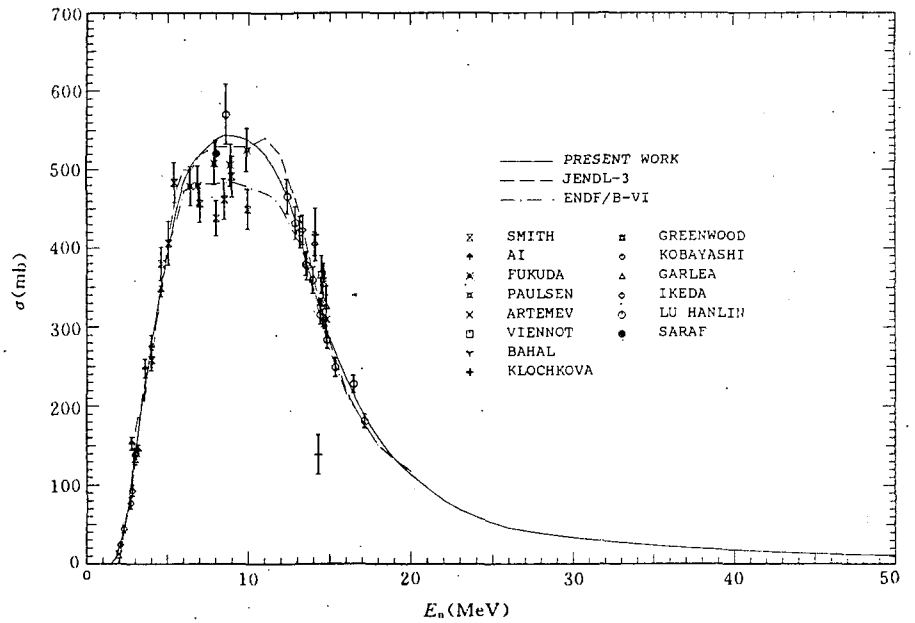

Fig. 2 Comparison among evaluated data with experimental data for $^{54}Fe(n,x)^{54}Mn$ reaction cross section

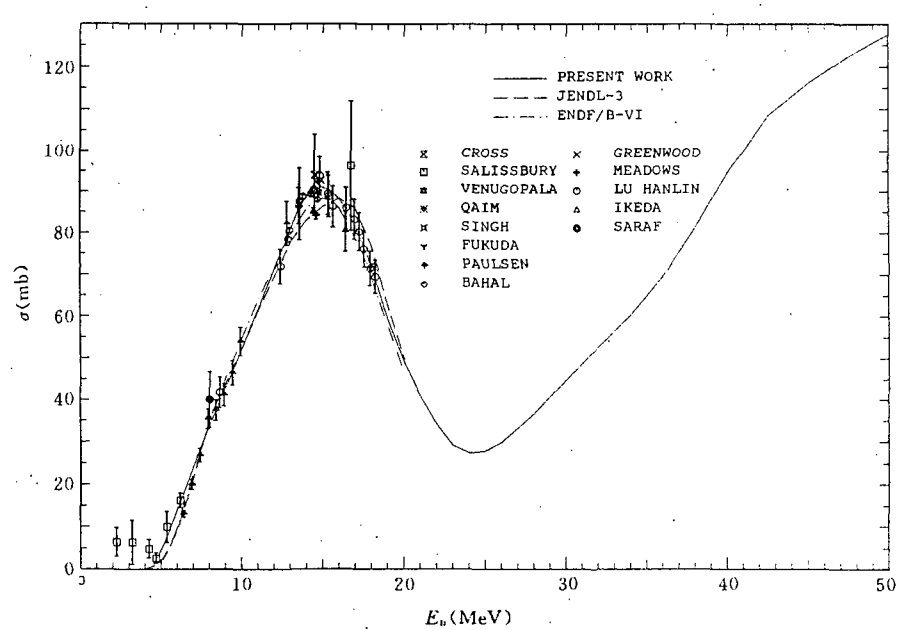

Fig. 3 Comparison among evaluated data with experimental data for $^{54}Fe(n,x)^{51}Cr$ reaction cross section

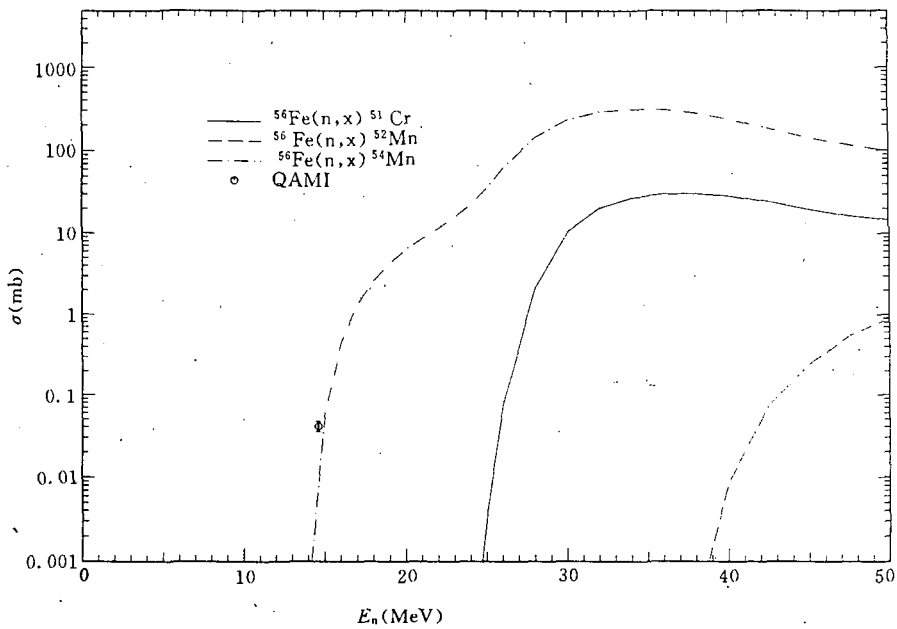

Fig. 4 Recommended data for $^{56}Fe(n,x)^{51}Cr$, $^{52,54}Mn$ reaction cross sections

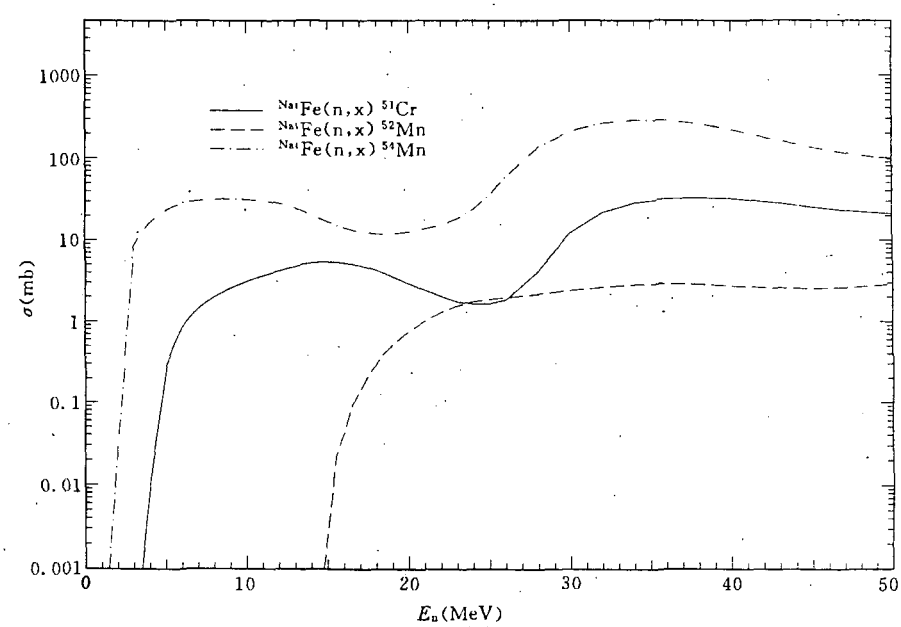

Fig. 5 Recommended data for $^{Nat}Fe(n,x)^{51}Cr$, $^{52,54}Mn$ reaction cross sections

Acknowledgements

The authors are indebted to IAEA, CNNC and CIAE for their supports and thanks to Drs. N. P. Kocherov, Wang Dahai, T. Benson, O. Schwerer, Lu Hanlin and Zhao Wenrong for their kind help and suggestions.

References

[1] Shen Qingbiao et al., CNDP No. 11 (1994)
[2] T. W. Woo et al., Conf. on Nucl. Cross Section for Tech., Knoxvill, p. 853, 1979
[3] A. P. Baerg et al., EXFOR 11542004
[4] S. M. Qaim et al., EXFOR 20522005
[5] S. M. Qaim et al., Nucl. Phys., A295, 150(1978)
[6] D. L. Smith et al., Nucl. Sci. Eng., 58, 314(1975)
[7] C. E. Ai et al., J NSF, 14, 1(1977); EXFOR 30457003
[8] K. Fukuda et al., NEANDC(J)-56 / U, 44(1978)
[9] A .Paulsen et al., Nucl. Sci. Eng., 72, 113(1979)
[10] O. I. Artemev et al., Atomic Energy, 49, 195(1980); EXFOR 88021006
[11] M. Viennot et al., Conf. on Nucl. Data for Sci. and Tech. p. 406, 1982, Antwerp; Nucl. Sci. Eng., 108, 289(1991)
[12] B. M. Bahal et al., GKSS-84-E(1984)
[13] L. I. Klochkova et al., 1987 KIEV, 3, 15(1987); EXFOR 40699010
[14] L. R. Greenwood et al., EOC-ER-0046-21, 15 (1985)
[15] K. Kobayashi et al., Conf. on Nucl. Data for Sci. and Tech., p. 261(1988), 1988 Mito, Japan
[16] I. Garlea et al., ZFK 562, 126(1985)
[17] Y. Ikeda et al., JAERI-1312 (1988)
[18] Lu Hanlin et al., J. Chinese Nucl. Phys., 7, 242(1985)
[19] S. K. Saraf et al., Nucl. Sci. Eng., 107, 365(1991)
[20] Lu Hanlin et al., INDC(CPR)-16 (1989)
[21] W. G. Cross et al., EANDC (CAN)-16 (1963)
[22] S. R. Salisbury at al., Phys. Rev., B140, 350(1965)
[23] P. Venugopala Rao et al., Phys. Rev., 154, 1023(1965)
[24] S. M. Qaim et al., 1971 CANT, 121(1971); EXFOR 20554005
[25] J. J. Singh et al., J. ANS, 15, 147(1972); EXFOR 10309003
[26] J. W. Meadows et al., J. ANE, 14, 489(1987); EXFOR 12969012

A Method for Evaluation of Uncertainties for DDX

Zhao Zhixiang Liu Tong

(Chinese Nuclear Data Center, IAE)

Introduction

The uncertainty information of DDX (double differential cross section) for structural materials such as Fe is significant in fusion reactor applications. Usually, DDX is obtained by a consistent theoretical calculation through adjusting the model parameters to fit the measured data available. By means of study of covariance matrix for the the model parameters, the uncertainty information for DDX could be obtained[1~3]. But This method is limited in practice due to the fact that huge calculations have to be done for sensitivity matrix of the calculated quantities to the parameters. In present work, a simplified method to evaluate uncertainty information of DDX is used on the basis of an analysis of measured DDX and the uncertainty information of DDX obtained in this way can be given in File 36 format suggested by Vonach[4].

1 Method

For many important nuclides, the measured DDX are available for total neutron emission around 14.5 MeV (for example, given by Refs. [5~ 7], 18.0 MeV[7], for total proton emission and alpha emission at 14.8 MeV[8].

Fig. 1 shows a comparison of the total neutron spectrum measured at 14.1 MeV for ^{56}Fe with those calculated by model theory. It is found from Fig. 1 that in the secondary neutron energy region from 3 MeV to 9 MeV, the neutrons mainly come from the contribution of continuum inelastic process, and from 0 MeV to 2 MeV, the (n,2n) reaction is a dominant process. It should be remembered that the uncertainties for elastic and inelastic to discrete levels, which contribute the spectrum above 9 MeV, can be given in file 33 and file 34. Therefore, by fitting measured angular distributions at given secondary neutron energy in the range from 3 MeV to 9 MeV with 3 order Legendre polynomial, the covariance matrix for Legendre coefficients f_0, f_1, f_2 and f_3 of neutron DDX in continuum inelastic process are obtained. Similarly, by fitting measured angular distributions at given secondary neutron energy in the range from

0 MeV to 2 MeV, the uncertainty information can be obtained for (n,2n) reaction. On the assumption that the spectra of both (n,np) and (n,nα) reactions are similar to those given by (n,2n) process in shape. The relative uncertainties of neutron DDX for reactions (n,np) and (n,nα) can be taken as same as those for (n,2n) reaction.The relative uncertainties obtained in this way should be enlarged in the case that the agreement between the evaluated and measured DDX is not so good.

The relative uncertainties for proton and for alpha DDX from (n,p) and (n,np), and from (n,α) and (n,nα) process can also be obtained on the basis of a similar analysis of measured total proton and alpha DDX.

The covariance matrix for Legendre coefficients obtained in this way for 14.8 MeV is used in other energy region where no measured DDX available.

For γ–ray DDX, relative covariance matrix of multiplicity can be given. Defined $M_\gamma(x)$, $\sigma_\gamma(x)$ and $\sigma(x)$ as γ multiplicity, γ production cross section and cross section for x reaction channel, we have

$$M_\gamma(x) = \sigma_\gamma(x) / \sigma(x) \tag{1}$$

and

$$\text{Var}\ (M_\gamma(x)) / M_\gamma^2(x) = \text{Var}\ (\sigma_\gamma(x)) / \sigma_\gamma^2 + \text{Var}\ (\sigma(x)) / \sigma^2(x) \tag{2}$$

Due to the uncertainties of cross sections have been given in File 33, only the relative covariance matrix for γ production cross sections are needed for obtaining uncertainties of γ multiplicities. The relative covariance matrix for γ production cross sections are generated on the basis of a comparison of the sum of production cross sections of several discrete γ–rays between measured values (for example, by Dickens[8]) and calculated by model code. In the energy region in which the agreement between measured and calculated values is good, experimental uncertainties are adopted. Otherwise, the experimental uncertainties are enlarged.

The uncertainties information obtained in the way above can be easily described by using file 36 format suggested by Vonach[4].

2 Typical Results

The method presented above has been used in ^{56}Fe evaluation and uncertainty files for DDX of neutron, proton, alpha and γ emited in (n,2n), (n,p), (n,α), (n,np), (n,nα) reactions and in inelastic process of discrete levels. In

general, the correlations among these coefficients are rather weak (correlation coefficients are usually less than 0.2) and can be neglected. A typical example for (n,2n) reaction at 18 MeV are given in Table 1 and Table 2.

Table 1 Relative error and correlation matrix for E_n = 18 MeV and $E_{n'}$ = 3 MeV

Coef.	STD (%)	Correlation Matrix		
a_0	5.0	100.0		
a_1	38.0	5.3	100.0	
a_2	80.0	−8.7	14.7	100.0

Table 2 Relative error and correlation matrix for E_n = 18 MeV and $E_{n'}$ = 4 MeV

Coef.	STD (%)	Correlation Matrix		
a_0	5.8	100.0		
a_1	34.0	10.8	100.0	
a_2	48.6	−2.4	20.4	100.0

Acknowledgements

The authors would like to thank Dr. Zhou Delin for helpful discussion.

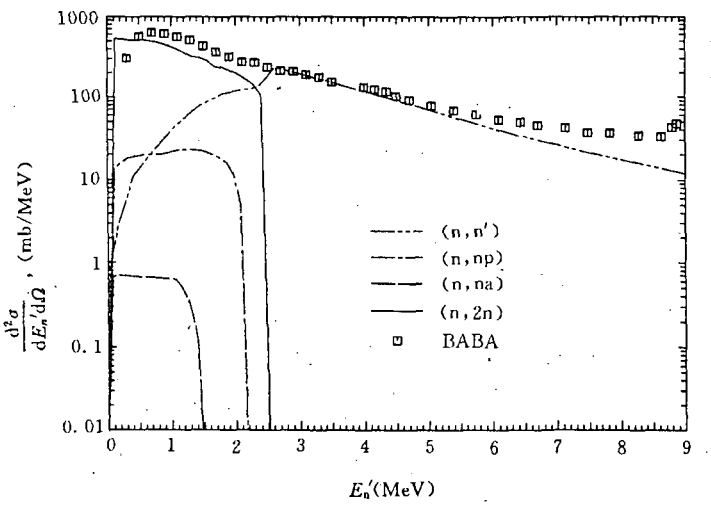

Fig. 1 Secondary neutron spectrum for ^{56}Fe at E_n = 14.1 MeV

References

[1] Zhao Zhixiang et al., ORNL / TM−11672, 1990

[2] R. W. Muir, "Review of Uncertainties in Results of Nuclear Model calculation", H4. SMR614 / 23, 1992

[3] Y. Kanda et al., Rome, p. 98, 1986

[4] H. Vonach, Proc. NEANSC Specialists' Meeting on Covariance Evaluation, ORNL, 1992

[5] O. A. Salnikov et al., YK−7, 102, 1972

[6] A. Takahashi et al., OKTAV−A−83−1, 1983

[7] N. Yabata et al., NETU−47, 1986

[8] J. K. Dickens et al., ORNL / TM−11671, 1990

Nuclear Data Sheets Update for $A = 195$

Zhou Chunmei

(Chinese Nuclear Data Center, IAE)

The 1989 version of Nuclear Data Sheets for $A = 195$[1] has been updated mainly on the basis of the experimental results from the $^{198}Pt(\alpha,xn\gamma)$, ^{195}Bi (from $^{181}Ta(^{20}Ne,6n)$ and $^{185}Re(^{16}O,6n)$) EC decay, $^{181}Ta(^{18}O,xn\gamma)$, $^{186}W(^{15}N,6n\gamma)$, and so on. The detailed level schemes and decay schemes, and experimental reaction and decay data on which they are based are summarized and presented for all nuclides with mass number $A = 195$. The experimental data are evaluated; the inconsistencies and discrepancies are noted; and adopted values for levels and their γ−radiations, as well as for other nuclear properties are presented. The references, spin and parity arguments, and necessary comments are given in the text.

References

[1] Zhou Chunmei, Nuclear Data Sheets, Vol. 57, 1(1989)

Level Spin Assignment of Superdeformed Bands for $A \sim 190$ Region

Zhou Chunmei Liu Tong

(Chinese Nuclear Data Center, IAE)

It is one of the most significant progresses in nuclear spectroscopy in recent years that the nuclear superdeformed (SD) band is discovered experimentally. About 50 superdeformed bands in nuclei with $A \sim 190$, 150, and 130 regions have been observed. But the level spins of SD bands can not be fully determined from the experimental measurements. The level energy formula of nuclear rotational bands can be used to fit transition γ–ray energies within SD band to assign the level spins.

$$E\ (I,K) = E_K + A\ [\ I\ (\ I+1\ )\ ] + B\ [\ I\ (\ I+1\ )\ ]^2 + C\ [\ I\ (\ I+1\ )\ ]^3 + \cdots \qquad (1)$$

where, $E(I,K)$ is the total energy of the level with spin I within K rotational band, E_K is to the energy of the band head, I is the quantum number of the total angular momentum for the intrinsic state, K is the projection of I onto the nuclear symmetry axis, coefficients A, B, and C are fitting parameters.

In order to extend the above rotational model to SD bands the following reasonable assumptions are required :

a) spins of the SD bands can be known as integer or half–integer depending on even or odd of the nuclear mass number A–value.

b) all the gamma transitions within the SD bands have multipolarity $L = 2$, $\Delta I = L = 2$, which can be determined from measurements.

c) spin of the SD band head, I_1, can be considered as quantized fitting parameter under the above conditions.

The least–square fit can be done to the experimental level energies of SD bands by using rotational level energy expression (1), where I_1 is quanti zed fitting–parameter. The correct spin of the SD band head, I_1, can be determinded by means of the minimum of root–mean–square (rms) deviation of experimen-

tal level energies for SD bands and fitting–calculated ones. Therefore, the spin value of the SD band head, I_1, and hence all the spins of the SD band levels can be assigned. Obviously, this fitting procedure is quite simple and straightforward. The level spins extracted from these fits of 27 SD bands in nuclei of $A \sim 190$ region are obtained and compared with those of others.

IV PARAMETER AND PROGRAM LIBRARIES

Progress on Chinese Evaluated Nuclear Parameters Library (CENPL) (III)

Su Zongdi Ge Zhigang Zhou Chunmei Ma Lizhen Chen Zhonglin

(Chinese Nuclear Data Center, IAE)

Liu Jianfeng

(Zhengzhou University)

Huang Zhongfu

(Guangxi University)

Yu Ziqiang Zuo Yixin

(Nankai University)

The setting up work of each sub–library of CENPL has got some new progresses at the past period. They are introduced as follows :

1. Atomic Mass and Characteristic Constant for Nuclear Ground State Sub–Library (CENPL–MCC)

We added the function of retrieving for natural isotopic composition in the management–retrieval code system, i. e. user can retrieve abundance, atomic mass, mass excess,binding energy and spin, parity of ground state of all stable isotopes for an element. The retrieval system can also retrieve the separation energies of neutron, proton, deuteron, triton, ^{3}He, α, 2n and 2p and the decay en-

ergy of β^+ and β^- for an isotopes.

Neutron reaction retrieval system of this sub-library has been finished. With this retrieval system user can get, for a target, the Q value and the threshold energy E_{th} of each reaction channel included in up to the third reaction process. According to retrieved E_{th}, user can choose a code from four type of popular fast neutron codes for model computations, and retrieve the mass of all nuclides required in the input data file of the chosen code.

2. Discrete Level Scheme and Branch Ratio of γ Decay Sub-Library (CENPL-DLS).

The data of DLS sub-library were taken from the Evaluated Nuclear Structure Data File, which is a computer file of evaluated experimental nuclear structure data maintained by the National Nuclear Data Center, Brookhaven National Laboratory. We have defined the data format in the DLS data file. For each level we give its order number, energy, spin, parity and half-life. For γ decay we give the order number of the final state level, the relative transition branch ratio and the multipolarity of γ radiation. The code of transforming format from ENSDF to DLS has been finished and some examples were provided. We are completing the code and setting up the DLS data file.

3. Level Density Parameter Sub-Library (CENPL-LDP)

By means of the moment method, likelihood method and a new method used to give Bayesian estimation provided by Wigner distribution, we have re-evaluated D_0 at the neutron binding energy and obtained the neutron resonance strength function S_0. Based on the work, we set up the file of "Four kinds of experimental data related to level density" (version 1993). This file contains the values of D_0 and the cumulative number of levels N_0 for 332 nuclei from ^{17}O to ^{254}Es, the radiative capture width GW at B_n for 208 nuclei from ^{33}S to ^{280}Bk and the neutron strength function S_0 for 202 nuclei from ^{24}Na to ^{254}Es.

4. Giant Dipole Resonance Parameter for γ-Ray Strength Function Sub-Library (CENPL-GDP)

We have improved and perfected the data file and the management-retrieval system further, which has been provided for using[1].

5. Fission Barrier Parameter Sub–Library (CENPL–FBP)

This sub–library was improved and perfected further, which could be used now[2].

6. Optical Model Parameter Sub–Library (CENPL–OMP)

A data file of global optical model parameters of neutron and charged particle is being built. From this file not only OMP can be retrieved, but also the information and comment on the potential can be got.

The data file of adjusted OMP from CENDL–1, 2 has been set up with dBASE method.

Our following work is to expend the data file and decide the management–retrieval scheme.

Ms. Zhang Limin, Mrs. Jin Yongli, Sun Zhenjun, Zhao Fengquan (CNDC), Drs. Ma Gonggui (Sichuan Univ.), Yao Lishan (Shaanxi Normal Univ.), Zhu Yaoyin (Jilin Univ.) et al. took part in partial work and related activities.

This work is supported by the International Atomic Energy Agency under contract No. 7431 / RB.

References

[1] Zuo Yixin et al., CNDP, 11, (1994)

[2] Zhang Limin et al., CNDP, 10, 88(1993)

The Sub–Library of Giant Dipole Resonance Parameters for γ–Ray (CENPL–GDP–1)

Zuo Yixin

(Department of Mathematics, Nankai University)

Liu Jianfeng Zhang Xizhi

(Department of Physics, Zhengzhou University)

Ge Zhigang Su Zongdi

(Chinese Nuclear Data Center, IAE)

Abstract

The data file and management–retrieval code system of the giant dipole resonance parameter sub–library (CENPL–GDR) are described. Because there are no giant dipole resonance parameters obtained from the experimental data for many nuclei, a treatment method in the management–retrieval code system was presented. Some problem on the giant dipole parameters are discussed in the report.

Introduction

The giant resonance parameters (GRP) of γ–ray strength function characterize the average electromagnetic properties of excited nuclei. Besides their fundamental importance for nuclear structure, γ–ray strength function is an indispensable component for nuclear reaction model calculations too. The giant dipole resonance parameters are necessary and important in the calculations of average radiation widths, radiative capture cross sections, γ–ray production cross sections and γ–ray spectra. Over the years, a considerable body of data on photoneutron cross sections obtained with monoenergetic photons has been acquired at Livermore, Saclay and several other laboratories. In view of the need, these photoneutron cross sections and integrated cross section data obtained

with monoenergetic photons have been compiled by S. S. Dietrich and B. L. Berman[1]. The data in the table of Ref. [1] include the integrated photoneutron yield cross sections, integrated total photoneutron cross sections and the first and second moments of the integrated total cross section. The table also lists the parameters of Lorentz curves fitted to giant dipole resonance. Numerous quantities interested in physics can be derived from these integrated cross sections and giant dipole resonance parameters. For example, they are necessary and important for the calculations of (n,γ) cross section, the other cross sections, γ production cross sections, γ–spectra and so on. In the first version of GDP sub–library of CENPL the giant dipole resonance parameters were collected and the data file of GDPs and the management–retrieval code system was set up. The data file and management–retrieval code system are described in section 1 and 3 respectively. In section 2, the treatment method in management–retrieval code system is introduced when there are no experimental giant dipole parameters in Ref. [1]. Discussion is given in section 4.

1 GDP–1 Data File

(1) Contents

GDR–1 data file, a sub–library of Chinese Evaluated Nuclear Parameter Library (CENPL), contains giant dipole resonance parameters for γ–ray strength function. These parameters of Lorentz curves fitted to the total photoneutron cross section data were compiled by Samuel S. Dietrich and Barry L. Berman[1] for 102 nuclides from ^{51}V to ^{239}Pu in 1987.

(2) Format

Each record of the file contains Z, EL, A, NL, NG, E1, CS1, E2, CS2, REF, LAB and No as defined below :

Z: the charge number, column 1～3;

EL: the element symbol, column 4～6;

A: the mass number, column 7～10;

NL: data set numbers for same nucleus, column 11～13;

NG: for NG = 1, single peak; for NG = 2, double peaks, column 14～16;

E1: the peak energy of the first peak, column 17～23;

CS1: the peak cross section of the first peak, column 24～30;

GW1: the peak full width of the first peak at half–maximum, column 31～36;

E2: the peak energy of the second peak, column 37～43;

CS2: the peak cross section of the second peak, column 44～50;

GW2: the peak full width of the second peak at half–maximum, column 51～56;

REF: the publication reference, bibliographic information is given in a chronological listing following the table, column 57～63;

LAB: the laboratory at which the data were obtained and the experimental method employed, column 64～67.

L Livermore, annihilation photons;

S Saclay, annihilation photons;

GA General Atomic, annihilation photons;

I Illinois, tagged bremsstrahlung.

No: the order number, column 68～71.

2 Treatment Method for Retrieving Giant Dipole Parameters

There are no experimental giant dipole parameters for many nuclei in Ref. [1], and these parameters are necessary in practical calculation of nuclear reaction cross sections. This requirement had been considered, when we set up the GDP–1 management–retrieval code system. The method provided the giant dipole parameters in GDP–1 code system according to different case are as fellows :

(1) If there are the giant dipole parameters for a retrieved nucleus in the GDP data file, the code system will directly retrieve the required ones from the GDP file. If there are several kinds of the giant dipole parameters from different laboratories, the retrieved parameters are the latest ones. (denoted by 'E')

(2) If there is only a set of the giant dipole parameters for some isotope, such as natural isotopic composition or some nucleus of the isotope, this set of parameters can be taken to replace ones of other nucleus, for which there are no giant dipole parameters. (denoted by 'R')

(3) If there are the giant dipole parameters at least two nuclei for same isotope, the parameters will be obtained by interpolation for the others except for the nuclei mentioned above. (denoted by 'I')

(4) A set of recommended systematics formulae as used to calculate the giant dipole parameters for required nucleus, for which there are no giant dipole parameters. After analysis and comparison the following systematic formulae in the sub–library are used[1, 2]:

$$E = 45.0Z^{-1/3}A^{0.05} \qquad (\text{MeV})$$

$$\Gamma = 5.0 \quad (\text{MeV})$$
$$\sigma = 168NZ/(\pi A\Gamma) \quad (\text{mb})$$

where the Lorentz parameters E, Γ and σ are the resonance energy and full width at half–maximum and peak cross section, respectively. (denoted by 'S')

The management–retrieval code system of GDP–1 can retrieve the giant dipole parameters for a single nucleus (SN retrieval) and also for a neutron induced reaction (NR retrieval). The later one can retrieve for all related residual nuclei with possible neutron reactions according to user's choice from three popular fast neutron reaction model codes (i. e. MUP, FUP, UNF and commonly used processing for up to third reaction processes with emissions of γ, n, p and α only).

3 GDP–1 Management–Retrieval Code System and Examples

We take ^{65}Ga, ^{64}Zn as examples for SN retrieval and ^{75}As for NR retrieval respectively, when user runs 'GDP', the following information will be displayed on screen, and then the routine procedures for retrieving:

There are two ways for retrieving :

1. retrieving for a single nucleus; (SN)
2. retrieving for possible residual nuclei in a neutron induced reaction (NR).

Choosing the retrieving way. (SN or NR)
SN (return)
The charge number Z = ?
31 (return)
The mass number A = ? (For natural nucleus A = 0)
65 (return)
Retrieving for other nucleus in this way? (Y or N)
Y (return)
The charge number Z = ?
30 (return)
The mass number A = ? (For natural nucleus A = 0)
64 (return)
Showing the reference? (Y or N)

Y (return)
Retrieving for other nucleus in this way? (Y or N)
N (return)
Continue to retrieve? (Y or N)
Y (return)

If the retrieval mode "NR" is chosen, then the retrieval process is :

Choosing the retrieving calculation code type (1 / 2 / 3 / 4)
3 (return)
The charge number of target Z = ?
33 (return)
The mass number of target A = ?
75 (return)
Retrieving for other nucleus in this way? (Y / N)
N (return)
Continue to retrieve? (Y or N)
N (return)
Print the retrieved parameters? (Y or N)
N (return)
Fortran stop

After the retrieval procedures the retrieved parameters have been put into the output file OUTGDP.DAT :

*** * * * * * * * * Retrieving G D R parameters for SN : * * * * * * ***

	E_1 (MeV)	CS1 (mb)	GW1 (MeV)	E_2 (MeV)	CS2 (mb)	GW2 (MeV)		Z	A
1	16.69	107.0	6.91				R	(31,	65)
2	16.23	41.4	3.27	19.19	56.1	5.98	E	(30,	64)

*** * * Reference : * * ***

2 P. Carlos, H. Beil, R. Bergere, J. Fagot, A. Lepretre,
A. Veyssiere, G. V. Solodukhov, Nucl. Phys., A258, 365(1976).

*** * * * Retrieving G D R parameters for NR : n+(33, 75) in UNF * * * ***

1st reaction process :

E_1 (MeV)	CS1 (mb)	GW1 (MeV)	E_2 (MeV)	CS2 (mb)	GW2 (MeV)	Z	A	Re–Channel
15.23	69.2	4.52	18.24	74.6	7.75	R (33,	76)	(n,γ)
15.23	69.2	4.52	18.24	74.6	7.75	E (33,	75)	(n,n)
15.02	41.7	3.14	17.92	87.7	9.81	I (32,	75)	(n,p)
14.52	23.9	1.92	17.02	102.3	8.18	E (32,	74)	(n,d)
16.61	115.8	7.69				I (32,	73)	(n,t)
16.69	107.0	6.91				R (31,	73)	(n,^{3}He)
16.69	107.0	6.91				R (31,	72)	(n,^{4}He)

2nd reaction process :

E_1 (MeV)	CS1 (mb)	GW1 (MeV)	E_2 (MeV)	CS2 (mb)	GW2 (MeV)	Z	A	Re–Channel
15.23	69.2	4.52	18.24	74.6	7.75	R (33,	74)	(n,2n)
14.52	23.9	1.92	17.02	102.3	8.18	E (32,	74)	(n,2p)
16.69	107.0	6.91				R (31,	71)	(n,n^{4}He)
14.52	23.9	1.92	17.02	102.3	8.18	E (32,	74)	(n,pn)
16.69	107.0	6.91				R (31,	74)	(n,2p)

3rd reaction process :

E_1 (MeV)	CS1 (mb)	GW1 (MeV)	E_2 (MeV)	CS2 (mb)	GW2 (MeV)	Z	A	Re–Channel
15.23	69.2	4.52	18.24	74.6	7.75	R (33,	73)	(n,3n)

4 Discussion

At present, the CENPL–GDP–1 has been set up at CNDC, and users can retrieve the giant dipole parameters for a single nucleus and the fast neutron model computation. In order to obtain a overall understanding on the giant dipole parameters and their variation features with the increase of the mass number, the peak energies, peak full widths at half–maximum and peak cross sections compiled in Ref. [1] and systematic results in Refs. [2] and [3], are plotted in Figs. 1～3 respectively. For the experimental data from Ref. [1] the circle denotes double peaks and the triangle denotes single peak.

The following are noteworthy :

(1) Fig. 1 shows the peak energy from Refs. [1～3] respectively. It is found

from the figure that the calculated results (dashed line) from Zhen–Yang's systematics formula[2] are better than those (full line) from Fuller and Hayward[3] in agreement with the experimental peak energies from Ref. [1] and relative deviation of Zhen–Yang's systematics formula for all nuclei with single peak energies values in Ref. [1] are less than ± 20%. Therefore, Zhen–Yang's systematic formula is used in GDP–1 sub–library.

(2) It seems the peak cross section CS1 from Ref. [1] have shell structure (Fig. 2). The systematics formula (full line) could not agree with the experimental data and for $A < 150$ the systematics results are higher than the experimental one for single peak nuclei. The relative deviation could exceed ± 20% for 50% of the experimental data.

(3) In the Fig. 3 the behavior of GW1 experimental data with the increase of the mass number shows clear shell structure. The systematics formula of Fuller–Hayward can not reproduce GW1 experimental data for single peak. The relative deviation exceed ± 20% for one third of experimental data.

(4) At present the GDP–1 file only includes the systematics for single peak. It needs to be improved for the problems mentioned above.

For GDP–1, we will use the total photoneutron cross–sections data provided by references to get the Lorentz giant dipole parameters for the theoretical calculations.

We will improve the systematics formula for the single peak nuclei and develop a new systematics formula for the double peaks Lorentz giant dipole resonance.

This work is supported by the International Atomic Energy Agency under contract No. 7431 / RB.

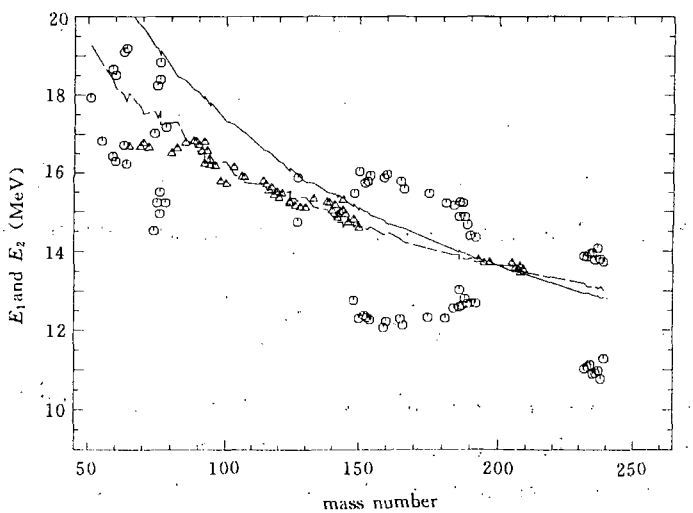

Fig. 1 The variation of peak energy with mass number

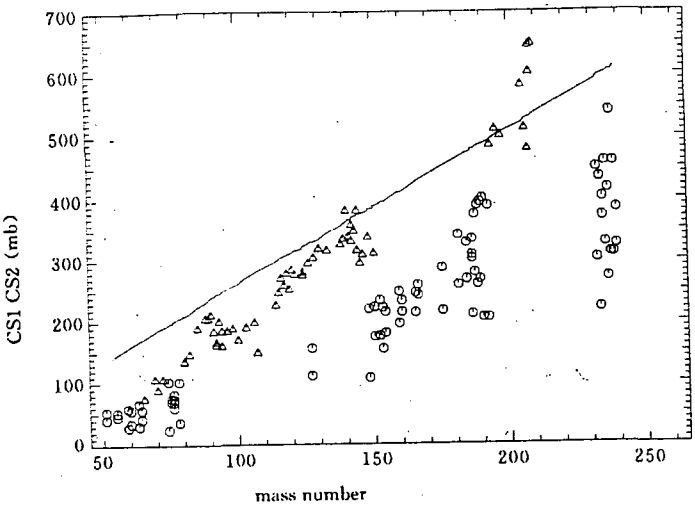

Fig. 2 The variation of peak cross section with mass number

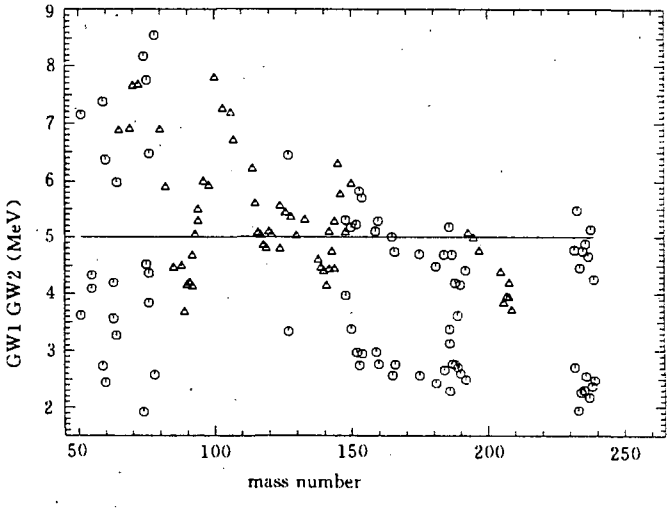

Fig. 3 The variation of peak width with mass number

References

[1] S. S. Dietrich et al., Atomic Data and Nuclear Data Tables, 38, 199(1988)

[2] Zhen Jinyuan et al., Chin. J. of Nucl. Phys., 2, 245(1980)

[3] E. G. Fuller et al., Nuclear Reaction, Vol., 2 113(1962) (Edited by P. M. Smith et al., North-Holland)

Atomic Mass and Characteristic Constant of Nuclear Ground State (CENPL.MCC) (I)

Su Zongdi Ma Lizhen Zhou Chunmei Ge Zhigang

(Chinese Nuclear Data Center, IAE)

Abstract

Atomic mass and characteristic constants for nuclear ground states are basic data for nuclear physics, and necessary ones for basic researches, theoretical calculations, as well as many applied researches. The atomic mass of exotic nuclei quite far from the valley stability are also very important for astrophysics researches. The above–requirement is paid attention to in our setting up this file. The recent and as many as possible data (such as the half–lives of the new nuclides ^{202}Pt, ^{208}Hg and ^{185}Hf and the mass excess of ^{199}Ir, which were produced and distinguished by Chinese scientists) have been collected, and put into the computer–based data file in brief table format.

1 Contents

This data file, which is a sub–library (Version 1) of Chinese Evaluated Nuclear Parameter Library (CENPL), consists of calculated, and in most cases also measured mass excess ME, atomic mass M, total binding energy B, half –life $T/2$ or abundance AB, spin J and parity P of nuclear ground state, etc. of 4800 nuclides ranging from $Z=0$, $A=1$ to $Z=122$, $A=318$. Most of these data were taken from Refs. [1～4], a few of them were collected and complied by us, and M, B were derived from ME.

2 Format

Each record of the file contains Z, EL, A, ME, M, B and $T/2$ or AB, J, P. They are defined as follows :

Z : Charge number, column 1～3.
EL : Element symbol, column 5～6.

A : Mass number, column 8～10.

ME : Mass excess *M*～*A* and its uncertainty, column 13～28.

Most of mass excesses are the experimental data, compiled by A. H. Wapstra et al. (Ref. [1]). An appended "s" denotes that the value is from systematics (see the contribution of Ref. [1]). An appended "t" denotes that the value is the mass excess calculated by P. Moller et al. (Ref. [2]), using a nuclear mass formula with a finite–range droplet model and a folded–Yukawa single–particle potential.

M : Atomic mass and its uncertainty, column 31～48, the meaning of "s", "t" is the same as above.

B : Total binding energy, column 51～60.

T / 2 or *AB* : Half–life or abundance, column 63～80.

These data are given followed by time units ("%" symbol in case of abundance), and then the uncertainty. The uncertainty given is in the last significant figures. For some very short–lived nuclei, level widths rather than half–lives are given, followed by energy units (e. g. eV, keV, or MeV) and then uncertainty if known.

J, *P* : Spin and parity of ground state, column 83～92.

Some examples are given in Table 1.

This work is supported by the International Atomic Energy Agency under contract No. 7431 / RB.

References

[1] A. H. Wapstra et al., At. Nucl. Data Tables, 39, 281(1988)

[2] P. Moller et al., At. Nucl. Data Tables, 39, 225(1988)

[3] Evaluated Nuclear Structure Data File–a computer file of evaluated experimental nuclear structure data maintained by the National Nuclear Data Center, Brookhaven National Laboratory. (File as of March 1991)

[4] N. E. Holden, Table of the Isotopes, 71st edition (1990)

Table 1 Some examples

Z	EL	A	ME (MeV)		M (micro-u)		B (MeV)	T/2 or AB		J	P
0	n	1	8.071	0	1008665	0	0.000	10.4	m	2	1/2+
1	H	1	7.289	0	1007825	0	0.000	99.985	%	1	1/2+
1	H	2	13.136	0	2014102	0	2.224	0.015	%	1	1+
1	H	3	14.950	0	3016049	0	8.482	12.33	a	6	1/2+
1	H	4	25.840	380	4027740	410	5.663				2-
2	He	3	14.931	0	3016029	0	7.718	0.000137	%	3	1/2+
2	He	4	2.424	0	4002602	0	28.297	99.999863	%	3	0+
.	.	.	.	.	.	.	.	.	.		
26	Fe	47	-8.402 t		46990980 t		367.416 t				
26	Fe	48	-18.130	110	47980537	120	385.215				0+
26	Fe	49	-24.580	160	48973612	170	399.736	75	ms	10	(7/2-)
26	Fe	50	-34.470	60	49962995	60	417.698				0+
26	Fe	51	-40.217	15	50956826	20	431.516	310	ms	5	(5/2-)
26	Fe	52	-48.331	10	51948115	10	447.701	8.275	h	8	0+
26	Fe	53	-50.943	2	52945311	0	458.385	8.51	m	2	7/2-
26	Fe	54	-56.250	1	53939614	0	471.763	5.9	%	2	0+
26	Fe	55	-57.476	1	54938297	0	481.060	2.73	a	3	3/2-
26	Fe	56	-60.603	1	55934941	0	492.259	91.72	%	15	0+
26	Fe	57	-60.178	1	56935397	0	499.905	2.1	%	1	1/2-
26	Fe	58	-62.151	1	57933279	0	509.950	0.28	%	2	0+
26	Fe	59	-60.661	1	58934878	0	516.531	44.496	d	7	3/2-
26	Fe	60	-61.406	4	59934078	0	525.347	1.5E+6	a	3	0+
.	.	.	.	.	.	.	.	.	.		
92	U	225	27.729 t		225029768 t		1716.354 t	50	ms	30	
92	U	226	27.170	30	226029168	30	1724.984	0.5	s	2	0+
92	U	227	28.970 s	110 s	227031100 s	120 s	1731.256 s	1.1	m	3	
92	U	228	29.209	16	228031357	20	1739.088	9.1	m	2	0+
92	U	229	31.181	9	229033474	10	1745.187	58	m	3	(3/2+)
92	U	230	31.600	6	230033924	10	1752.840	20.8	d		0+
92	U	231	33.780	50	231036264	50	1758.731	4.2	d	1	(5/2-)
92	U	232	34.587	4	232037130	0	1765.995	68.9	a	4	0+
92	U	233	36.915	3	233039630	0	1771.739	1.592E+5	a	2	5/2+
92	U	234	38.141	2	234040946	0	1778.584	0.0055	%	5	0+
92	U	235	40.915	2	235043924	0	1783.882	0.720	%	1	7/2-
92	U	236	42.441	2	236045562	0	1790.427	2.3415E7	a	14	0+
92	U	237	45.387	2	237048725	0	1795.552	6.75	d	1	1/2+
92	U	238	47.305	2	238050784	0	1801.706	99.2745	%	15	0+
92	U	239	50.570	2	239054289	0	1806.512	23.50	m	5	5/2+
92	U	240	52.711	5	240056587	10	1812.442	14.1	h	1	0+
92	U	241	55.849 t		241059956 t		1817.376 t				
.	.	.	.	.	.	.	.	.	.		
122		317	255.372 t		317274151 t		2207.807 t				
122		318	257.518 t		318276455 t		2213.732 t				0+

UNFTOOLS – An Auxiliary Plotting Code of UNF Code and the Intercomparison of the Double Differential Cross Section for ^{56}Fe

Liu Tong Zhao Zhixiang Zhang Jingshang

(Chinese Nuclear Data Center, IAE)

Introduction

During the years from 1990 to 1992, the code UNF was already developed by Zhang Jingshang[1]. In the recent years, this code has been widely used to calculate the fast neutron data. As we know, in order to do a consistent calculation for neutron induced data, the evaluator must compare the calculated cross sections, angular distributions, energy spectra, as well as the double differential cross sections with the experimental and the other evaluated data. To perform the comparison, a lot of pictures must be plotted. Some of them have to be plotted many times. But the evaluator can not plot them directly from the output files (UNF.OUT, PLO.OUT) of UNF code, especially for the double differential cross sections. In order to help evaluator to use UNF more conveniently, an auxiliary code, UNFTOOLS, was developed and used to do the intercomparison. In this paper the functions of the UNFTOOLS code are introduced. As an example, some pictures of n + ^{56}Fe are given.

1 The Functions of UNFTOOLS and Some Examples

UNFTOOLS has the following main functions : plotting the curves of cross section, spectrum and double differential cross section directly from the UNF output (UNF.OUT or PLO.OUT); plotting simultaneously the experimental data in comparison with those calculated by UNF code; plotting the evaluated neutron nuclear data in ENDF / B format (Only for MF = 3 and MF = 4).

UNFTOOLS is developed on MICRO–VAX–II, and has been converted to PC–486 (DOS 3.3, NDP 2.1). If a VT240, VT340, or a PC terminal is available, the user can see the picture on the screen easily, and can also adjust the

position of note easily by using the "arrow key". The user's manual and the code can be obtained from the authors.

The evaluation of neutron induced data on ^{56}Fe has been completed[2] on the basis of a consistent theory calculation by means of UNF code. During the evaluation, UNFTOOLS has been used to compare the UNF result with the experimental data and the evaluated data from other nuclear libraries. The functions of UNFTOOLS are shown in detail by means of the examples of intercomparison of double differential cross sections for n+^{56}Fe.

1.1 Cross Section

Plotting the cross section of each reaction channel.

1.2 Gamma Production Cross Sections

UNF code has the function to output the γ–production cross section between two levels, they can be plotted by UNFTOOLS.

1.3 Particle Production Cross Sections

Plotting the particle production cross section (Only for γ, neutron, proton, α, ^{3}He, deuteron, triton).

1.4 Energy Spectrum at Given Angle

Plotting the double differential cross sections at given angle. Two typical examples for this function are shown in Figs. 1 and 2. (The result in ENDF / B–6 format is obtained from DDXB1[3] code).

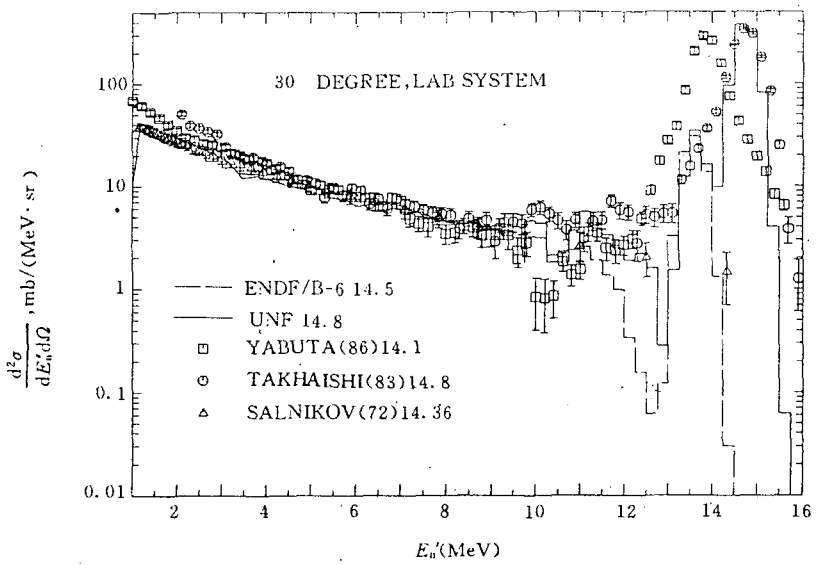

Fig. 1 Comparison of neutron emission spectrum with the experimental data and the data of ENDF / B-6 library for n+^{56}Fe

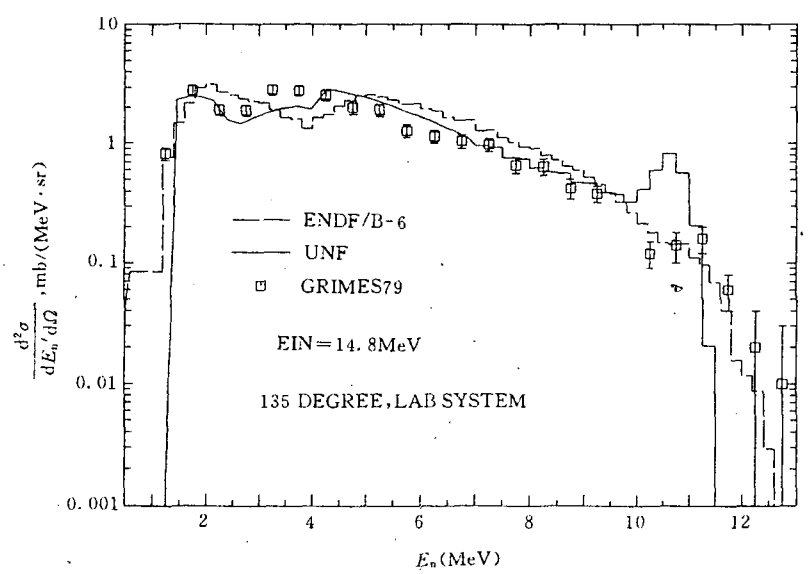

Fig. 2 Comparison of proton emission spectrum with the experimental data and the data of ENDF / B-6 library for n+^{56}Fe

1.5 Angular Distribution at Given Secondary Energy

Plotting the differential cross section at given secondary energy. An example for this case is shown in Fig. 3.

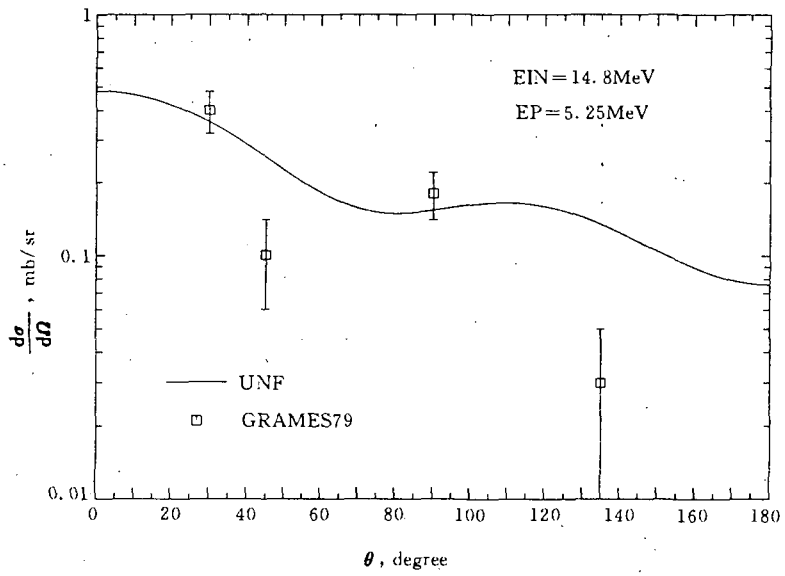

Fig. 3 Comparison of deuteron emission angular distribution with the experimental data for n+^{56}Fe

1.6 Spectrum for Particle Production

Plotting the total alpha production spectrum (integrated over angles). In Fig. 4, it can be seen that the UNF result is consistent with the experimental data.

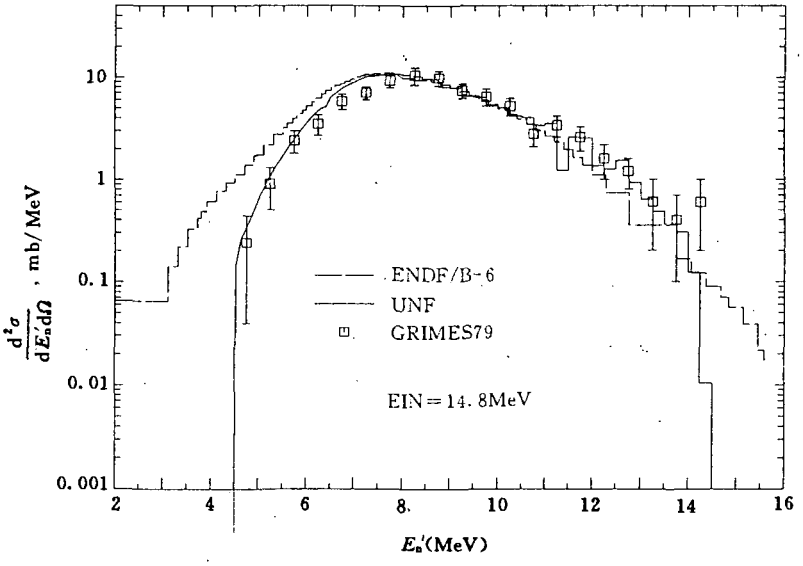

Fig. 4 Comparison of alpha emission spectrum with the experimental data and the data of ENDF / B–6 library for n+^{56}Fe in CM system

In the functions 4 ~ 6, LAB system or CM system can be selected according to the experimental data.

2 Some Special Treatments

2.1 Spectrum of the Discrete Levels

The spectrum of each discrete levels is extended by Gauss function and summed up together in the energy bin to make the histogram.

$$P(E)=\frac{1}{\sqrt{2\pi}\,\sigma}\ \exp\left\{-\frac{(E-E_0)^2}{2\sigma^2}\right\}$$

Where σ is a adjustable parameter. If the default value (0.2 MeV) does not fit the experimental data very well, the user can adjust it very easily. E_0 is the emission particle energy to the discrete level.

2.2 Transformation Between Two Coordinate Systems

From CM system to LAB system, it must be emphasis that the forbidden angular region for some outgoing energy exist[4]. UNFTOOLS takes it into account.

3 The Merit and Bugs of UNFTOOLS

3.1 This code adopted the "Input card" and the interactive mode together, so it can be used and learned easily.

3.2 UNFTOOLS is independent with the plotting facilities, so the user can easily convert the code to the plotting device themselves.

3.3 Up to now, UNFTOOLS can directly compare the ENDF / B library data only for MF = 3 and MF = 4. In order to compare the other files of ENDF / B library, the user must use other code first. (DNFTOOLS will be extended to other files of ENDF / B library in the future if necessary).

Acknowledgement

The authors would like to thank IAEA for their support under a CRP contract No. 7048 / R1 / RB, and Dr. Zhang Jin for using his unpublished plotting library, and Dr. Tang Guoyou for his helpful advices.

References

[1] Zhang Jingshang, Nucl. Sci. & Eng., 114, 55(1993)

[2] Zhao Zhixiang et al., CNDP No. 11 (1994)

[3] Zhang Jin et al., Programming in Standard FORTRAN 77, Program Library in CNDC, 1993

[4] Zhang Jingshang et al., CNDP No. 9, 17(1993)

Management Program System of Chinese Evaluated Nuclear Decay Database

Huang Xiaolong Zhou Chunmei

(Chinese Nuclear Data Center, IAE)

Abstract

The organization structure of Chinese Evaluated Nuclear Decay Database and its management program system are presented briefly.

Introduction

The nuclear decay data and their decay drawing of radioactive nuclides (called as nuclear decay data for short) are very useful and important nuclear data. They are basic data for nuclear engineering design and nuclear technical application, and widely used in the fields of industry, agriculture, geology, prospecting, biology, medicine, environmental protection, energy development, and other science researches. It can be anticipated that their applications will be more and more in the future.

The Chinese Evaluated Nuclear Decay Database[1] is set up according to the relevant user's needs. Being based on the Chinese evaluated nuclear decay data developed before and having refered to the international recent measured and evaluated ones, revising, updating, adding, correcting of the evaluated decay data have been done and then radioactive nuclear decay data in this library are recommended and stored in MICRO-VAX-II computer at CNDC (Chinese Nuclear Data Center) with ENSDF[2] data format (about forty-five thousand records included). More than 300 radioactive nuclides (which include fission-product nuclides, transactinium nuclides, structure material nuclides, and X- and γ-ray standard nuclides for detector calibration) and their relevant data (decay mode, half-life, ray energy and intensity, branching ratio, internal conversion coefficient, level energy, spin and parity, and so on) are comprised in this library. They are very frequently used in practice. The management program system has been written and completed in order to manage well the library and be convenient to the users. Using this management

program system, the decay data in A–chain, in one nuclide of A–chain or one nuclide with special decay mode in A–chain can be convenient to be updated, added, deleted, checked in data format and physics contents; meanwhile, it also can be output to the terminal screen, printer, diskette in original–input data format, and listing data table or plotting decay drawing.

1 Fundamental Structure of Database

The ENSDF data format is adopted in the database. The decay data sets are arranged in the order of mass number A from low to high in Chinese Evaluated Nuclear Decay Database. Each A–number corresponds to a few ${}^{A}_{Z}X$ nuclides, moreover, each ${}^{A}_{Z}X$ nuclide also has its corresponding decay data set. In general, for decay data set of every ${}^{A}_{Z}X$ nuclide, the following contents may be embodied : (1) identification card (recording the mass number and element symbol of daughter–nuclide and parent–nuclide, parent nuclide decay mode, etc.); (2) a brief comment of experimental conditions and measured data; (3) a brief comment of choosing "best" data; (4) comment of data analysis and calculation; (5) the data set body with numeric data card (including P, N, L, G, E, A and B cards, etc.); (6) blank line (end of data set).

2 Management of Database

The management program system is written in order to manage the library well and be convenient for users.

2.1 Main Programs and Functions

The main programs and their functions for the management program system of database are listed in Table 1 and shown in Fig. 1. The management program system is written in standard FORTRAN–77 and stored in MICRO–VAX–II computer at CNDC.

Table 1 The programs and functions of the management system

Code	main functions
FMTCHK*	checking data in format
PANDOR*	checking data in physics
NSDSC	establishing database
NSDCC	changing data from binary system to decimal system
NSDDC	deleting data
NSDUC	updating data
NSDAC	adding data
NSDRC	retrieving data
NSDIN	setting up index file for database
TREND*	listing data table
PREND*	plotting decay diagram

* transplanted

2.2 Adding and Deleting

The decay data set to be added must be checked in format and physics contents before put into database. To add data into database may be completed by running the code NSDAC after passing through checking. There are three choices in code NSDAC. First, if the decay data in A–chain to be added, the mass number of parent nuclide is input; secondly, when the decay data in one nuclide of A–chain to be added, the mass number and element symbol of parent nuclide must be input; and finally, while the decay data in one nuclide with special decay mode in A–chain to be added, the mass number, element symbol and decay mode of parent nuclide should be input. Similarly, as to deleting relevant data in database, there is also three choices identical to code NSDAC in code NSDDC.

2.3 Updating

Whenever the newly measured and / or evaluated decay data are received and the decay data in database must be updated, the code NSDUC may be

used. To update the decay data, the following steps can be adopted : the decay data set to be updated will be retrieved from database by running code NSDRC[3] first; and then deleted from database by running code NSDDC; finally, it is added to database by running code NSDAC after correcting and passing through checking data format and physics. There is two functions in code NSDUC : at first, to update all decay data sets in A–chain; and secondly, to update decay data set in one nuclide (including the decay data set in one nuclide with special decay mode) under A–chain.

References

[1] The Chinese Evaluated Nuclear Decay Database, Chinese Nuclear Data Center, 1993

[2] K. T. Jagdish, Evaluated Nuclear Structure Data File, BNL–NCS–51655, 1987

[3] Huang Xiaolong et al., The Retrieval Program of Chinese Evaluated Nuclear Decay Data File, Atomic Energy Science and Technology, to be published, 1994

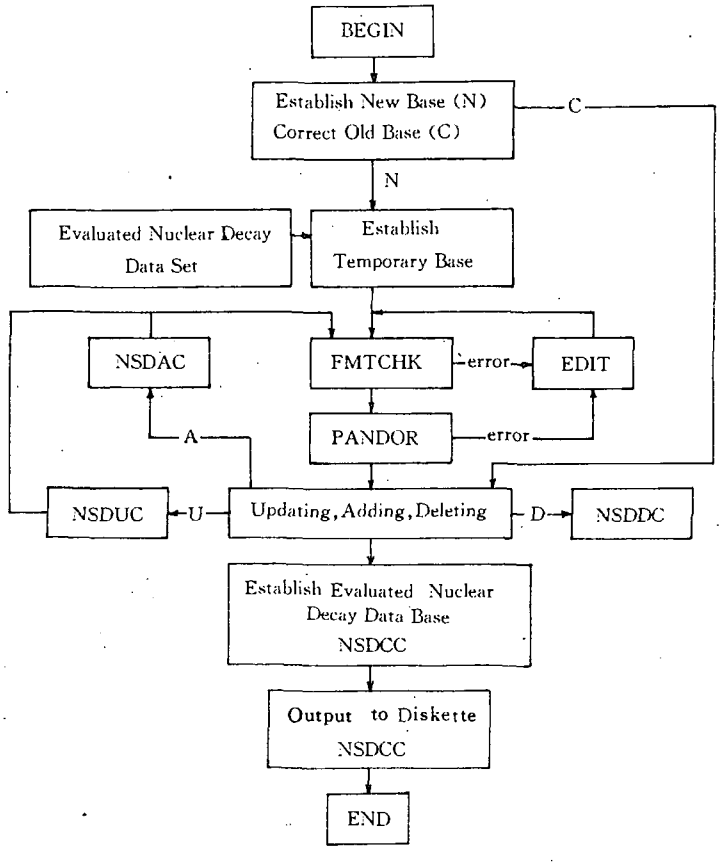

Fig. 1 A schematic diagram of management system for evaluated nuclear decay data file

V DATA PROCESSING

The Spline Fitting for Multi–Sets of Correlative Data

Liu Tingjin

(Chinese Nuclear Data Center, IAE)

Zhou Hongmo

(Nankai Univ., Tianjin)

There are many works on spline function fit[1~3], but they all do not take account of the correlation of the data.

Keeping the main features of our early work[3] (any order spline as base, knot optimization and accurate calculation of the error for fit values), this paper is its development, aimed at dealing with multi–sets of correlative data. The formulas were deduced (section 1, 2), the program was developed, the correctness of the program was tested (section 3), the effects of the correlation on fit values were studied, and some problems concerned were discussed (section 4).

1 Spline Fit for Multi–Sets of Correlative Data

Suppose there are R sets of correlative data

$$\{ x_i^{(r)}, y_i^{(r)}, \sigma_r \} \qquad r = 1, 2, \cdots, R, \quad i = 1, 2, \cdots, L_r \tag{1}$$

and their covariance matrixes for each set of experimental data :

$$V^{(r)} = \begin{bmatrix} V_{11}^{(r)} & V_{12}^{(r)} & \cdots & V_{1L_r}^{(r)} \\ V_{21}^{(r)} & V_{22}^{(r)} & \cdots & V_{2L_r}^{(r)} \\ \cdots & \cdots & \cdots & \cdots \\ V_{L_r^1}^{(r)} & V_{L_r^2}^{(r)} & \cdots & V_{L_r L_r}^{(r)} \end{bmatrix} \qquad r = 1, 2, \cdots, R \tag{2}$$

where foot–note r means r–th set of experimental data, $y_i^{(r)}$ are the measured values at (for example, incident energy) $x_i^{(r)}$, L_r is the number of r–th set of data. σ_r is the width of r–th set of data, characterized its systematical error (called reliable degree in Ref. [1]). In the practice, σ_r could not be given by the experimentors, but by the evaluators, who collect all of R sets of measured data and compared them with each other.

Let W be the inverse matrix of V (weight matrix)

$$W_r = V_r^{-1} \qquad r = 1, 2, \cdots, R \tag{3}$$

and b_r is the systematical deviation of the r–th set of data from the expected value.

Now, take the extended knot partition of the spline function as

$$t_1 \leqslant \cdots \leqslant t_K \leqslant t_{K+1} \leqslant \cdots \leqslant t_N < t_{N+1} < t_{N+K} \tag{4}$$

So the spline function $S(x)$ can be expressed uniquely as

$$S(x) = \sum_{n=1}^{N} C_n B_n(x) \tag{5}$$

where $B_n(x)$ ($n = 1, 2, \cdots, N$) are normal B–spline functions with knots (4) (see Ref. [2]).

Because $y_i^{(r)}$ are measured data,

$$y_i^{(r)} - S(x_i^r) \tag{6}$$

is a Gauss random variable with mathematical expected value b_r and variance

$V_{ii}^{(r)}$.

The joint probability density of the multi-dimension random variable, consisting of random variables b_1, b_2, ···, b_R and random variable group (6), can be expressed as (a constant factor was omitted) :

$$F = \exp\left[-(1/2)\sum_{r=1}^{R}\sum_{i=1}^{L_r}\sum_{j=1}^{L_r}(y_i^{(r)} - S(x_i^r) - b_r) \times W_{ij}^{(r)}(y_j^{(r)} - S(x_j^{(r)}) - b_r) - (1/2)\sum_{r=1}^{R}(b_r/\sigma_r)^2\right] \tag{7}$$

where $W_{ij}^{(r)}$ is the element of matrix W_r.

Based on the maximum like-hood principle, it can be got that

$$b_r = \sum_{j=1}^{L_r}(y_j^{(r)} - S(x_j^r))/d(r) \quad (r = 1, 2, \cdots, R) \tag{8}$$

where

$$d(r) = \sum_{i=1}^{L_r}\sum_{j=1}^{L_r} W_{ij}^{(r)} + 1/\sigma_r^2 \quad (r = 1, 2, \cdots, R) \tag{9}$$

and the normal equation group, which determine the fit coefficients :

$$\sum_{n=1}^{N} A_{mn} C_n = R_m \tag{10}$$

$$A_{mn} = \sum_{r=1}^{R}\{[\sum_{i=1}^{L_r}\sum_{j=1}^{L_r} W_{ij}^{(r)} B_m(x_j^r)][\sum_{i=1}^{L_r}\sum_{j=1}^{L_r} W_{ij}^{(r)} B_n(x_j^r)]/d(r) - \sum_{i=1}^{L_r}\sum_{j=1}^{L_r} W_{ij}^{(r)} B_m(x_j^r) B_n(x_i^r)\}$$

$$(m, n = 1, 2, \cdots, N) \tag{11}$$

$$R_m = \sum_{r=1}^{R} \left[\sum_{i=1}^{L_r} \sum_{j=1}^{L_r} W_{ij}^{(r)} y_j^{(r)} \right] \left[\sum_{i=1}^{L_r} \sum_{j=1}^{L_r} W_{ij}^{(r)} B_m (x_j^r) \right]$$

$$/ d(r) - \sum_{i=1}^{L_r} \sum_{j=1}^{L_r} y_i^{(r)} W_{ij}^{(r)} B_m (x_j^r) \quad (m = 1, 2, \cdots, N) \tag{12}$$

From the linear Equation group (10), the coefficients can be solved. So, the fit spline function $S(x)$ can be calculated with Eq. (5).

2 The Covariance of the Fit Values

For convenience's sake, the Equation group (10) can be written in the matrix form.

Let

$$C = \left[c_1 \quad c_2 \quad \cdots \quad c_N \right]^{\mathrm{T}}$$

$$Y = \left[y_1^{(1)} \quad y_2^{(1)} \quad \cdots \quad y_{L_1}^{(1)} \quad \cdots \quad y_1^{(R)} \quad y_2^{(R)} \quad \cdots \quad y_{L_R}^{(R)} \right]^{\mathrm{T}}$$

$$D = \begin{bmatrix} d(1) & 0 \\ \cdots & \cdots \\ 0 & d(R) \end{bmatrix}$$

$$W = \begin{bmatrix} W_1 & 0 \\ \cdots & \cdots \\ 0 & W_R \end{bmatrix}$$

$$U=\begin{bmatrix} U_1^{(1)} & \cdots & U_{L_1}^{(1)} & 0 & \cdots & \cdots & \cdots & \cdots & 0 \\ 0 & \cdots & 0 & U_1^{(2)} & \cdots & U_{L_2}^{(2)} & 0 & \cdots & 0 \\ \cdots & \cdots & \cdots & \cdots & \cdots & \cdots & \cdots & \cdots & \cdots \\ 0 & \cdots & \cdots & \cdots & \cdots & \cdots & U_1^{(R)} & \cdots & U_{L_R}^{(R)} \end{bmatrix}$$

where

$$U_j^{(r)} = \sum_{i=1}^{L_r} W_{ij}^{(r)} \qquad (r=1, 2, \cdots, R, \quad j=1, 2, \cdots, L_r)$$

Also let

$$B = \begin{bmatrix} B_1^{(1)}(x_1) & \cdots & \cdots & B_N^{(1)}(x_1) \\ \cdots & \cdots & \cdots & \cdots \\ B_1^{(1)}(x_{L_1}) & \cdots & \cdots & B_N^{(1)}(x_{L_1}) \\ \cdots & \cdots & \cdots & \cdots \\ B_1^{(R)}(x_1) & \cdots & \cdots & B_N^{(R)}(x_1) \\ \cdots & \cdots & \cdots & \cdots \\ B_1^{(R)}(x_{L_R}) & \cdots & \cdots & B_N^{R}(x_{L_R}) \end{bmatrix}$$

$$E = B^{\mathrm{T}} (W - U^{\mathrm{T}} D U)$$

In this case, the Equation group (10) can be written as

$$A C = Y^{*} \tag{13}$$

where

$$A = E B \tag{14}$$

$$Y^{*} = E Y \tag{15}$$

So the vector C can be expressed as

$$C = A^{-1} Y^{*} \tag{16}$$

Note, the covariance matrix of Y is

$$V_Y = \begin{bmatrix} V_1 & \cdots & 0 \\ \cdots & \cdots & \cdots \\ 0 & \cdots & V_R \end{bmatrix}$$

From Eq. (15), the covariance matrix of Y^{*} can be got

$$V_{Y^{*}} = E V_Y E^{T}$$

Similarly, the covariance matrix of vector C is

$$V_C = A^{-1} V_{Y^{*}} (A^{-1})^{T} \tag{17}$$

So, the covariance matrix of fit values is

$$V_S = B V_C B^{T} \tag{18}$$

From Eq. (18), it can be seen that the variance V_x of the fit value at any point x is

$$V_x = B_x V_C B_x^{T} \tag{19}$$

where

$$B_x = [\, B_1(x) \; B_2(x) \; \cdots \; B_N(x) \,]$$

and the covariance matrix V_L of the fit values at any L points (x_1, x_2 , ···, x_L) is

$$V_L = B_L V_C B_L^{T} \tag{20}$$

where

$$B = \begin{bmatrix} B_1(x_1) & B_2(x_1) & \cdots & B_N(x_1) \\ \cdots & \cdots & \cdots & \cdots \\ B_1(x_L) & B_2(x_L) & \cdots & B_N(x_L) \end{bmatrix}$$

3 Program

According to the basic theory and method discussed above, a practical program SPC was developed. In principle, any number of data sets and any number of data points can be dealed with by the program, it is only limited by the computer used.

In the program the main features of our early program SPD[3] were kept,that is the order of spline function can be selected as base to fit various shape curves, the knot can be optimized automatically. Meanwhile, the program was developed to deal with multi–sets of correlative data. It is supposed that there are correlations among different data points of each set of data, but no correlations among different data sets. For the curve fitting of correlative data, in some cases, for example there are large discrepancies among different data sets and strong correlation among data points, so called PPP problem[4] may happen, some methods are offered in the program to deal with this kind of problems (discussed in detail in section 4).

Three input data files are necessary to run the program, one is for experimental data to be fitted, another is for fit parameters, like knots, output data points etc., and the other is for covariance matrix of input experimental data. For convenience, the input covariance matrix is allowed in different form: absolute, relative covariance matrix or correlation coefficients, and if some elements are the same, it is only needed to input one. The fit values and their covariance matrix are output in ENDF / B format. In addition, the covariance matrix of fit values in different form and some fit parameters, e. g. new knots and reduced χ^2 etc., are also output.

The correctness of the program has been tested in various ways. Firstly, the program is used for correlative data, no correlation is only its special case (the correlation coefficients are zero), which is just the case dealt with by our early program SPD. So, when the correlation coefficients or the nodiagonal elements of covariance matrix are zero, the results got with SPC and SPD should be the same, in fact it is true (the methods dealing with the matrix are completely different in two codes). Secondly, taken some sets of input data, which are around a constant, and select the fit parameters appropriately, a horizontal fit curve (the same fit values) can be got. Taken this same set of input data and regards them as at same selfvariable points,the weighted mean was got with our another code. The two calculations show that the constant fit values are the same as weighted mean. This is quite reasonable. Thirdly, the correctness of the program also can be seen from many examples calculated (which will be dis-

cussed in detail below).

4 Examples and Discussions

1) Example 1

Input two sets of data

x	1.0	2.0	3.0
y_1	1.2	2.2	3.2
y_2	0.8	1.8	2.8

take the order of spline $K=$ 1; 2 knots (1.0, 3.0), iteration time (for knot optimization) $T = 1$.

1 – 1 $$V_1 = V_2 = \begin{bmatrix} 0.01 & 0.009 & 0.009 \\ & 0.01 & 0.009 \\ & & 0.01 \end{bmatrix}$$

$$\sigma_1 = \sigma_2 = 1.0$$

1–2 $\sigma_1 = 0.1$, others are the same as (1–1)

1–3 $\sigma_1 = 0.01$, others are the same as (1–1)

1 – 4 $$V_2 = \begin{bmatrix} 0.01 & 1.0 \times 10^{-6} & 1.0 \times 10^{-6} \\ & 0.01 & 1.0 \times 10^{-6} \\ & & 0.01 \end{bmatrix}$$

others are the same as (1 – 1)

1 – 5 $$V_1 = \begin{bmatrix} 1.0 & 0.9 & 0.9 \\ & 1.0 & 0.9 \\ & & 1.0 \end{bmatrix}$$

$$V_2 = \begin{bmatrix} 1.0 \times 10^{-6} & 0.0 & 0.0 \\ & 1.0 \times 10^{-6} & 0.0 \\ & & 1.0 \times 10^{-6} \end{bmatrix}$$

others are the same as (1 – 1)

The calculated results are given in Table 1 and Fig. 1, from which it can be seen that :

(1) In the conditions of $\sigma_1 = \sigma_2$ and $V_1 = V_2$, the fit values are the arithmetical mean of the data as they were at the same x points;

(2) If $V_1 = V_2$ but $\sigma_1 < \sigma_2$, the fit values are close to data set 1 (the σ_1 smaller, the more close);

(3) If $\sigma_1 = \sigma_2$ but $V_2 < V_1$ (the elements of V_2 are smaller than the corresponding elements of V_1), the fit values are close to the data set 2 (the V_2 smaller, the more close);

All of these are reasonable in physics. In the case (1), the weights are equal, two sets of data were measured with same accuracy. In the case (2), the data set 1 was measured with higher accuracy. And in the case (3), the data set 2 was measured with higher accuracy.

2) Example 2

Let $V = [\ V_{ij}\ ]$, $R = [\ r_{ij}\ ]$ are absolute covariance matrix and correlation coefficient matrix respectively and Δy are the standard errors of data y_i, then $V_{ij} = r_{ij} \times \Delta y_i \times \Delta y_j$, so instead of absolute covariance matrix, the correlation coefficient matrix and standard error can be input. For convenience's sake, suppose all the elements of the correlation coefficient matrix are the same, e. g. $r_{ij} = r$ ($i \neq j$).

Input one set of data :

x_i	0.8	1.0	2.3	3.4	4.5	7.4	8.8	9.7
y_i	19.0	30.0	27.0	41.0	52.0	53.0	63.0	78.0
Δy_i	5.7	9.0	8.1	12.3	15.6	15.9	18.9	23.4

The order of spline function $K = 1$, two knots (0.8, 9.7), width $\sigma = 1.0$ and iteration time $T = 1$ are taken.

The fit values are shown in Table 2 and Fig. 2, from which it can be seen that when the correlation coefficient becomes larger, the fit values become smaller, the coefficient larger, the values smaller, and, finally, the fit values deviate from the experimental data, PPP problem happens. It should be noted that the mathematical expected values should be used in the construction of covariance matrix of experimental data, but, usually, instead of them the measured data are used directly[7]. When the measured data are consistent with each other, this is a quite well approximation, but when there are larger discrepancy and strong correlation, the problem becomes serious. Based on this basic idea, two ways are offered to solve the problem in the program.

(1) Correct original input covariance matrix

Iteration method is used, the procedure is as the following :

(a) Suppose V_{ij}^{A} are the elements of original input absolute covariance, the elements V_{ij}^{R} of its relative covariance matrix are given by

$$V_{ij}^{R} = V_{ij}^{A} / y_i / y_j \ ;$$

(b) With V_{ij}^{A}, the fit values, e. g. spline function $S(x)$ is calculated;

(c) The new absolute covariance matrix is calculated with V_{ij}^{R} and $S(x)$

$$V_{ij}^{A} = V_{ij}^{R} \ S(x_i) \ S(x_j) \ ;$$

(d) With new V_{ij}^{A} as input covariance matrix, the new spline function $S(x)$ is calculated. Repeat steps (c), (d) (the input covariance matrix is corrected repeatly) until the reasonable result is got.

As an example, the above procedures are completed with the input data of example 2 ($r = 0.95$). The results are shown in Fig. 3, from which it can be seen that with increasing the number of iteration time, the fit values become close to the measured data. In fact, for this example, all results are reasonable after one time of iteration.

(2) Appropriately select the order and knots of spline function

In the example 2, when the correlation coefficient becomes larger, the fit values deviate from the measured data. The other possible reason is the spline function, which has been used to fit the data and depends on the selected order

Table 1 The calculated results of example 1

	$S(x)$			$V(x)$		
	1.0	2.0	3.0	1.0	2.0	3.0
(1)	1.0	2.0	3.0	0.0049 0.0047	0.0047 0.0047	0.0044 0.0047 0.0049
(2)	1.192	2.192	3.192	0.0092 0.0090	0.0090 0.0090	0.0090 0.0090 0.0092
(3)	1.196	2.196	3.196	0.0094 0.0092	0.0092 0.0092	0.0089 0.0092 0.0094
(4)	0.9994	1.9994	2.9994	0.0036 0.0031	0.0031 0.0031	0.0027 0.0031 0.0036
(5)	0.930	1.930	2.930	0.11 0.11	0.11 0.11	0.11 0.11 0.11

Table 2 The calculated results of example 2

x	0.8	1.0	2.3	3.4	4.5	7.4	8.8	9.7	r
$S(x)$	21.7	22.8	30.2	36.5	42.7	59.2	67.2	72.3	0
$S(x)-y$	2.7	−7.2	3.2	−4.5	−9.3	6.2	4.2	−5.7	
$S(x)$	20.8	21.9	29.0	35.1	41.0	57.0	64.6	69.5	0.2
$S(x)-y$	1.8	−8.1	2.0	−5.9	−11.0	4.0	1.6	−8.5	
$S(x)$	19.6	20.6	27.3	33.0	38.0	53.5	60.8	65.4	0.4
$S(x)-y$	0.6	−9.4	0.3	−8.0	−13.4	0.5	−2.2	−12.6	
$S(x)$	17.5	18.4	24.4	29.4	34.5	47.8	54.3	58.4	0.6
$S(x)-y$	−1.5	−11.6	−2.6	−11.6	−17.5	−5.2	−8.7	−19.6	
$S(x)$	13.2	13.9	18.5	22.3	26.1	36.2	41.1	44.2	0.8
$S(x)-y$	−5.8	−16.1	−8.5	−18.7	−25.9	−16.8	−21.9	−33.8	
$S(x)$	5.4	5.7	7.5	9.1	10.6	14.7	16.7	18.0	0.95
$S(x)-y$	−13.6	−24.3	−19.5	−31.9	−41.4	−38.3	−46.3	−60.0	

Table 3 The fit result with 3 order spline and more knots for example 2 ($r=0.95$)

x	0.8	1.0	2.3	3.4	4.5	7.4	8.8	9.7
$S(x)$	17.7	27.9	24.9	39.8	46.3	49.8	58.9	72.1

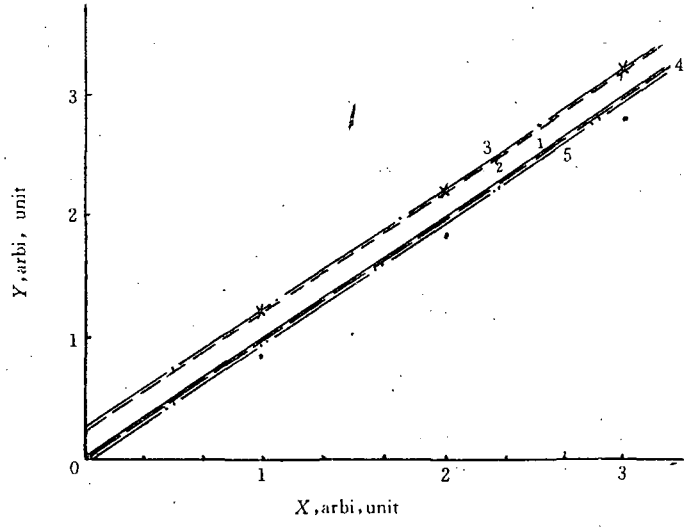

Fig. 1 The variation of fit values with width and covariance matrix of input data set (example 1)

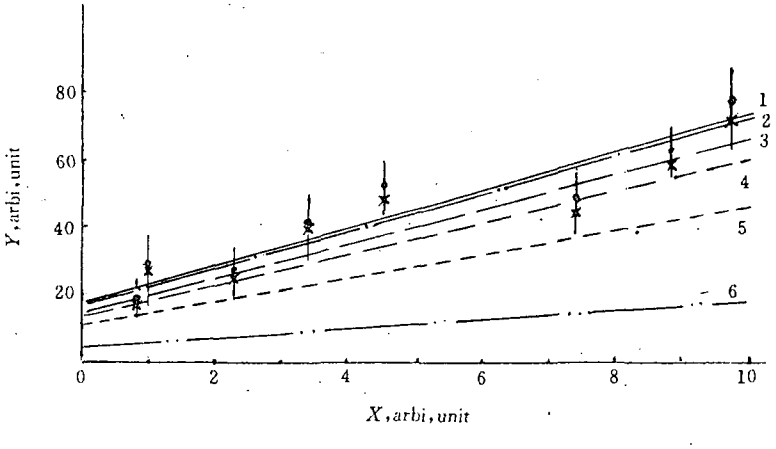

Fig. 2 The variation of fit values with correlation coefficients r (example 2)

curve 1, $r=0.0$; 2, $r=0.2$; 3, $r=0.4$; 4, $r=0.6$; 5, $r=0.8$; 6, $r=0.95$

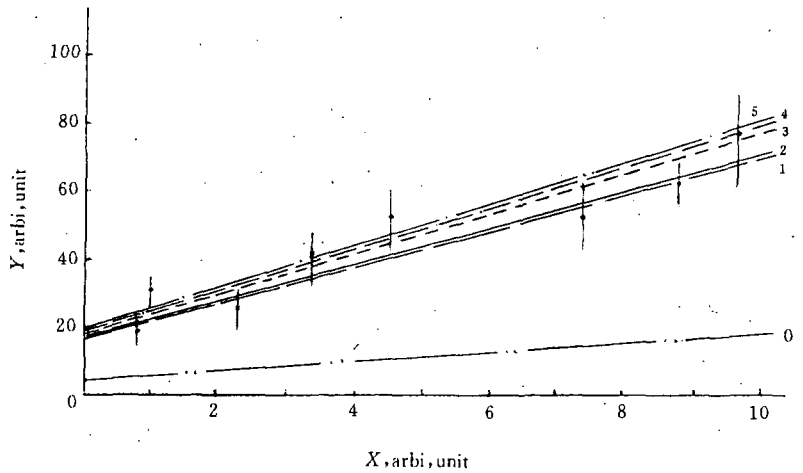

Fig. 3 The variation of fit values with iteration (for input covariance matrix) time (example 2, $r=0.95$)

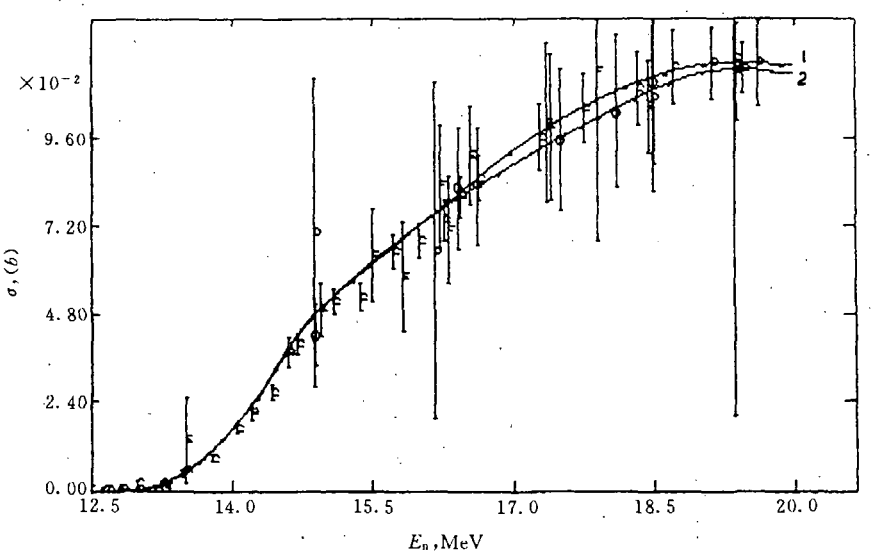

Fig. 4 A practical example of spline function fitting with program SPC : $^{23}Na(n,2n)$ cross section

ϕ etc. experimental data;

curve 1. Input data are correlative; curve 2. Input data are not correlative.

and knots, is not the correct one. In fact, in this example the order of spline function $K = 1$ and two knots are selected, which mean the expected values are linear function, but the real expected values may be another function form, which is more close to measured data, the problem happens due to selecting unappropriate function (the order and knots of spline function). So to solve the problem, we must choose more reasonable function form, which is more close to the measured data (this needs to be judged in physics). As mentioned above, the order and knots can be chosen wantonly, so, in principle, innumerable selections could be offered. Therefore, the satisfactory result can be got just through selecting the order and knots of spline function (of course, this must be reasonable in physics).

As an example, the input data in example 2 ($r = 0.95$) are fitted with spline order $K = 3$ and 4 knots (0.8, 1.0, 2.3, 9.7). The results are given in table 3. It can be seen that the fit values are reasonable.

3) Example 3

A practical example is shown in Fig. 4 for the application of the program. The data to be fitted are cross section of ^{23}Na(n,2n) reaction as function of incident energies. They were measured by 8 laboratories,including Prof. Lu Hanlin[5], CIAE. To fit the data, the order of spline $K = 3$ and 7 knots (12.5, 14.5, 15.0, 16.5, 18.5, 19.8, 21.0) were chosen. The results are shown in Fig. 4. The curve 1 is for correlative input data, the correlations of each set of data were determined according to the strict mathematical calculation or physical analysis estimation [6]. It is supposed for curve 2 that the input data are all not correlative.

References

[1] A. Horsley et al., Nucl. Instr. & Methods, 62, 29(1968)

[2] Zhou Hongmo et al., Atomic Energy Sci. & Technology, 4, 389(1987) (in Chinese)

[3] Liu Tingjin et al., CNDP, 2, 58(1989)

[4] R.Peelle, Private Commun. (1987)

[5] Lu Halin et al., Private Commun. (1987)

[6] Zhang Jianhua, CIAE Master thesis (1992)

[7] Zhao Zhixiang, ORNL / TM-12106

VI NUCLEAR DATA NEWS

Activities and Cooperations on Nuclear Data in China During 1993

Zhao Zhixiang

(Chinese Nuclear Data Center, IAE)

1 The Following Meetings Were Held by CNDC in 1993 :

"Examination and Acceptance Meeting of the Soft–ware for Compilation of EXFOR Neutron Data" June 15～17, 1993, held at Yantai City, Shandong. Reviewed the soft–ware system for compilation of EXFOR neutron data completed in the end of 1992 by Nankai University and CNDC.

"Working Meeting of China Committee of Nuclear Data on Nuclear Data Project in 1993～1994" Sep. 15, 1993, held at CIAE, Beijing. Worked out nuclear data work project of 1993～1994 in China and proposed nuclear data tasks of Chinese Nuclear Data Coordination Network.

"Workshop on Chinese Evaluated Nuclear Parameter Library(CENPL)", Oct. 18～20 , 1993, held at CIAE, Beijing. Communicated and reviewed the progress in CENPL, discussed the future work.

" Working Group Meeting of Nuclear Data Evaluation" , Dec. 15～18,1993, held at CIAE, Beijing. Communicated the progress and the trends in nuclear data evaluation. Reviewed the evaluations newly completed and the intercomparison among several evaluated nuclear data libraries. Discussed the contents which should be included in CENDL–2.1.

2 The Following International Meetings and Workshops in Nuclear Data Field Were Attended by Members of CNDC in 1993 :

" 19th Meeting of International Nuclear Data Committee" Mar. 8～12, 1993, held in Vienna, Austria.

"IAEA Advisory Group Meeting on Technical Aspects of A+M Data Pro-

cessing and Exchange" Sep. 18～26, 1993, held in Vienna, Austria.

"IAEA Advisory Group Meeting on Review of Uncertainty Files and Improved Multigroup Cross Section Files for FENDL" Nov. 8～12, 1993, held at JAERI, Japan.

"IAEA Specialists' Meeting on Comparison of Activation Cross Section Measurements and Experimental Techniques" Nov. 15～17, 1993, held at JAERI, Japan.

"1993 Symposium on Nuclear Data" Nov. 8～19, 1992, held at JAERI, Japan.

3 In 1992, two mumbers of CNDC as visiting scientists worked in ECN / Netherlands and ICTP / Italy in nuclear data field.

4 The Following Foreign Scientists in Nuclear Field Visited CNDC / CIAE in 1993

Dr. Y. Kikuchi, JAERI / NDC, Japan, Feb. 20 ～ Mar. 7, 1993;

Dr. A. Mengoni, Bologna / ENEA, Italy, Mar. 31～Apl. 15, 1993;

Prof. Kimura, Kyoto University, Japan, May 5, 1993;

Dr. Y. Kikuchi, JAERI / NDC, Japan, May 22～24, 1993;

Dr. A. Blokhin, IPPE / CJD, Russia, May 25～30, 1993;

Prof. P. Kahn, Stonybrook University, and Dr. V. Mclane, NNDC, USA, Sept. 14, 1993;

Dr. H. Klippel, ECN, Netherlands, Oct. 25～29, 1993;

Dr. T. V. Golashvili, ATOMINFORM, Russia, Dec. 22～23, 1993.

CINDA INDEX

Nuclide	Quantity	Energy (eV)		Lab	Type	Documentation			
		Min	Max			Ref	Vol	Page	Date
^{1}H	(n,n)	2.0+6	1.5+8	AEP	Theo	Jour CNDP	11	52	Jun 94
^{27}Al	(γ,n)	1.3+6	3.0+7	AEP	Theo	Jour CNDP	11	21	Jun 94
^{54}Fe	(γ,n)	1.6+6	2.6+7	AEP	Theo	Jour CNDP	11	21	Jun 94
	(n,x)	Thrsh	5.0+7	AEP	Eval	Jour CNDP	11	79	Jun 94
^{56}Fe	(n,x)	Thrsh	5.0+7	AEP	Eval	Jour CNDP	11	79	Jun 94
	Evaluation	1.0−5	2.0+7	AEP	Eval	Jour CNDP	11	72	Jun 94
Fe	(n,x)	Thrsh	5.0+7	AEP	Eval	Jour CNDP	11	79	Jun 94
^{64}Zn	(n,p)	4.0+6	7.0+6	BJG	Expt	Jour CNDP	11	1	Jun 94
^{66}Zn	(n,2n)	1.4+7	1.5+7	LNZ	Expt	Jour CNDP	11	5	Jun 94
^{67}Zn	(n,p)	1.35+7	1.48+7	LNZ	Expt	Jour CNDP	11	5	Jun 94
^{132}Ba	(n,p)	1.42+7		LNZ	Expt	Jour CNDP	11	5	Jun 94
	(n,2n)	1.42+7		LNZ	Expt	Jour CNDP	11	5	Jun 94
^{134}Ba	(n,p)	1.42+7		LNZ	Expt	Jour CNDP	11	5	Jun 94
	(n,2n)	1.42+7		LNZ	Expt	Jour CNDP	11	5	Jun 94
^{136}Ba	(n,p)	1.42+7		LNZ	Expt	Jour CNDP	11	5	Jun 94
^{137}Ba	(n,p)	1.42+7		LNZ	Expt	Jour CNDP	11	5	Jun 94
^{151}Eu	(n,γ)	2.2+4	1.1+6	SIU	Expt	Jour CNDP	11	9	Jun 94
^{153}Eu	(n,γ)	2.2+4	1.1+6	SIU	Expt	Jour CNDP	11	9	Jun 94
^{193}Ir	(n,2n)	1.48+7		LNZ	Expt	Jour CNDP	11	5	Jun 94
^{197}Au	(n,3n)	Thrsh	5.0+7	AEP	Eval	Jour CNDP	11	67	Jun 94
	(n,4n)	Thrsh	5.0+7	AEP	Eval	Jour CNDP	11	67	Jun 94
^{204}Pb	(n,2n)	1.35+7	1.5+7	LNZ	Expt	Jour CNDP	11	5	Jun 94
^{206}Pb	(n,α)	1.44+7		LNZ	Expt	Jour CNDP	11	5	Jun 94
^{209}Bi	(γ,n)	7.6+6	3.0+7	AEP	Theo	Jour CNDP	11	21	Jun 94
	(γ,abs)	7.6+6	3.0+7	AEP	Theo	Jour CNDP	11	21	Jun 94

Author, Comments
Shen Qingbiao, SIG, ANGDIST
Zhang Jingshang+, SIG, CALC
Zhang Jingshang+, SIG, CALC
Yu Baosheng+, SIG, CR–51, MN–52, MN–54
Yu Baosheng+, SIG, CR–51, MN–52, MN–54
Zhao Zhixiang+, FOR CENDL–2.1
Yu Baosheng+, SIG, CR–51, MN–52, MN–54
Tang Guoyou+, ACTIV, SIG, TBL
Yuan Junqian+, ACTIV, SIG, TBL
Yuan Junqian+, ACTIV, SIG, TBL
Yuan Junqian+, ACTIV, SIG, TBL
Yuan Junqian+, ACTIV, SIG, TBL
Yuan Junqian+, ACTIV, SIG, TBL
Yuan Junqian+, ACTIV, SIG, TBL
Yuan Junqian+, ACTIV, SIG, TBL
Yuan Junqian+, ACTIV, SIG, TBL
Xia Yijun+, ACTIV, SIG, TBL
Xia Yijun+, ACTIV, SIG, TBL
Yuan Junqian+, ACTIV, SIG, TBL
Yu Baosheng+, SIG, CR–51, MN–52, MN–54
Yu Baosheng+, SIG, CR–51, MN–52, MN–54
Yuan Junqian+, ACTIV, SIG, TBL
Yuan Junqian+, ACTIV, SIG, TBL
Zhang Jingshang+, SIG, CALC
Zhang Jingshang+, SIG, CALC

(京)新登字 077 号

图书在版编目(CIP)数据

核数据进展通讯 (11) =COMMUNICATION OF NUCLEAR DATA PROGRESS NO. 11:英文/中国核数据中心编. —北京:原子能出版社,1994. 6
ISBN 7-5022-1200-0

Ⅰ. 核… Ⅱ. 中… Ⅲ. 核技术-数据处理-进展-中国-英文 Ⅳ. TL-64

中国版本图书馆 CIP 数据核字 (94) 第 05990 号

原子能出版社出版发行
责任编辑:李曼莉
社址:北京市海淀区阜成路 43 号 邮政编码:100037
核科学技术情报研究所印刷
开本 787×1092 1/16 · 印张 8½ · 字数 134 千字
1994 年 6 月北京第一版 · 1994 年 6 月北京第一次印刷

1991

COMMUNICATION OF NUCLEAR DATA PROGRESS

ISBN 7-5022-1200-0